

SOLUTE PARTITIONING OF Fe-Cr-Mn-Ni-C
ALLOYS DURING SOLIDIFICATION

by

DAVID MALCOLM KUNDRAT

B.S. University of Cincinnati

Cincinnati, Ohio

1975

SUBMITTED IN PARTIAL FULFILLMENT
OF THE REQUIREMENTS FOR THE
DEGREE OF

DOCTOR OF SCIENCE

at the

MASSACHUSETTS INSTITUTE OF TECHNOLOGY

February 1980

© Massachusetts Institute of Technology 1980

Signature redacted

Signature of Author

Department of Materials Science and Engineering
January 11, 1979

Signature redacted

Certified by

John F. Elliott
Thesis Supervisor

Signature redacted

Accepted by

Regis M. N. Pelloux
Chairman, Department Committee

ARCHIVES
MASSACHUSETTS INSTITUTE
OF TECHNOLOGY

MAR 21 1980

LIBRARIES



77 Massachusetts Avenue
Cambridge, MA 02139
<http://libraries.mit.edu/ask>

DISCLAIMER NOTICE

Due to the condition of the original material, there are unavoidable flaws in this reproduction. We have made every effort possible to provide you with the best copy available.

Thank you.

The following pages were not included in the original document submitted to the MIT Libraries.

This is the most complete copy available.

ABSTRACT

SOLUTE PARTITIONING OF Fe-Cr-Mn-Ni-C
ALLOYS DURING SOLIDIFICATION

by

DAVID MALCOLM KUNDRAT

Submitted to the Department of Materials Science and Engineering on January 11, 1980 in partial fulfillment of the requirements for the degree of Doctor of Science.

The phase relationships between the liquid phase and primary solution phases were investigated in the iron-rich Fe-Cr-Mn-Ni-C system. The investigation consisted of experiments and thermodynamic modeling of the results.

The phase relationships determined experimentally were the tie-lines between the liquid and δ (BCC) phases and between the liquid and γ (FCC) phases, the δ -liquidus and the γ -liquidus and the two-fold equilibrium $L+\delta \rightleftharpoons L+\delta+\gamma$. The composition fields investigated were the iron-rich binary systems, ternary systems and selected quaternary systems of the composition pentahedroid bounded by 0 to 1 w/o C, 0 to 10 w/o Mn, 0 to 25 w/o Cr and 0 to 25 w/o Ni (bal. Fe). The liquidus of the nickel-rich Ni-Cr system was also determined experimentally.

The experimental results have been predicted within the experimental error with the use of a thermodynamic model. Parameters in the model were determined from thermodynamic measurements and analyses reported in the literature and from mathematical methods applied on the experimental results. A method to calculate equilibrium solidification paths in alloy systems has been developed and the use of the method in kinetic studies of the solidification process has been demonstrated.

Thesis Supervisor: John F. Elliott

Title: Professor of Metallurgy

TABLE OF CONTENTS

<u>Chapter</u>		<u>Page</u>
	TITLE PAGE	1
	ABSTRACT	2
	TABLE OF CONTENTS	3
	LIST OF FIGURES	7
	LIST OF TABLES	12
	ACKNOWLEDGEMENTS	14
1	INTRODUCTION	15
2	LITERATURE SURVEY	16
	2.1 Phase Diagrams	16
	2.1.1. Unary Systems	16
	2.1.2. Binary Systems	18
	2.1.3. Ternary Systems	20
	2.1.4. Quaternary Systems	23
	2.2 Thermodynamics	23
	2.2.1. The Pure Components	23
	2.2.2. Multicomponent Alloys	26
	2.2.2.1. Liquid Solutions	32
	2.2.2.2. Solid Solutions	41
3	OUTLINE OF RESEARCH	52
	3.1 Experimental Methods	54
	3.2 Modelling	57
4	METHOD OF CALCULATION AND PORTRAYAL OF THE PHASE EQUILIBRIA IN THE IRON-RICH Fe-Cr-Mn- Ni-C SYSTEM	58
	4.1 Methods of Calculation	59
	4.1.1. Method of Minimization of the Gibbs Energy	59

TABLE OF CONTENTS (Cont'd.)

<u>Chapter</u>		<u>Page</u>
	4.1.1.1. Numerical Techniques	61
	4.1.2. Method of Equal Chemical Potentials	64
	4.1.2.1. Numerical Techniques	67
	4.1.3. Comparison of Methods	68
	4.2. Spatial Representation	71
	4.2.1. The Concentration Simplex	72
	4.2.2. The Hyperconode	76
	4.2.3. The Continuum	78
	4.2.3.1. The Ternary System	79
	4.2.3.2. The Quaternary System	79
	4.2.3.3. The Quinary System	83
	4.2.4. Method of Projection	86
5	EXPERIMENTAL	87
	5.1. Differential Thermal Analysis	87
	5.1.1. Materials	88
	5.1.2. Apparatus	88
	5.1.3. Procedure	91
	5.1.4. Source of Experimental Error	91
	5.2. Equilibrium Couples	96
	5.2.1. Materials	96
	5.2.2. Apparatus	96
	5.2.3. Procedure	96
	5.2.4. Source of Experimental Error	101
6	THERMODYNAMIC MODELLING OF PHASE DIAGRAMS	105

TABLE OF CONTENTS (Cont'd.)

<u>Chapter</u>		<u>Page</u>
6.1.	The Integral Molar Free Energy	108
6.1.1.	Interaction Models of Solution Phases	108
6.1.1.1.	Selection of a Solution Model	110
6.1.1.2.	The Quasi-Regular Solution Model	112
6.2.	Methods to Determine Thermodynamic Parameters from Phase Diagrams	116
6.2.1.	Optimization Procedure	120
6.2.1.1.	Calculation of the Weighting Factor	122
6.2.1.2.	Linear Functional Relationships	125
6.2.1.3.	Non-Linear Functional Relationships	127
6.2.1.4.	Direct Search	129
7	RESULTS	131
8	DISCUSSION OF RESULTS	162
8.1.	Binary Systems	162
8.2.	Ternary Systems	166
8.3.	Quaternary Systems	179
9	CALCULATION OF SOLIDIFICATION PATHS	188
9.1.	Equilibrium Solidification	190
9.1.1.	Two-phase Equilibrium	191
9.1.2.	Three-phase Equilibrium	192
9.2.	Non-equilibrium Solidification	193
10	SUMMARY AND CONCLUSIONS	196

TABLE OF CONTENTS (Cont'd.)

<u>Chapter</u>	<u>Page</u>
APPENDICES:	
A. The Chemical Potential Expressed as a Function of the Intensive Thermodynamic Variables	198
B. Effect of Contamination on the Measurement of Temperature and Composition of the Two-phase Equilibrium	201
C. Tabulated Results	204
D. Recommendations for further research	236
REFERENCES	237
BIBLIOGRAPHY	242

LIST OF FIGURES

<u>Figure</u>		<u>Page</u>
2.1	Schematic representation of the single-phase fields in the iron-rich Fe-Cr-C system (13)	21
4.1	Schematic representation of the tie-lines of the equilibrium between two phases in the Fe-X ₁ -X ₂ system.	63
4.2	Representation of neighboring equilibrium states of the equilibrium between two phases in a multi-component system.	65
4.3	Schematic representation of the chemical potential and the integral molar free energy of a binary system (Const. T, P).	69
4.4	The concentration simplex for a three-component system (Const. T, P).	74
4.5	The concentration simplexes of the Fe-Cr-Mn-Ni-C system (Const. T, P).	75
4.6	The hyperconodes (phase simplexes) of the multi-component system.	77
4.7	Schematic representation of the procedure to calculate the continuum of tie-lines of the equilibrium between two phases in a ternary system (Const. T, P).	80
4.8	Schematic representation of the procedure to calculate the continuum of tie-triangles of the equilibrium among three phases in a ternary system (Const. P).	81
4.9	Schematic representation of the procedure to calculate the continuum of tie-lines of the equilibrium between two phases in a quaternary system (Const. T, P).	82

LIST OF FIGURES (Cont'd.)

<u>Figure</u>		<u>Page</u>
4.10	Schematic representation of the procedure to calculate the continuum of tie-lines of the equilibrium among three phases in a quaternary system (Const. T, P).	84
4.11	Schematic representation of the liquidus of the quinary system projected into two-dimensional space (Const. T, P).	85
5.1	The experimental apparatus for DTA.	89
5.2	Schematic diagram of the sequence of thermalgrams of the freezing points of Fe and the alloys Fe-C, Fe-Mn-C and Fe-C-Mn-Cr.	95
5.3	The experimental apparatus for the directional solidification of alloy melts.	97
5.4	Photographs of an etched ingot exhibiting the interface between the quenched pre-solid gamma and liquid phases (A). The microstructure of the cross-section of the ingot at positions a, b and c are also shown (B) (6% Nital etch).	100
5.5A & 5.5B	Schematic drawings of two types of composition profiles observed in the quenched equilibrium couples.	103
6.1	The experimental and calculated isotherms of a surface of saturation in the ternary system Fe-X ₁ -X ₂ at T _A .	123
7.1	The Fe-C system determined experimentally from equilibrium couples and DTA and calculated by the model.	133
7.2	The Fe-Ni system determined experimentally and by calculation.	134
7.3	The Fe-Mn and Fe-Cr systems determined experimentally and by calculation.	135
7.4	The Ni-Cr system determined experimentally and by calculation.	136
7.5	The liquidus in the Fe-Cr-C system determined experimentally and by calculation.	137

LIST OF FIGURES (Cont'd.)

<u>Figure</u>		<u>Page</u>
7.6	The equilibrium between the liquid (L) and BCC (δ) phases in the Fe-Cr-C system determined experimentally and by calculation.	138
7.7	The equilibrium between the liquid (L) and FCC (γ) phases in the Fe-Cr-C system determined experimentally and by calculation.	139
7.8	The peritectic reaction in the Fe-Cr-C system determined experimentally and by calculation.	140
7.9	The liquidus in the Fe-Mn-C system determined experimentally and by calculation.	141
7.10	The equilibrium between the liquid (L) and BCC (δ) phases in the Fe-Mn-C system determined experimentally and by calculation.	142
7.11	The equilibrium between the liquid (L) and FCC (γ) phases in the Fe-Mn-C system determined experimentally and by calculation.	143
7.12	The liquidus in the Fe-Ni-C system determined experimentally and by calculation.	144
7.13	The equilibrium between the liquid (L) and BCC (δ) phases and between the liquid and FCC (γ) phases in the Fe-Ni-C system determined experimentally and by calculation.	145
7.14	The peritectic reaction $L + \delta \rightarrow L + \delta + \gamma$ in the Fe-Ni-C system determined experimentally and by calculation.	146
7.15	The liquidus in the Fe-Cr-Ni system determined experimentally and by calculation.	147
7.16	The equilibrium between the liquid (L) and FCC (γ) phases in the Fe-Cr-Ni system determined experimentally and by calculation.	148
7.17	The peritectic reaction in the Fe-Cr-Ni system determined experimentally and by calculation.	149

LIST OF FIGURES (Cont'd.)

<u>Figure</u>		<u>Page</u>
7.18	The liquidus in the Fe-Cr-Mn system determined experimentally and by calculation.	150
7.19	The liquidus in the Fe-Mn-Ni system determined experimentally and by calculation.	151
7.20	The experimental and calculated tie-lines of the L- δ equilibrium in the Fe-Cr-Mn-C system projected orthogonally onto the Fe-Cr-C and Fe-Mn-C basal planes.	152
7.21	The experimental and calculated tie-lines of the L- γ equilibrium in the Fe-Mn-Ni-C system projected (orthogonally) onto the Fe-Ni-C and Fe-Mn-C basal planes.	153
7.22	The experimental and calculated tie-lines of the L- δ equilibrium in the Fe-Cr-Ni-C system projected (orthogonally) onto the Fe-Cr-C and Fe-Ni-C basal planes ($\theta^L_{\text{(FeCrNiC)}} = 0$; $\theta^\delta_{\text{(FeCrNiC)}} = 0$).	154
7.23	The experimental and calculated tie-lines of the L- γ equilibrium in the Fe-Cr-Ni-C system projected (orthogonally) onto the Fe-Cr-C and Fe-Ni-C basal planes ($\theta^L_{\text{(FeCrNiC)}}$, $\theta^\gamma_{\text{(FeCrNiC)}} = 0$).	155
7.24	The experimental and calculated tie-lines of the L- γ equilibrium in the Fe-Cr-Ni-C system projected (orthogonally) onto the Fe-Cr-C and Fe-Ni-C basal planes ($\theta^L_{\text{(FeCrNiC)}} = -1000000$; $\theta^\gamma_{\text{(FeCrNiC)}} = -1400000$).	156
8.1	The liquidus in the Fe-Cr-C system determined experimentally by Chochol and calculated with the quasi-regularly solution model (13).	169
8.2	Comparison of the equilibrium between the liquid (L) and BCC (δ) phase in the Fe-Cr-C system determined experimentally in this study and by Chochol (13).	171

LIST OF FIGURES (Cont'd.)

<u>Figure</u>		<u>Page</u>
8.3	Comparison of the isotherms of the liquidus in the Fe-Cr-C system calculated with the quasi-regular solution model with (continuous line) and without (dotted lines) the ternary parameters.	172
8.4	Comparison of the liquidus in the Fe-Ni-C system determined experimentally by Hume-Rothery and calculated with the quasi-regular solution model.	175
8.5	The liquidus in the Fe-Cr-Ni system determined experimentally by Chochol and calculated with the quasi-regular solution model (13).	176
8.6	Orthogonal projection of the liquidus in the Fe-Cr-Ni-C system at 1493°C onto the Fe-Cr-Ni basal plane. Calculated with the quasi-regular solution model ($\theta^{\gamma}_{(\text{FeCrNiC})} = -1400000$; $\theta^{\text{L}(\delta)}_{(\text{FeCrNiC})} = -1000000$; $\theta^{\text{L}(\gamma)}_{(\text{FeCrNiC})} = 0$; $\theta^{\delta}_{(\text{FeCrNiC})} = 0$).	183
8.7	The L- δ - γ equilibrium in the Fe-Cr-Ni-C system (Constant T, P) depicted as a continuum of tie-triangles.	184
8.8	Orthogonal projection of the surface of two-fold saturation $L \rightleftharpoons L + \delta + \gamma$ in the Fe-Cr-Ni-C system onto the Fe-Cr-Ni basal plane. Calculated with quasi-regular solution model ($\theta^{\phi}_{(\text{FeCrNiC})} = 0$; $\phi = \delta, L, \gamma$).	186
8.9	Progress of the two-fold equilibrium $L + L + \delta \rightleftharpoons L + \delta + \gamma$ with temperature in the Fe-Cr-Ni-C system (orthogonally) projection onto the Fe-Ni-C and the Fe-Cr-C basal planes.	187
9.1	The solidification paths of the liquid and gamma phases in the Fe-Cr-C system beginning at the composition $\underline{P}(X_i^{\circ})$. Parentheses indicate the fraction of liquid phase at selected temperatures during equilibrium solidification. Brackets indicate the fraction of liquid phase when segregation of Cr and C is assumed during solidification (See text).	195

LIST OF TABLES

<u>Table</u>		<u>Page</u>
2.1	Equilibrium transformation temperatures of the pure elements.	17
2.2	Relative phase stabilities of the pure components ($1000^{\circ}\text{C} < T < 1600^{\circ}\text{C}$; 1 atm. pressure).	24
2.3	Equilibrium and metastable melting points of the pure components calculation from Table (2.2) (1 atm).	25
2.4	Interaction coefficients of carbon (atom fraction) in liquid iron (1500 to 1570°C).	33
2.5	Interaction coefficients of carbon (atom ratio) in liquid iron (38).	34
2.6	Parameter λ_{ic} (Eq. 2.19) in the expression for the activity coefficient of carbon in liquid iron from the central atom model (1550°C) (32, 39).	35
2.7	Binary parameters in the quasi-regular solution model for phase proposed by Kaufman	37
2.8	Interaction coefficient and the activity coefficient at infinite dilution (atom fraction) of substitutional elements in liquid iron (33, 34).	38
2.9	Binary parameters in the quasi-regular solution model for the liquid phase (Rao-Tiller).	40
2.10	Interaction coefficients of carbon (atom ratio) in Austenite (40, 37).	42
2.11	Parameter λ_{ic} in the expression for the activity coefficient of carbon in Austenite developed from the central atom model (32, 39).	43
2.12	The parameters in the Zupp-Stevenson model of the activity coefficient of carbon in alloyed Austenite (e.g., 2.21).	45
2.13	Binary parameters in the quasi-regular solution mode for the gamma (FCC) phase (Kaufman) proposed by Kaufman	46

LIST OF TABLES (Cont'd.)

<u>Table</u>		<u>Page</u>
2.14	Binary parameters in the quasi-regular solution model for the Delta (BCC) phase proposed by Kaufman.	48
2.15	Parameters in the quasi-regular solution model of substitutional solid solutions ($T > 1000^\circ\text{C}$).	49
2.16	Summary of partial molar properties of iron-base binary alloys ($T > 1000^\circ\text{C}$).	51
5.1	Calculated additions and corresponding chemical analyses of DTA ingots..	92
7.1	Relative phase stabilities of the liquid and BCC and the liquid and FCC forms of the pure elements $\Delta G_i^{\circ L \rightarrow \phi}$ (cal/mole).	157
7.2	Binary interaction parameters in the quasi-regular solution model.	158
7.3	Ternary parameters in the quasi-regular solution model determined from experimental tie-lines.	160
7.4	Quaternary parameters in the quasi-regular solution model determined from experimental tie-lines.	161
8.1	The peritectic reaction $L + \delta \rightleftharpoons L + \delta + \gamma$ determined experimentally in the binary systems and calculated from the quasi-regular model.	164
8.2	Experimental and calculated minimum in the liquidus of the Fe-Cr system.	165
8.3	The ternary parameter in the quasi-regular solution-model for the liquid phase calculated from thermo-chemical models reported in the literature.	168

ACKNOWLEDGEMENTS

This thesis is dedicated to Kjell Hellesøe, a physicist who has inspired in the author a desire to know.

"To know is to know all; not to know all is not to know. To know all, it is necessary to know very little, but to know that very little, one must first know pretty much."

Gurdjieff

The author expresses his gratitude to Professor John Elliott for his able guidance and staunch support. The metaphysical support of his parents and the encouragement of his friends is also kindly appreciated. In particular, he thanks Linn Eichler and his colleagues David De Young and David Lee.

The author thanks Professor Antonio Laurachi for his helpful comments during completion of the manuscript and Professors Kent Bowen and Thomas King for their efforts and suggestions which have brought the thesis to its final form. He also thanks Dick Stanton for his technical assistance with building the experimental apparatus, and to Linda Sayegh for typing the manuscript of the thesis.

The author is indebted to Copperweld Specialty Steel Company for the chemical analyses of the unusually large number of specimens and to the American Iron and Steel Institute for their financial support.

CHAPTER 1INTRODUCTION

The solute elements Cr, Mn, Ni and C in iron constitute the compositional base of corrosion resistant alloys. When more than one of these elements are present in significant concentrations in iron, the phase relationships in the multicomponent system cannot, in general, be determined by extrapolation from the limiting binary systems. Precise knowledge of these phase relationships in the alloy system is essential to control the processes that occur during solidification and during heat treating.

With improved control of the solidification of the alloy steels, the quality of the casting is improved. This has a two-fold importance today. Because of the demands of high-technology, stricter tolerances of the properties of the product must be met. And, with escalating costs of the alloying additions and energy consumed per unit of production, it is cost-effective to increase the yield of the finished product.

The focus of this study is thermodynamic modeling of the equilibrium phase relationships which have been determined experimentally in the iron-rich Fe-Cr-Mn-Ni-C system at solidification temperatures. With a thermodynamic model of the alloy system available, the usefulness of the experimental results is extended by permitting extrapolation and interpolation within the composition field investigated. In addition, kinetic process that occur during solidification of these alloys can be studied in a quantitative manner with reference to the equilibrium state of the system.

CHAPTER 2

LITERATURE SURVEY

Reliable data on both the phase diagrams and thermodynamics of binary and ternary alloys in the Fe-Cr-Mn-Ni-C system have accumulated in the past thirty years. In particular, the influence of alloying elements on the phase relationship in the Fe-C system and on the activity of carbon in iron has been well documented. This chapter is concerned with information published on the phase relationship and thermochemical properties of the iron-rich alloys in the composition region bounded by 0 to 25% Cr, 0 to 10% Mn, 0 to 25% Ni and 0 to 1% C (bal. Fe) at solidification temperatures ($1000^{\circ}\text{C} < T < 1600^{\circ}\text{C}$). All temperatures refer to the 1968 International Temperature Scale.

2.1. Phase Diagrams

Phase diagrams of binary alloys in the Fe-Cr-Mn-Ni-C system have been constructed from the results of numerous investigators. There are few investigations of the phase diagrams of the ternary and quaternary alloys. Hansen, Elliott, Shunk, Hultgren and most recently, A.S.M. (vol.8) have reviewed critically the binary systems (1,2,3,4,5). Prince lists references of the ternary and quaternary systems investigated from 1952 through 1973 (6). Recent work on the phase diagrams of the iron-rich alloys at solidification temperatures are reviewed presently. Relevant data on these phase diagrams are portrayed in Chapter 7.

2.1.1. Unary Systems

Table 2.1 lists equilibrium transformation temperatures of the pure

Table 2.1. Equilibrium transformation temperatures of the pure elements (1 atm.)

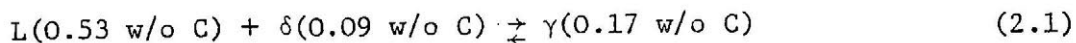
Element	Equilibrium	Transformation temperatures °C	Reference
Fe	$L \rightleftharpoons \delta$	1538	(7)
	$\delta \rightleftharpoons \gamma$	1394	
Cr	$L \rightleftharpoons \delta$	1859	(4)
Mn	$L \rightleftharpoons \delta$	1246	(4)
	$\delta \rightleftharpoons \gamma$	1139	
Ni	$L \rightleftharpoons \gamma$	1555	(4)
C	$L \rightleftharpoons \text{Gr}$	3927	(8)

elements. δ , γ and Gr refer to the BCC, FCC and graphitic crystalline structures, and L refers to the liquid phase.

2.1.2. Binary Systems

Fe-C

In 1972 Chipman reviewed critically thermodynamic and phase diagram data on the Fe-C system and reconstructed the phase diagram (7). The peritectic reaction is reported to occur at 1495°C:



In the composition region less than 1.0 w/o C, the liquidus and solidus are linear with temperature. Equations of these lines are as follows:

$$\delta\text{-Liquidus} \quad T(^{\circ}\text{C}) = 1538.0 - (81.1) \times (\text{w/o C}) \quad (2.2)$$

$$\delta\text{-Solidus} \quad T(^{\circ}\text{C}) = 1538.0 - (477.8) \times (\text{w/o C}) \quad (2.3)$$

$$\gamma\text{-Liquidus} \quad T(^{\circ}\text{C}) = 1531.1 - (68.2) \times (\text{w/o C}) \quad (2.4)$$

$$\gamma\text{-Solidus} \quad T(^{\circ}\text{C}) = 1528.4 - (177.8) \times (\text{w/o C}) \quad (2.5)$$

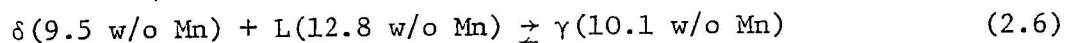
Fe-Cr

Hellewell and Hume-Rothery have employed DTA (differential thermal analysis) to determine the liquidus and solidus in the Fe-Cr system up to 40% Cr (10). The equilibrium between the liquid and delta (BCC) phases is observed to occur throughout the entire composition region investigated. A minimum in the liquidus with respect to temperature is observed at 1516°C and is estimated to occur in the vicinity of 21% Cr. The liquidus is in good agreement with that of earlier investigators; however, the maximum width of the liquidus-solidus gap is reported to be 4°C at 10% Cr,

which is smaller than reported by Hansen (1,2).

Fe-Mn

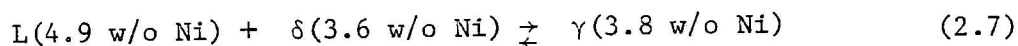
The same investigators have redetermined the liquidus and solidus of the entire composition range (10). They reported the iron-rich peritectic reaction to occur at 1477°C:



Loss of manganese from the liquid phase due to vaporization during experimentation and the use of impure materials are likely to account for the inconsistent information in the literature on this system. However H. and H.-R. reported negligible loss of manganese and they used materials of substantially lower impurity content.

Fe-Ni

H and H.-R. also investigated the liquidus and solidus in the iron-rich Fe-Ni system up to 15% Ni (10). The peritectic reaction was observed to occur at 1516°C:



As with the Fe-Mn system, there is disagreement on the temperature and compositions of the peritectic reaction determined by earlier investigators. Equation (2.7) is considered to be the most reliable.

2.1.3. Ternary Systems

Fe-Cr-C

The general features of the liquidus up to 10% C were established by the work of Austin in 1923, Griffing in 1962 and Jackson in 1970 (11, 12, 21). Figure (2.1) is a schematic representation of the single-phase fields of the solution phases L, δ and γ , and corresponding surfaces of saturation with respect to the carbides and with respect to each other (13). The isotherms at intervals of 5°C of the δ -liquidus (surface of liquid phase saturated with respect to the delta phase, (A-B-C-H) in the composition region bounded by 0 to 1% C and 0 to 20% Cr (bal. Fe) was determined recently by DTA by Chochol (13). He also investigated by DTA the γ -liquidus (E-H, extending to K), δ -solvus (A-D-F-E) and the peritectic surface $L+\delta \rightleftharpoons L+\delta+\gamma$ (F-E-C-H). Tie-lines between the liquid and delta phase also were determined from liquid-solid equilibrium couples. It is seen from Figure 2.1 that the delta and gamma single-phase fields exhibit at lower temperatures surfaces of saturation (solvi) with respect to the carbides $M_{23}C_6$, M_7C_3 , M_3C_2 and Gr, where M designates the total number of moles of metal atoms (Fe+Cr) in each carbide. The extent of the saturation of the delta phase and the gamma phase with the carbides in the composition field up to 1150°C is due to the efforts of Benz, Elliott and Chipman (14). From this work and the earlier investigations of Austin and Griffing, no intermediate phases (i.e., carbides) in equilibrium with the solution phases are expected to occur above 1275°C, at which temperature the onset of liquid phase in equilibrium with M_7C_3 is expected to occur. Selected results on this system are discussed in Chapter 8.

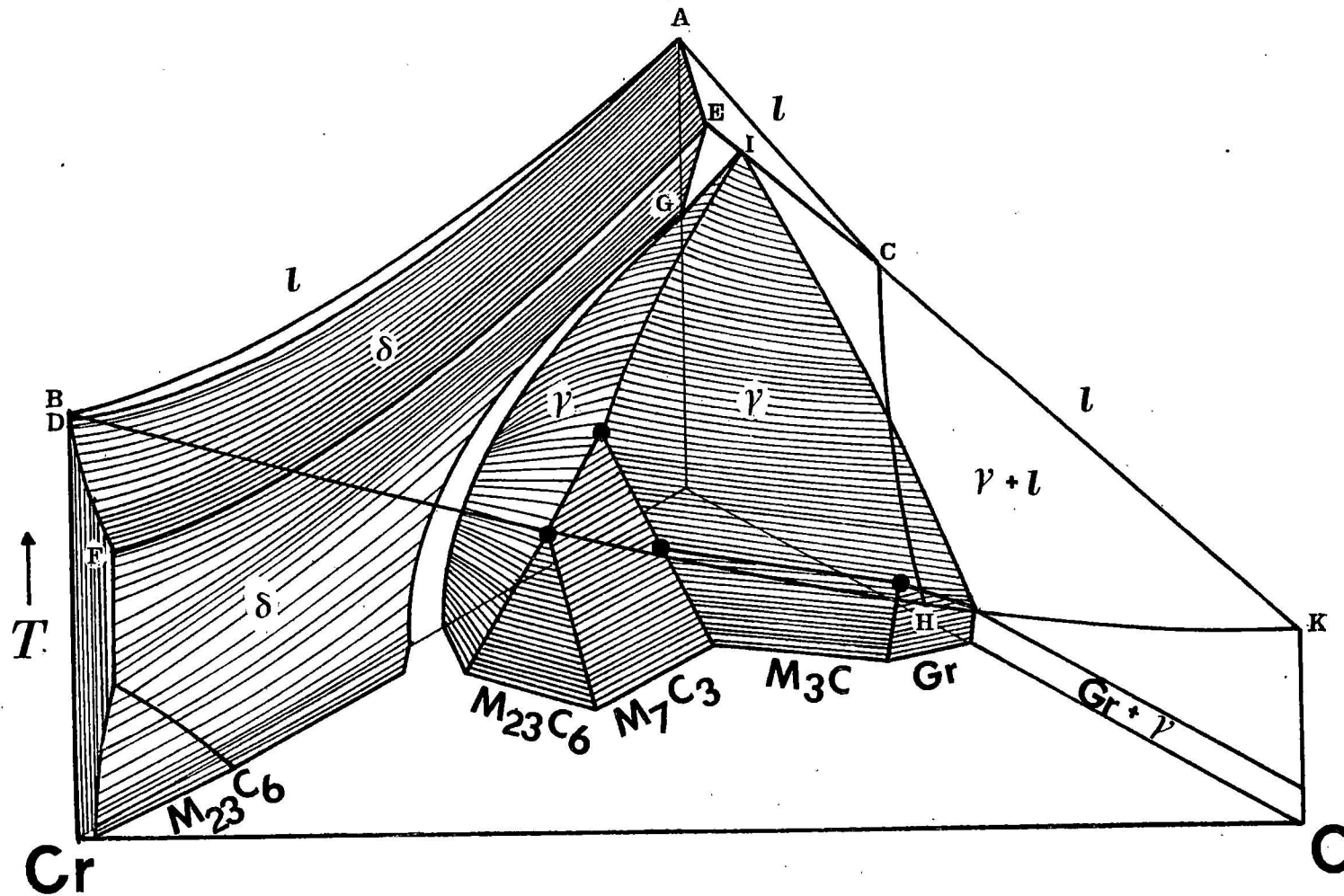


Figure 2.1 - Schematic Representation of the single-phase fields in the iron-rich Fe-Cr-C System (13)

Fe-Ni-C

Buckley and Hume-Rothery determined by DTA the liquidus in the iron-rich Fe-Ni-C system in the composition region bounded by 0 to 1% C and 0 to 40% Ni (bal. Fe) (15). These results substantiate that the peritectic reaction originates in the Fe-Ni system at 1517°C and terminates in the Fe-C system at 1498°C. In addition, they reported no intermediate phases at the temperatures and compositions investigated.

Fe-Mn-C

Isobe has determined the general features of the liquidus and solidus in the Fe-Mn-C system, up to 10% carbon (16). The carbide M_3C was observed to be the only intermediate solid phase in equilibrium with the liquid phase and was found to extend continuously from the Fe-C system as a metastable phase to the Mn-C system as a stable phase. Benz, Elliott and Chipman determined the phase relationship in the temperature range 600 to 1100°C (17).

Fe Cr-Ni

Chochol has determined the liquidus isotherms of the equilibrium with respect to the delta phase and the equilibrium with respect to the gamma phase (13). The contours of the γ -isotherm are in agreement with Jellinghams but not with Jenkins et al. (18, 19).

Fe-Cr-Mn

Burgess and Forger have summarized the investigations done on this system up through 1938 (20). Their observations confirm that Cr additions to Fe-Mn alloys stabilize the delta phase and shift the three-fold equilibrium between the delta, gamma and liquid phase to higher manganese contents. Accordingly, additions of Mn to Fe-Cr alloys were observed to

stabilize the equilibrium between the liquid and gamma phases. In the past thirty years, there has been no reported investigations of this system at solidification temperatures (6).

Fe-Mn-Ni

There has been no investigation reported of the iron-rich Fe-Mn-Ni system at solidification temperatures.

2.1.4. Quaternary Systems

The only quaternary phase diagram in the Fe-Cr-Mn-Ni-C system to be constructed at solidification temperatures is the Fe-Cr-Ni-C system. Chochol recently determined the location of the δ -liquidus and the γ -liquidus by DTA and deduced the location of the surface of two-fold saturation of liquid saturated with respect to the delta and gamma phases (13). These results are discussed in Chapter 8.

2.2. Thermodynamics

The solution phases that are stable in the Fe-Cr-Mn-Ni-C system are amenable to thermodynamic analysis. In particular, there is considerable thermodynamic information reported in the literature on the liquid and gamma but not delta solution phases in the binary and ternary systems at solidification temperatures. This section summarizes the thermodynamics of the solution phases and the corresponding composition and region temperature over which the analysis is valid.

2.2.1. The Pure Components

The difference in the Gibbs energies of different structural forms of the elements Cr, Mn, Ni and C are listed in Table 2.2. It is noted that some of the crystalline forms are not stable at one atm.

Table 2.2. Relative phase stabilities of the pure components
(1000°C < T < 1600°C; 1 atm.)

Element i	Phase		$G_i^{\circ, \phi_2} - G_i^{\circ, \phi_1}$ (cal/mole)	Reference
	ϕ_1	ϕ_2		
Fe	L	δ	$-3300.0 + 1.822xT$	(7)
	δ	γ	$-227.0 + 0.135xT$	(7)
Cr	L	δ	$-4050.0 + 1.900xT$	(21)
	L	δ	$-4350.0 + 2.000xT$	(23)
	δ	γ^*	$4356.0 - 1.716xT$	(22)
	δ	γ^*	$2500.0 + 0.150xT$	(23)
	δ	γ^*	$627.4 - 1.058xT + 0.465x10^{-3}xT^2 - 0.045x10^{-6}xT^3$	(26)
Mn	L	δ	$-3500.0 + 2.300xT$	(54)
	δ	γ	$-430.0 + 0.305xT$	(54)
Ni	L	γ	$4210.0 - 2.436xT$	(25)
	δ^*	γ	$-940.0 - 0.982x10^{-3}xT^2 + 0.116x10^{-5}xT^3 - 0.337x10^{-9}xT^4$	(25)
C	L	Gr	$27300.0 + 6.500xT$	(8)
	L	δ^*	$7800.0 + 3.000xT$	(8)
	δ^*	γ^*	-2000.0	(8)

* unstable phase

Table 2.3. Equilibrium and metastable melting points of
the pure components calculated from Table (2.2)
(1 atm.)

Element	Equilibrium phase	Equilibrium melting point (°C)	Metastable phase	Metastable melting point (°C)	Reference
Fe	δ	1538	γ	1529	(7)
Cr	δ	1859	γ	1390	(22)
	δ	1830	γ	483	(23)
Mn	δ	1249	γ	1234	(21)
					(54)
Ni	γ	1555	δ	1103	(21)
C	Gr	3927	δ	2327	(8)
			γ	1660	(8)

The quantity $G_i^{\phi_2} - G_i^{\phi_1}$ is referred to as the relative phase stability. Table 2.3 gives the equilibrium and the metastable melting points of the pure components calculated from Table 2.2. In addition to Table 2.2 the following differences in reference states are useful (9):

$$C(\text{Gr}) = \underline{C} (-\text{Fe}) \quad (2.8)$$

$$\Delta G^\circ (\text{cal/mole}) = 5400 - 3.98 \times T$$

$$C(\text{Gr}) = \underline{C} (-\text{Fe})$$

$$\Delta G^\circ (\text{cal/mole}) = 10520 - 4.21 \times T \quad (2.9)$$

2.2.2. Multicomponent Alloys

Activity measurements on liquid and on solid-solution alloys in the iron-rich Fe-Cr-Mn-Nr-C system are numerous. Several models have been used to represent analytically the measurements of the thermodynamic behavior of each solution phase. These models range between two extremes: those which are strictly empirical and those which are based on statistical thermodynamics. Models based on the statistical thermodynamics of interstitial solutions are in general different from those of substitutional solutions (short or long range order). As a consequence, solution phases of alloys in which C is dissolved interstitially are described by a different model from that of alloys containing only the substitutional solute elements Cr, Mn and Ni. On the other hand, empirically-based models are generally insensitive to the details of the ordering of atoms in solutions and have been used to describe the thermodynamic interactions of liquid and solid, interstitial and substitutional

solutions.

Each of the solution phases is treated in a separate section. Emphasis is placed on the models reported in the literature and on the composition and temperature region in the Fe-Cr-Mn-Ni-C system in which the model is valid. Models which have been applied successfully on more than one solution phase are discussed firstly to avoid repetition. These include the use of interaction coefficient in a Taylor expansion of the activity coefficient to describe the behavior of multicomponent solutions, the application of the quasi-regular and central atoms models to describe concentrated binary solutions and concentrated ternary solutions containing carbon dissolved as an interstitial element, respectively.

Interaction Coefficients

An approximate analytic expression for the activity coefficient of a solute in a dilute solution phase was first utilized by Wagner and by Chipman and subsequently extended to multicomponent systems by Lupis and Elliott (27,28). The expression which results from a second-order Taylor expansion of the activity coefficient about the infinitely dilute solution reference state (phase ϕ) is

$$\begin{aligned} \ln \Gamma_i &= \ln \Gamma_i^\circ + \sum_{j=2}^N \bar{a}_i^j \xi_j + \sum_{j=2}^N \bar{a}_i^j \xi_j^2 \\ &+ \sum_{j=2}^N \sum_{\substack{k=2 \\ j \leq k}}^N \bar{a}_i^{j,k} \xi_j \xi_k + O(\xi^3) \end{aligned} \quad (2.10)$$

where Γ_i is the activity coefficient of component i in phase ϕ , in the system of N components based on composition coordinate ξ_i , and Γ_i° is

the value at infinite dilutions. The coefficients \dot{a}_i , \ddot{a}_i^j and $\ddot{a}_i^{j,k}$ also depend upon the choice of coordinate system for the solute and solvent species. If the atom fraction coordinate system is employed, Equation (2.10) becomes

$$\begin{aligned} \ln \gamma_i &= \ln \gamma_i^\circ + \sum_{j=2}^N \epsilon_i^j X_j + \sum_{j=2}^N \rho_i^j X_j^2 \\ &+ \sum_{j=2}^N \sum_{k=2}^N \rho_i^{j,k} X_j X_k + O(X^3) \end{aligned} \quad (2.11)$$

where γ_i is the activity coefficient based on atom fraction as the composition coordinate. Investigators have evaluated the coefficients ϵ_i^j , ρ_i^j and $\rho_i^{j,k}$ from measurements of the activity coefficient, and application of Equation (2.11) is valid up to the compositions where the higher-order coefficients are determined to be statistically insignificant. In more concentrated solutions, coefficients of the higher-order and the cross terms may be needed.

Chipman has adopted an atom ratio coordinate system to express the thermodynamic properties of solutions in which one of the components is interstitial (31). The composition coordinate is stated in terms of the atom ratios

$$y_i = \frac{n_i}{N} ; Z_k = \frac{n_k}{N} \quad (2.12)$$

$$\sum_{j=2}^N n_j \quad \sum_{j=2}^N n_j - n_k$$

where i is any component and j and k are the substitutional and interstitial components of the N -component system, respectively. The Taylor

expansion of the activity coefficient of carbon dissolved in iron rich Fe-C-i solutions takes the form

$$\begin{aligned} \log \psi_c &= \log \psi_c^\circ + \theta_c^c y_c + \theta_c^i y_i \\ &+ \pi_c^{c,c} y_c^2 + \pi_c^{c,i} y_c y_i \end{aligned} \quad (2.13)$$

where ψ_c is the activity coefficient of carbon in the solution based on the atom ratio Z_c as the coordinate system; i.e.,

$$\psi_c = a_c / \{y_c / (1 - y_c)\} \quad (2.14)$$

It is noted that Equation (2.13) is suitable to describe the behavior of iron-carbon alloys, since, in general, the activity of a dilute interstitial component is proportional to the ratio of filled to unfilled interstitial sites. It has been used for both liquid and solid solutions of ternary iron-carbon alloys up to moderate concentrations of the substitutional components.

The Quasi-regular Solution Model

Kaufman has estimated parameters in the quasi-regular solution model to account for the variation of the activity coefficient over the entire composition field of the binary systems (25). The excess partial free energies of components i and j in the binary system i-j according to this model are:

$$RT \ln \gamma_i^\phi = X_j^2 \{ \theta_i + (2X_j - 1)(\theta_j - \theta_i) \} \quad (2.15)$$

$$RT \ln \gamma_j^\phi = X_i^2 \{ \theta_i + 2X_j (\theta_j - \theta_i) \} \quad (2.16)$$

θ_i and θ_i are parameters which usually are assumed to have a linear dependence on temperature.

The parameters in Equations (2.11) and (2.12) can be evaluated from activity coefficients where they have been determined experimentally. However, Kaufman's approach is to estimate the parameters based on a theoretical analysis of the relative phase stabilities of all possible competing phases in the alloy system (29). An essential aspect of this approach is that the enthalpy and entropy differences between structural forms of the pure elements should be essentially the same in a given Group in the Periodic Table. The advantage is that a description of the thermodynamic properties of mixing of solution phases is possible over compositions and temperatures in which the phase is metastable or unstable, or has not yet been measured. Kaufman has shown that the general features of the binary phase diagrams of alloys in the Fe-Cr-Mn-Ni-C system when calculated from his parameters are in reasonable agreement with experiment. However, in point of fact, Equation (2.11) employing these parameters does not always predict the binary excess enthalpies and entropies of mixing to within their experimental error over all composition and temperature regions investigated.

The Central Atoms Model

Foo and Lupis have generalized the central atoms model to multi-component interstitial solutions of short and long range ordering (30). The model has been applied to carbon in the liquid and the γ (FCC) phase in iron alloys and describes successfully the activity of carbon at both low and high concentrations to within its experimental error. The

logarithm of the activity coefficient of carbon in a ternary solution Fe-C-i is given by the following expression:

$$\ln \gamma_C = \ln \gamma_C^\circ - \ln(1 + C + r) y_C + 2z' \ln A_{CC} + 2Z' \ln A_{iC} \quad (2.17)$$

The activity coefficient of carbon is based on the atom ratio y_C : i.e., $\gamma_C = a_C / y_C$ (Equation 2.12a). Z' and z' designate respectively the number of substitutional and interstitial nearest neighbors to an interstitial site and r is defined as the ratio of the total number of interstitial sites to the total number of substitutional sites. For liquid and FCC solutions Z' , z' and r are assumed to be 6, 12, and 1, respectively. The parameters A_{CC} and A_{iC} are a function of composition given by the following expressions:

$$A_{CC} = 2 / \{ (1 - y_C + ((1 - y_C)^2 + 4(1 - \lambda_{CC}) y_{CC})^{1/2}) \} \quad (2.18)$$

and

$$A_{iC} = 2(1 + y_i) / \{ (1 + y_i)(1 - y_C) + \lambda_{iC}(y_C - y_i) \} + \{ (1 + y_i)(1 - y_C) + \lambda_{iC}(y_C - y_i) \}^2 + 4(1 - \lambda_{iC}) y_C (1 + y_i)^2 \}^{1/2} \quad (2.19)$$

where y_C and y_i are given by Equation (2.12). These variables are related to the atom fractions in iron-rich ternary solution by the following equations for the case of carbon as the only interstitial element:

$$y_C = \frac{X_C}{1 - X_C} \quad (2.20a)$$

and

$$y_i = \frac{X_i}{1 - X_C} \quad (2.20b)$$

The parameters X_{CC} and X_{iC} are evaluated from measurements of the activity of carbon in the ternary solution. It is noted that the central atoms model has also been extended to dilute interstitial multi-component solutions and can be used to predict interaction coefficients of carbon in dilute solutions (30).

2.2.2.1. Liquid Solutions

Interstitial Solutions

Table 2.4 gives the interaction coefficients corresponding to Equations (2.11) for carbon in iron-rich melts. The activity coefficient of carbon in the melt at infinite dilution relative to pure solid as the standard state is $\log \gamma_C^\circ = -2.01 + 2718/T$. The interaction coefficients were evaluated by different investigators from the activity coefficient of carbon in iron-rich melts of the Fe-Cr-Mn-Ni-C system that was determined experimentally in the temperature range of 1500 to 1570°C.

Table 2.5 also gives the interaction coefficient of carbon in the iron-rich Fe-C and Fe-Cr-C melts. Pure solid graphite is the standard state and $\log \psi_C^\circ = (1180/T) - 0.87$. These coefficients are based on atom ratio corresponding to Equation (2.12). It is noted that the temperature dependence of the effect of chromium on carbon in the melt has been determined.

Table 2.6 gives the value of the parameter λ_{i-C} in Equation (2.19) corresponding to the central-atoms model. The activity coefficient of carbon at infinite dilution relative to pure solid graphite as the

Table 2.4. Interaction coefficients of carbon (atom fraction)
in liquid iron (1500 to 1570°C)

Alloying element i	Interaction Coefficient			Range of X_i a/o	Reference
	$\epsilon_C^{(i)}$	$\epsilon_{C_i}^{(i)}$	$\epsilon_C^{(i,C)}$		
C	$7830/T + 3.66$	$15600/T + 5.32$	-	$0 < X_C < 10$	(35)
Cr	-5.1	-	-	$0 < X_{Cr} < 25$	(35)
	-5.4	1.2	-3		(32)
Mn	-1.89	-	-	$0 < X_{Mn} < 5$	(33)
	-2.73	-	-		(34)
Ni	2.4	-	-	$0 < X_{Ni} < 25$	(32)
	2.7	-	-		(36)

Table 2.5. Interaction coefficients of carbon (atom ratio)
in liquid iron (38)

Alloying Element i	Interaction Coefficient		Range of y_i
	$\theta_C^{(i)}$	$\pi_C^{(C,i)}$	
C	$3860/T$	0	$0 < y_C < 0.1$
Cr	$-9500/T + 3.05$	$12800/T - 4.61$	$0 < y_{Cr} < 0.10$

Table 2.6. Parameter λ_{iC} (Eq. 2.19) in the expression for the activity coefficient of carbon in liquid iron from the central atom model (1550°C) (32, 39)

Alloying element i	λ_{iC}	Range of Y_i
C	0.21	$0 < Y_C < 0.1$
Cr	-0.45	$0 < Y_{Cr} < 0.25$
Mn	-0.20	$0 < Y_{Mn} < 0.05$
Ni	0.20	$0 < Y_{Ni} < 0.25$

standard state is $\lambda_{iC}^{\circ} = 0.37$. The parameters were determined from the experimental activity coefficient of carbon in iron melts at 1550°C.

The carbon solubility in Fe-Cr-Ni-C melts ($0 < y_{Ni} + y_{Cr} < 0.3$) at 1550°C at a constant carbon activity (fixed CO/CO₂ ratios) has been measured by Lupis (32). The experimental results indicate that the parameters λ_{iC} evaluated from ternary melts are adequate to describe the equilibrium carbon concentrations in the quaternary alloys.

To determine from the quasi-regular solution model the effect of alloying elements on the activity of carbon in solution, it is necessary to utilize the parameters of the limiting binary systems of the multi-component system. The parameters of liquid alloys of the ten binary system of the Fe-Cr-Mn-Ni-C system have been estimated by Kaufman and are listed in Table 2.7. The parameters relate to the pure liquid phase (1 atm.) as the standard state of each component, including carbon.

Substitutional Solutions

Table 2.8 gives the interaction coefficients and activity coefficients at infinite dilution relative to the pure liquid phase as the standard state for the substitutional elements in iron-rich melts. The coefficients are based on the atom fraction as the composition coordinate.

It is noted that the parameters in Table 2.7 can be used to calculate the activities of components in the substitutional liquid solutions in the Fe-Cr-Mn-Ni-C system (solutions without carbon).

Kubachewski and Müller have investigated the Fe-Cr system and have determined parameters in a third-order power series model of the excess enthalpy of mixing based on the thermochemical and phase diagram

Table 2.7. Binary parameters in the quasi-regular solution model
for the liquid phase (proposed by Kaufman)

Binary system		Parameters		Source
i	j	θ_j	θ_i	
Fe	Cr	$4970 - 2.500xT$	$4970 - 2500xT$	(25)
Fe	Mn	$-5460 + 4.060xT$	$-4700 + 4.060xT$	(54)
Fe	Ni	$-2000 + 0.650xT$	$-7700 + 2.200xT$	(25)
Fe	C	$-37300 + 11.700xT$	$-21900 + 2.520xT$	(8)
Cr	Mn	$-3000 + 2.500xT$	$-3000 + 2.500xT$	(54)
Cr	Ni	-2000	-2000	(25)
Mn	Ni	$-15395 + 2.600xT$	$-18395 + 2.600xT$	(54)
Cr	C	-33000	-33000	(8)
Mn	C	$-39790 + 11.400xT$	$-23795 - 1.100xT$	(55)
Ni	C	$-23800 + 3.600xT$	$-2660 + 10.300xT$	(8)

Table 2.8. Interaction coefficient and activity coefficient at infinite dilution (atom fraction) of substitutional elements in liquid iron (33, 34)

Alloying element i	Interaction Parameter			$\ln \gamma_i^\circ$
	ϵ_{Cr}^i	ϵ_{Mn}^i	ϵ_{Ni}^i	
Cr	0.004	0.90	0.004	0
Mn	0.90	0	-1.79	491/T
Ni	0.004	-1.79	0.166	-2516/T + 0.91

measurements of several investigators (41). This expression is:

$$\Delta H_M^{E,L} = X_{Cr} X_{Fe} \{4973 + 19 (X_{Cr} - X_{Fe}) + 119(X_{Cr} - X_{Fe})^2 - 93(X_{Cr} - X_{Fe})^3\} \quad (2.20)$$

where the standard states are pure liquid chromium and iron.

Rao and Tiller have deduced parameters in the quasi-regular model of the excess Gibbs energies of mixing for the Fe-Cr, Fe-Mn and Fe-Ni melts (42, 43). The parameters were determined from a simultaneous analysis of thermochemical and phase diagram measurements, with the use of a linear programming technique. The standard states correspond to pure liquid manganese, chromium, nickel and iron. These parameters are listed in Table 2.9.

Activities of the components for Fe-Cr-Ni alloys at 1600°C were measured by Gilby and St. Pierre in 1968 and Belton and Fruehan in 1969. Empirical expressions of the activity coefficients of iron, chromium and nickel were determined by the investigators from their results:

$$(X_{Fe} > 0.6)$$

$$\ln a_{Fe} = -0.08 X_{Ni}^2 \quad (2.21a)$$

$$\ln a_{Cr} = 0.09 - 0.08 X_{Ni}^2 \quad (2.21b)$$

$$\ln a_{Ni} = -0.26 - 0.08 (1 - X_{Ni})^2 \quad (2.21c)$$

Rao and Tiller have extended the α -formalism of Darken to ternary and quaternary alloy solutions and have found that the activities of chromium, nickel and iron calculated from their model based on binary data are in good agreement with the experimental data on the ternary system reported in the literature (46).

Table 2.9. Binary parameters in the quasi-regular solution model for the liquid phase (Rao-Tiller)

Binary System		Parameter	
i	j	θ_j	θ_i
Fe	Cr	$5090 - 2.530xT$	$521 - 0.732xT$
Fe	Mn	$-7555 + 5.65xT$	$-5610 + 4.01xT$
Fe	Ni	$-5960 + 1.095xT$	$-3065 + 0.528xT$

2.2.2.2. Solid Solutions

Austenitic Solutions.

Table 2.10 lists the interaction coefficients of carbon in alloyed austenite (1 atm.). The coefficients refer to pure solid graphite as the standard state and to the atom ratio (Equation 2.14) as the composition coordinate. The value of the activity coefficient at infinite dilution relative to pure graphite as the standard state is $\log \psi_C^\circ = (2300/T) - 0.92$.

Table 2.11 gives the parameter λ_{iC} (Equation 2.19) as a function of temperature for each alloying element. The activity coefficient of carbon at infinite dilution related to solid graphite as the standard state is $\ln \gamma_C^\circ = -2.1 + 5300/T$.

Two models of the thermodynamic behavior of ternary austenitic solutions have been developed, by Zupp and Stevenson and by Bodsworth et al. (48, 52). As with the central-atoms model, these models are based on analysis of the interactions between carbon and the host atoms. The Zupp-Stevenson model is discussed here. The expression for the activity coefficient of carbon in solution according to Z-S model is

$$\ln \gamma_C = \ln \gamma_C^\circ + \ln \left\{ y_C / (1 - H \times \exp(K_i y_i) y_C) \right\} + K_Z y_i \quad (2.21)$$

where i refers to the substitutional alloying element, γ_C° is the activity coefficient of carbon at infinite dilution relative to pure solid graphite as the reference state and H and K_i are parameters determined from Fe-C and Fe-C- i alloys respectively. y_C and y_i refer to the atom ratios

Table 2.10. Interaction coefficients of carbon (atom ratio)
in austenite (40, 37)

Alloying Element i	Interaction Coefficient θ_{C}^i	Range of Y_i
C	$3860/T$	$0 < Y_C < 0.1$
Cr	$-9500/T - 3.05$	$0 < Y_{Cr} < 0.1$
Mn	$-2200/T$	$0 < Y_{Mn} < 0.6$
Ni	$2000/T + 0.30$	$0 < Y_{Ni} < 0.25$

Table 2.11. Parameter λ_{iC} in the expression for the activity coefficient of carbon in austenite developed from the central atom model (32, 39)

Alloying Element i	λ_{iC}	Range of Y_i
C	$1 - \text{Exp}[-0.10 - 290/T]$	$0 < Y_C < 1.0$
Cr	-1.0	$0 < Y_{Cr} < 0.30$
Mn	$0.155 - 650/T$	$0 < Y_{Mn} < 0.30$
Ni	0.34	$0 < Y_{Ni} < 0.30$

defined by Equation (2.12). Z-S give the value of H as 4.9 and $\log \gamma_C^\circ$ as $(2191/T) - 0.754$. Table 2.12 gives the parameter K_i and the temperature and composition range in which the model was applied.**

The model accounts successfully for phenomenological expression developed to represent the influence of substitutional solutes on the carbon solubility in alloyed austenite. This expression is

$$y_C^* = y_C \exp(k_i y_i) \quad (2.22)$$

where y_C^* refers to the atom ratio for the Fe-C binary system, i.e.

$$y_C^* = n_C / n_{Fe}$$

Greenbank has measured the activities of C in alloys of austenite in the Fe-Ni-C and Fe-Cr-C systems (49). His analysis indicates that the ternary data correlated to an equation analogous to Equation (2.13) is adequate to predict the observed carbon solutions at equilibrium in Fe-Cr-Ni-C alloys at constant activity of carbon. The composition triangle and temperatures in which these observations were made are

$$0 < y_{Cr} + y_{Ni} < 0.40 \quad 900^\circ\text{C} < T < 1050^\circ\text{C}$$

$$0 < y_C < 0.12$$

Table 2.13 lists parameters proposed by Kaufman, which refer to the quasi-regular solution model of the FCC phase of alloys of the Fe-Cr-Mn-Ni-C system. The parameters refer to the pure components having the FCC structure, which is not stable for Cr and C at one atm. (see Table 2.2).

**

$$0 < y_C < 0.06$$

Table 2.12. The parameters in the Zupp-Stevenson model of the activity coefficient of carbon in alloyed austenite (Eqn. 2.21)

Alloying element i	Parameter $K_i/2.3$	Temperature $^{\circ}\text{C}$	Range of Y_i
Cr	-3.8	1000	$0 < Y_{\text{Cr}} < 0.06$
Mn	-1.39	1000	$0 < Y_{\text{Mn}} < 0.15$
Ni	1.98	930	$0 < Y_{\text{Ni}} < 0.25$
	1.54	1000	$0 < Y_{\text{Ni}} < 0.25$
	1.26	1200	$0 < Y_{\text{Ni}} < 0.25$

Table 2.13. Binary parameters in the quasi-regular solution mode for the gamma (FCC) phase (proposed by Kaufman)

Binary System		Parameters		Source
i	j	θ_j	θ_i	
Fe	Cr	$1700 - 1.500xT$	$1700 - 1.500xT$	(25)
Fe	Mn	$-4509 + 4.059xT$	$-4509 + 4.059xT$	(54)
Fe	Ni	$-8320 + 0.583x10^{-2}xT^2$ $-0.249 x 10^{-5}xT^3$	$500 - 0.916x10^{-3}T^2$ $+0.390 x 10^{-6}xT^3$	*25)
Fe	C	$-37100 + 1.390xT$	$-22600 - 0.700xT$	(8)
Cr	Mn	$-4200 + 2.500xT$	$-4200 + 2.500xT$	(54)
Cr	Ni	$-2000 + 0.112x10^{-2}xT^2$ $-0.186x10^{-5}xT^3$	$-6000 + 0.227x10^{-2}xT^2$ $-0.623x10^{-6}xT^3$	(25)
Mn	Ni	$-12400 + 2.600xT$	$-15395 + 2.600xT$	(54)
Cr	C	-	-	-
Mn	C	$-68885 + 11.397xT$	$-33790 - 0.971xT$	(55)
Ni	C	$-26000 + 16.180xT$	$-19000 + 1.030xT$	(8)

Interstitial BCC Solutions

Table 2.14 lists parameters proposed by Kaufman which refer to the quasi-regular solution model of the BCC phase of alloys of the Fe-Cr-Mn-Ni-C system. The parameters refer to the pure components having the BCC structure, which is not stable for Cr and C at one atm. (see Table 2.2). No data on the activity of carbon in BCC alloys at solidification temperatures have been reported in the literature; and, as a consequence, the parameters estimated by Kaufman for this phase are useful to estimate activities in this phase.

BCC and FCC Substitutional Solutions

Investigators have evaluated parameters in the quasi-regular solution model, Equations (2.15, 2.16), from thermochemical measurements on BCC Fe-Cr, Fe-Mn and Fe-Ni solutions ($T > 1000^\circ\text{C}$). The standard states refer to pure BCC manganese, chromium and iron for BCC alloys in the Fe-Cr and Fe-Mn systems, pure FCC iron and nickel for FCC alloys in the Fe-Ni system, and pure FCC iron and FCC Cr (hypothetical) for the FCC alloys in the Fe-Cr system (1 atm.). These parameters are given in Table 2.15.

It is noted that parameters in Table 2.13 and 2.14 can also be used to calculate activities of the components in BCC and FCC alloys of the Fe-Cr-Mn-Ni system.

The activity of chromium referred to pure solid chromium (BCC) (1 atm.) as the standard state was measured between 900 and 1200°C in the BCC and FCC alloys of the Ni-Cr, Fe-Cr and Fe-Ni-Cr systems (52). However, the results has not been expressed as an analytical function of composition and temperature. The results show that Ni increases the activity

Table 2.14. Binary parameters in the quasi-regular solution model for the delta (BCC) phase (proposed by Kaufman)

Binary System		Parameters		Source
		θ_{ij}	θ_{ji}	
Fe	Cr	$5900 - 2.500xT$	$5900 - 2.500xT$	(25)
Fe	Mn	$1240 + 0.360xT$	$980 + 1.120xT$	(54)
Fe	Ni	$-3915 + 8.46x10^{-3}xT^2$ $-3.15x10^{-6}xT^3$	$320 + 3.17x10^{-4}x10^2$ $-3.790x10^{-7}xT^3$	(25)
Fe	C	$-22900 - 6.950xT$	$-8400 - 9.040xT$	(8)
Cr	Mn	$-2100 + 2.500xT$	$-2100 + 2.500xT$	(54)
Cr	Ni	$12800 - 6.500xT$	$-3200 - 0.50xT$	(25)
Mn	Ni	$-10895 + 0.870xT$	$-13895 + 0.870xT$	(54)
Cr	C	-32000	-32000	(8)
Mn	C	$-64285 + 11.400xT$	$-28295 - 1.100xT$	(55)
Ni	C	-	-	(8)

Table 2.15. Parameters in the quasi-regular solution model for substitutional solid solutions ($T > 1000^\circ\text{C}$)

Binary System i	System j	Alloy phase	Parameters		Source
			θ_j	θ_i	
Fe	Cr	BCC	$5950 - 2.15xT$	$5940 - 3.235xT$	(43)
		BCC	$6000.0 - 2.8xT$	$6000.0 - 28xT$	(41)
		FCC	0	0	(22)
Fe	Mn	BCC	$-5340 + 4.42xT$	$-3270 + 2.86xT$	(42)
		FCC	$-15000 + 7.3xT^*$	$-15000.0 + 7.3xT^*$	(50)
Fe	Ni	FCC	$-5255 + 0.875xT$	$-1920 + 0.208xT$	(43)

* based on atom-ratio as the coordinate system.

of Cr in the FCC ternary solutions and that this effect is greater at both higher Cr concentrations and lower-temperatures.

Smith has measured the activity of manganese referred to pure solid FCC manganese (1 atm.) as the standard state in Fe-Mn, Mn-Ni and Fe-Mn-Ni FCC and BCC solutions at 960°C. The data have not been expressed as an analytical function of composition but they indicate that the ternary solution exhibits non-regular solution behavior.

Table 2.16 summarizes qualitatively, the partial molar properties determined by experiment at solidification temperature in the iron-rich binary systems of the Fe-Cr-Mn-Ni-C system.

Table 2.16. Summary of the thermodynamic behavior of the iron-base binary alloys ($T > 1000^\circ\text{C}$)

System	Solute	Liquid solutions		Solution	Solid solutions	
		Standard state	Deviation from ideality		Standard state	Deviation from ideality
Fe-C	C	Gr	Large positive	γ (FCC)	Gr	Large positive
Fe-Cr	Cr	Liquid Cr	Small negative	δ (BCC)	BCC Cr	Large positive
				γ (FCC)	FCC Cr	Ideal
Fe-Mn	Mn	Liquid Mn	Large positive	γ (FCC)	FCC Mn	Positive
Fe-Ni	Ni	Liquid Ni	Negative	γ (FCC)	FCC Ni	Large negative

CHAPTER 3OUTLINE OF RESEARCH

The liquidus and solidus of each of the limiting binary systems in the Fe-Cr-Mn-Ni-C system have been well established by the work of recent investigators. This is not the case for the ternary and higher order systems. The investigations have been concerned with determining the location of the liquidus, and there is little reported on the compositions of the tie-lines of the equilibrium between the liquid and primary solution phases. Nonetheless, these results have established the general features of the liquidus of the equilibrium with each solid solution phase which is stable in the limiting binary systems as well as the liquidus of the equilibrium with each intermediate phase (i.e., carbide). For example, Cr and Mn but not Ni have been observed to form carbides in the ternary system Fe-X-C. Accordingly, addition of Ni to Fe-Cr-C or to Fe-Mn-C would be expected to decrease the tendency to form carbides in the quaternary systems and shift the field of stability of each carbide to lower temperatures and higher concentrations of Cr and of Mn. The purpose of this research was to develop more precise knowledge of the phase-relationships in the higher-order systems at solidification temperatures. The composition fields investigated were the iron-rich binary systems, ternary systems and selected quaternary systems of the composition pentahedroid bounded by 0 to 1 w/o C, 0 to 10 w/o Mn, 0 to 25 w/o Cr and 0 to 25 w/o Ni (bal. Fe). The phase relationships investigated in the composition field were the tie-lines between the liquid and δ (BCC) phases and between the liquid and γ (FCC) phases, the δ -liquidus and the γ -liquidus and the two fold equilibrium

$L+\delta \rightleftharpoons L+\delta+\gamma$.

The approach to establish the phase relationships was primarily experimental. That is, experiments were conducted to measure the composition of solid phase in equilibrium with the liquid phase of a selected composition and to measure the temperature of the liquidus as a function of composition. The composition of the latter measurement which corresponds to the composition of the conjugate liquid phase established the temperature of the tie-line.

In contrast to the experimental approach is calculation of the phase relationships from knowledge of the Gibbs energies of the coexisting phases and the relative phase stabilities of the pure components. The latter approach was not practical as the only means to establish the phase relationships; the Gibbs energies of δ (BCC) and γ (FCC) phases have not been measured in the multicomponent system at the compositions and temperatures of the equilibrium with the liquid phase.

The thermochemical information which has been reported in the literature was employed as parameters in a model which, in turn, was used to predict the phase relationships determined by experiment. The parameters which refer to the thermodynamic behavior of the components in each of the stable phases in the higher-order systems were determined by application of mathematical methods to the phase relationships determined by experiment. Prediction of the experimental results within the experimental error by the model was possible. This reduced the number of experiments needed to complete the investigation in the composition field. Moreover, the model enabled the enormous amount of information of the phase relationships in the higher-order systems to be accommodated and handled more easily in subsequent analyses.

3.1. Experimental Methods

The compositions of the equilibrium between two phases can be determined by chemical analyses of the quenched liquid and pre-solid phases of the alloys which have been equilibrated at a constant temperature in the composition-temperature field in which the equilibrium is stable. So that the compositions can be determined accurately by chemical analysis, a separation of the liquid and solid phases prior to quenching is desirable and can be achieved in a number of ways.

A diffusion couple can be made by holding a pre-formed pellet of solid phase in contact, at a constant temperature, with a melt having initially a composition near that of saturation with respect to the solid phase (51). The compositions of the equilibrium are established when the diffusion gradients in the couple are depleted. However in δ and γ iron the solute elements Cr, Mn and Ni have diffusivities on the order of 10^{-7} to 10^{-8} cm^2/sec at solidification temperatures and, as a consequence, equilibrium would not be reached in a reasonably short period of time.

A relatively recent method is the application of an electromagnetic force field to effect agglomeration of particles of solid phase in equilibrium with an alloy melt at a constant temperature (26). Although wetting of the bulk solid phase can lead to spurious measurements of the composition of the solidus, the method is superior to other methods for the determination of tie-lines of refractor systems at very high temperatures. Another method, similar to the electromagnetic method, is the separation of solid phase and liquid phase by applying hydrostatic pres-

DISCLAIMER NOTICE

MISSING PAGE(S)

p. 55

sure to a slurry of the liquid phase and sheared dendrites (56). The process conditions can be controlled to insure complete equilibrium between the dendrites and the liquid phase. However, application of the technique at steel-making temperatures would be limited by materials problems.

These methods can be classified as isothermal methods. A non-isothermal, but relatively simple method would be to solidify a solid phase from the alloy melt. Under conditions of a high ratio of thermal gradient to solidification rate, the solidification front is planar. For multicomponent systems the criterion is (71)*

$$\frac{G_L}{R} \gtrsim \sum_{i=1}^{N-1} \frac{m_i X_i^0 (1-K_i)}{K_i D_i^L} \quad (3.1)$$

where G_L is the thermal gradient perpendicular to the solidification front moving at rate R , m_i is the slope of the liquidus with respect to solute element i , X_i^0 is the mole fraction of solute element i in the alloy and K_i and D_i^L are the partition coefficient and diffusivity of i in the liquid-solid equilibrium and in the liquid phase, respectively.

At solidification rates on the order of 1 cm/hr, equilibrium can be assumed at the liquid solid interface (58). Because the experimental conditions and parameters (thermal gradient, solidification rate, etc.) can be controlled relatively easily to grow equilibrium couples of alloys in the Fe-Cr-Mn-Ni-C system, this method was employed in the present study.

Errors in the measurement of temperature at solidification front were unavoidable since a relatively high thermal gradient (approximately 50°/cm) across the solidification front was required. However, the

* assumes that the cross-diffusivities in the multicomponent system are negligible.

composition of the liquid phase of the equilibrium couple also corresponds to a point on the composition coordinate of the liquidus. The temperature coordinate of the liquidus at this composition can be determined by differential thermal analysis. This technique and the method to obtain equilibrium couples were employed to measure the temperature and compositions of the equilibrium between the liquid and the solution phases in the Fe-Cr-Mn-Ni-C system and are discussed in detail in Chapter 5.

3.2. Modelling

Thermodynamic modelling of the phase relationships involve directly the equations stating the conditions of equilibrium of the alloy system. These conditions can be expressed mathematically in two different classes of equations. One class is a function of the amounts and compositions of each phase in the equilibrium system at a constant temperature and pressure, while the other class is a function only of the compositions of each phase. Nonetheless, resolution of both classes of equations yields identical solution matrices.

Each class of equations is solvable by application of several numerical techniques. The efficiency of the numerical techniques to solve each class of equations and the method of calculation chosen for the present analysis is discussed in Chapter 4.

The application of the equations of equilibrium and method of solution to determine the thermodynamic parameters from the experimental results are discussed fully in Chapter 6.

CHAPTER 4METHOD OF CALCULATION AND PORTRAYAL OF THE PHASE EQUILIBRIA IN THE IRON-RICH Fe-Cr-Mn-Ni-C SYSTEM

The equilibrium compositions of coexisting phases in a multicomponent system at constant temperature and pressure can be calculated by resolving the equations stating the conditions of chemical equilibrium of the system. However, these conditions are expressible mathematically as two different classes of equations. The method of equal chemical potentials is based directly on the classical concept of equality of chemical potential of each component in each of the coexisting phases at a constant temperature. The method of minimization of the Gibbs energy is based on the fact that the conditions of equilibrium also correspond to the minimum of the Gibbs energies of the coexisting phases at a fixed total composition and temperature of the system. Null has shown for a multicomponent system that the condition of minimum Gibbs energy satisfies mathematically the criterion of equality of chemical potential (58).

Lupis, Ansara, Counsel and Chochol have applied different numerical techniques to determine the minimum in the Gibbs energy of the equilibrium between two phases in a multi-component system (59, 60, 61, 13). Kaufman and Pike have applied the same numerical technique to solve the system of equations of equal chemical potentials to calculate the equilibrium between two phases and the equilibrium between three phases in ternary systems, respectively (29,62). It is found in the present analysis that the efficiency of the calculations depends considerably on the numerical technique employed, and in some cases, the method of equal chemical potentials is superior to the method of the minimization

of the Gibbs energy, regardless of the numerical technique employed.

This chapter begins with the development of the two methods to calculate phase equilibria. Numerical techniques for the resolution of each class of equations are compared and the technique employed in the present study is discussed in detail. Geometric constructions representing spatially the solution matrix of the equations are reviewed and, finally, the method to portray the equilibrium between two phases and the equilibrium between three phases in the iron-rich Fe-Cr-Mn-Ni-C system is discussed.

4.1. Methods of Calculation

A general review of the development of the equations for the calculation of equilibrium compositions of coexisting phases is given by Ansara (60). These equations are now developed in more detail and numerical techniques appropriate to the method of calculation of the equilibrium compositions of coexisting solution phases are presented.

4.1.1. Method of Minimization of the Gibbs Energy

The equilibrium state of a chemical system at a specified temperature, pressure and total composition is defined completely when its molar Gibbs energy is a minimum with respect to the independent thermodynamic variables. This quantity is equal to

$$G_{T,P}^S = \sum_{\phi=1}^R n^{\phi} G^{\phi} \quad (4.1)$$

where n^{ϕ} is the fraction of phase ϕ in the system of R Stable phases and G^{ϕ} is the molar Gibbs energy of phase ϕ , which, in turn, is expressed as the molar Gibbs energy of mixing of the components in phase ϕ , referred

to the same standard state:

$$G^\phi = \sum_{i=1}^N \{ \Delta G_M^\phi(X_i) - X_i \Delta G_i^{\circ, \phi \rightarrow R} \} \quad (4.2)$$

X_i is the mole fraction of component i in phase ϕ ($\phi=1,R$) and ΔG_M^ϕ is the molar Gibbs energy of mixing of phase ϕ and $\Delta G_i^{\circ, \phi \rightarrow R}$ is the difference in the molar Gibbs energies of the pure component i in phases ϕ and R (constant T and P).

The number of variables in Equation (4.1) is $R(1+N)$. A mass balance on the system provides $(N+R)$ additional relationships:

$$\sum_{\phi=1}^R m_i^\phi = M_i \quad (4.3)$$

$$\sum_{i=1}^N m_i^\phi = m^\phi \quad (4.4)$$

$$\sum_{i=1}^N M_i = M \quad (4.5)$$

where M_i is the specified total mass of component i of the chemical system of mass M , m^ϕ is the total mass of phase ϕ and m_i is the mass of component i in phase ϕ . Equations (4.3) to (4.5) are rearranged to yield mass balance relationships among the intensive thermodynamic variables n^ϕ , X_i^ϕ ($i=1,N$; $\phi=1,R$):

$$\sum_{i=1}^N X_i^\phi = 1 \quad (4.6)$$

$$\sum_{\phi=1}^R n^\phi = 1 \quad (4.7)$$

$$\sum_{\phi=1}^R n^{\phi} X_i^{\phi} = X_i^{\circ} \quad (i = 1, N) \quad (4.8)$$

where

$$X_i = \frac{m_i^{\phi}}{m^{\phi}} \quad (4.9)$$

$$n^{\phi} = \frac{m^{\phi}}{M} \quad (4.10)$$

$$X_i^{\circ} = \frac{M_i}{M} \quad (4.11)$$

Equation (4.1) combined with Equation (4.6) to (4.8) can be rewritten:

$$G_{T,P}^S = \sum_{\phi=1}^{R-1} n^{\phi} (G^{\phi} - G^R) \quad (4.12)$$

subject to:

$$||n^{\phi}|| = ||X_i^{\phi} - X_i^R||^{-1} \cdot ||X_i^{\circ} - X_i^R|| \quad (4.13)$$

$$\begin{aligned} \phi &= 1, R \\ i &= 2, N \end{aligned}$$

The equilibrium compositions of a group of R coexisting phases of specified total composition are calculated at each temperature by minimizing $G_{T,P}^S$ with respect to the $N(R-1)$ independent variables.

4.1.1.1. Numerical Techniques

The minimum in the function $G_{T,P}^S$ with respect to the independent variables corresponds mathematically to

$$\frac{\partial G_{T,P}^S}{\partial \theta_r} = 0 \quad (4.14)$$

$$r = 1, N(R-1)$$

where θ_r is the independent variable.

This is an optimization problem which is solvable by a number of techniques, among them direct search, gradient and quadratic minimization procedures (63). One type of search technique is the simplex tableau method developed by Nelder and Mead (64). No differentiation is required; Equations (4.12) and (4.13) are evaluated at a selected number of points (about 10) which indicate the direction of steepest descent. Lupis and Chochol have each applied a similar procedure in which the minimization begins at a pre-selected "approximate" solution. The function $G_{T,P}^S$ is tested iteratively at small deviations of the approximate solution for an improved solution (13, 59).

To avoid a time-consuming search and to guarantee convergence, it is imperative that the minimization procedure be initiated in the vicinity of the global minimum. Chochol and Lupis have each developed a stepwise procedure to calculate the continuum of compositions of the equilibrium between the alpha and beta phase in multicomponent systems; i.e., the α - β tie-lines (see Figure 4.1). The procedure takes advantage of the solution at a minimum found previously in the function $G_{T,P}^S$. Chochol has calculated the sequence of tie-line in a quaternary system in this manner. After a tie-line is calculated, the total composition vector $P(x_i^o)$ is incremented by an amount ΔP . To provide a starting point at each minimization, an approximate tie-line is determined by extrapolation from the two tie-lines calculated previously through point $P+\Delta P$, beginning at a limiting binary system. Lupis has developed a different stepwise procedure in which the approximate tie-lines are calculated much more precisely. The difference in the Gibbs energy between two

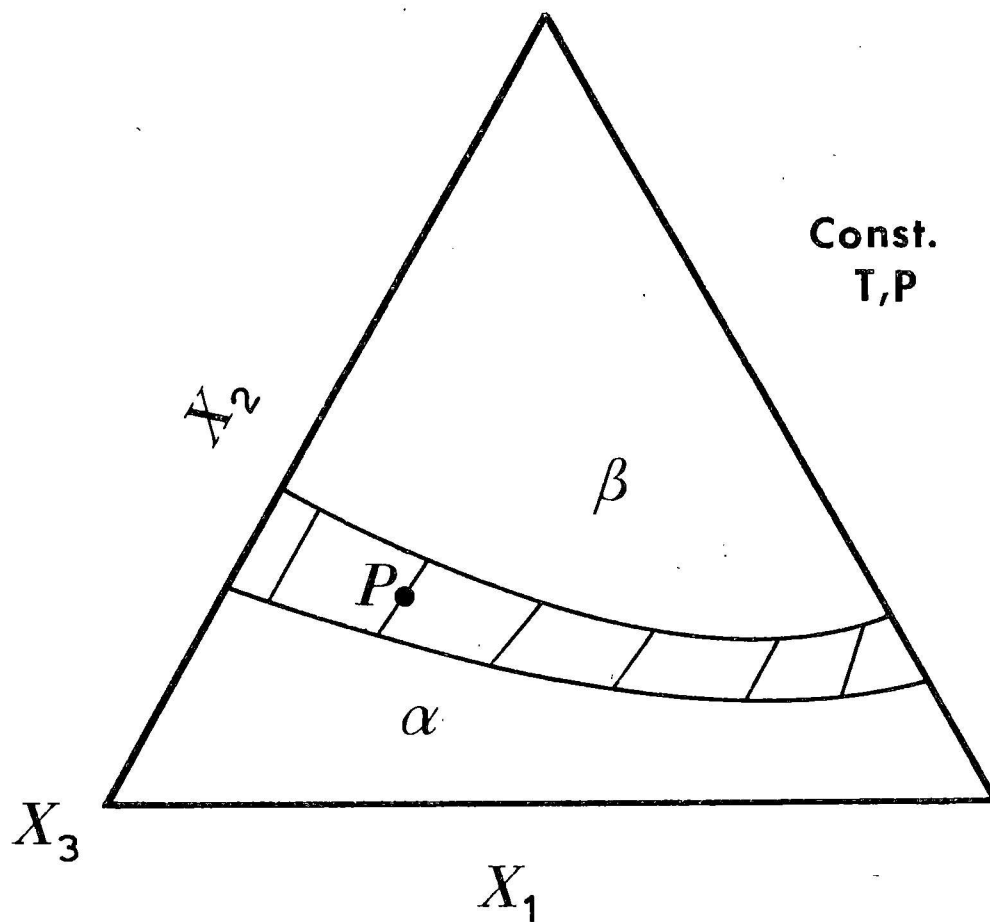


Figure 4.1 - Schematic representation of the tie-lines of the equilibrium between two phases in the Fe- X_1 - X_2 system

equilibrium states at P' and P'' ($P''=P'+dP$) is approximated by a second-order Taylor series expansion in terms of the N independent variables dn^α , dX_i^α , dX_i^β ($i=2,N$) (See Figure 4.2). Accordingly, coordinates of the tie-line through point P'' are calculated by summing the solution vector calculated at point P' and the solution vector of the system of equations

$$\frac{\partial \Delta G_{T,P}^S}{\partial d\theta_r} = 0 \quad (4.15)$$

where $\Delta G_{R,P}^S$ is the difference in the Gibbs energy of the two equilibrium states $G_{T,P}^{S''}$ and $G_{T,P}^{S'}$ and $d\theta_r$ is the independent variable. A distinct advantage of this method is that, for "small" increments dP , the coordinates of the tie-line calculated at $P'+dP$ is within the range of applicability of the Taylor expansion and can be taken as the true equilibrium tie-line.

4.1.2. Method of Equal Chemical Potentials

A second method to calculate equilibrium compositions of coexisting phases at a constant temperature and pressure is to invoke directly the fact that the chemical potential of each component is the same in all of the phases coexisting at equilibrium. These conditions are expressed mathematically as follows:

$$\Delta\mu_i^R = \Delta\mu_i^1 + \Delta\mu_i^{\circ,R-1} = \Delta\mu_i^2 + \Delta\mu_i^{\circ,R-2} = \dots = \Delta\mu_i^\phi + \Delta\mu_i^{\circ,R-\phi} \quad (4.16)$$

$$i = 1, N$$

$$\phi = 1, (R-1)$$

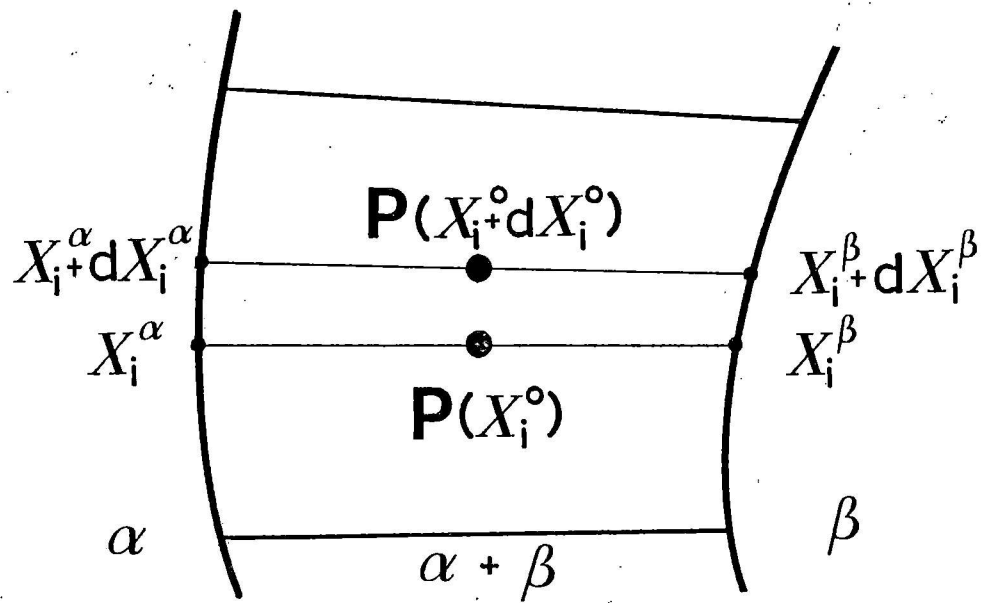


Figure 4.2 - Representation of neighboring equilibrium states of the equilibrium between two phases in the Fe- X_1 - X_2 system

where $\Delta\mu_i^\phi$ is the difference in the chemical potential of component i in solution in phase ϕ and the chemical potential of pure component i in phase ϕ and $\Delta\mu_i^{\circ, \phi \rightarrow R}$ is the difference in the chemical potential of pure component i in phases ϕ and R . (Table 2.2).

The chemical potential is expressed as a function of the molar Gibbs energy of mixing of phase ϕ , ΔG_M^ϕ ($\Delta G_M^\phi(X_1)$), by the following derived in the appendix:*

$$\Delta\mu_i^\phi = \Delta G_M^\phi + \sum_{j=1}^{N-1} (\delta_{ij} - X_j) \frac{\partial \Delta G_M^\phi}{\partial X_j} \quad (4.17)$$

It is noted that Equation (4.8) but not (4.9) or (4.10) provides an additional relationship. Consequently, the system of equations of equal chemical potentials (4.16) is a function of $(R)(N-1)$ independent variables, and themselves, consist of $(N)(R-1)$ independent equations. Thus, the total degrees of freedom at a constant temperature and pressure is:

$$F = (R)(N-1) - (N)(R-1) \quad (4.18)$$

which is a statement of the Gibbs phase rule. The equilibrium compositions of a group of R coexisting phases are calculated by solving simultaneously the system of Equations (4.16) subject to F of any of the independent variables held constant.

*

The chemical potential of each component can also be expressed as the partial molar quantity rather than as a function of the integral molar quantity.

4.1.2.1. Numerical Techniques

The system of Equations (4.16) are transcendental and can be highly non-linear. However a number of numerical techniques for their resolution are available (63). In particular, the Newton-Rhapson method has been used by Kaufman and Pike to calculate compositions of equilibria of two and three phases, respectively (29,62). The Newton-Rhapson technique linearizes the system of equations and calculates the solution vector X by an iterative method: *

$$X^{(K+1)} = X^{(K)} + \Delta X^{(K)} \quad (4.19)$$

where

$$\Delta X^{(K)} = |J^{(K)}|^{-1} E(X^{(K)}) \quad (4.20)$$

$E(X^{(K)})$ represents the vector of function values at point $X^{(K)}$ and $J^{(K)}$ represents the Jacobian evaluated at $X^{(K)}$

$$J = \begin{matrix} \frac{\partial (E(X_i))}{\partial (X_j)} & i = 1, (R(N-1)-F) \\ & j = 1, (R(N-1)-F) \\ & i \neq j \end{matrix} \quad (4.21)$$

The test for convergence to the solution is set by specifying the residual

ϵ :

$$| X^{(K+1)} - X^{(K)} | \leq \epsilon | X^{(K+1)} | \quad (4.22)$$

*

| | refers to absolute value.

4.1.3. Comparison of Methods

Both methods discussed require the same measurable thermodynamic quantities in order to calculate the equilibrium compositions of coexisting phases: the molar Gibbs energy of mixing of each phase (Chapter 6) and the differences between standard states (the relative phase stabilities) of the pure components. However, there are significant differences in the efficiency by which the methods can be applied to yield the calculations. The sensitivity of the methods to perturbations in the independent variables is shown schematically for the case of equilibrium between two phases in a binary system in Figure 4.3. In general, the magnitude of the chemical potential is more sensitive to the curvature of the Gibbs energy function $G_{T,P}^S$ than to the magnitude of the function itself. For small perturbations in the composition of component 2 of the equilibrium between the α and the β phase in the binary system, δX_2^α , there is a relatively small change in the Gibbs energy of the α phase but a relatively large change in the direction of the tangent at $X_2^\alpha + \delta X_2^\alpha$, which corresponds to a large change in the chemical potential of component 2. As a consequence, the method of equal chemical potentials is generally more sensitive to perturbations of the independent composition variables during convergence to the solution than with the method of minimization of the Gibbs energy and will converge to the solution in fewer iterations. An exception to this generality is the case in which the Gibbs energies of the coexisting phases referred to the same standard state, are similar in magnitude and have small first and second derivatives with respect to composition and temperature.

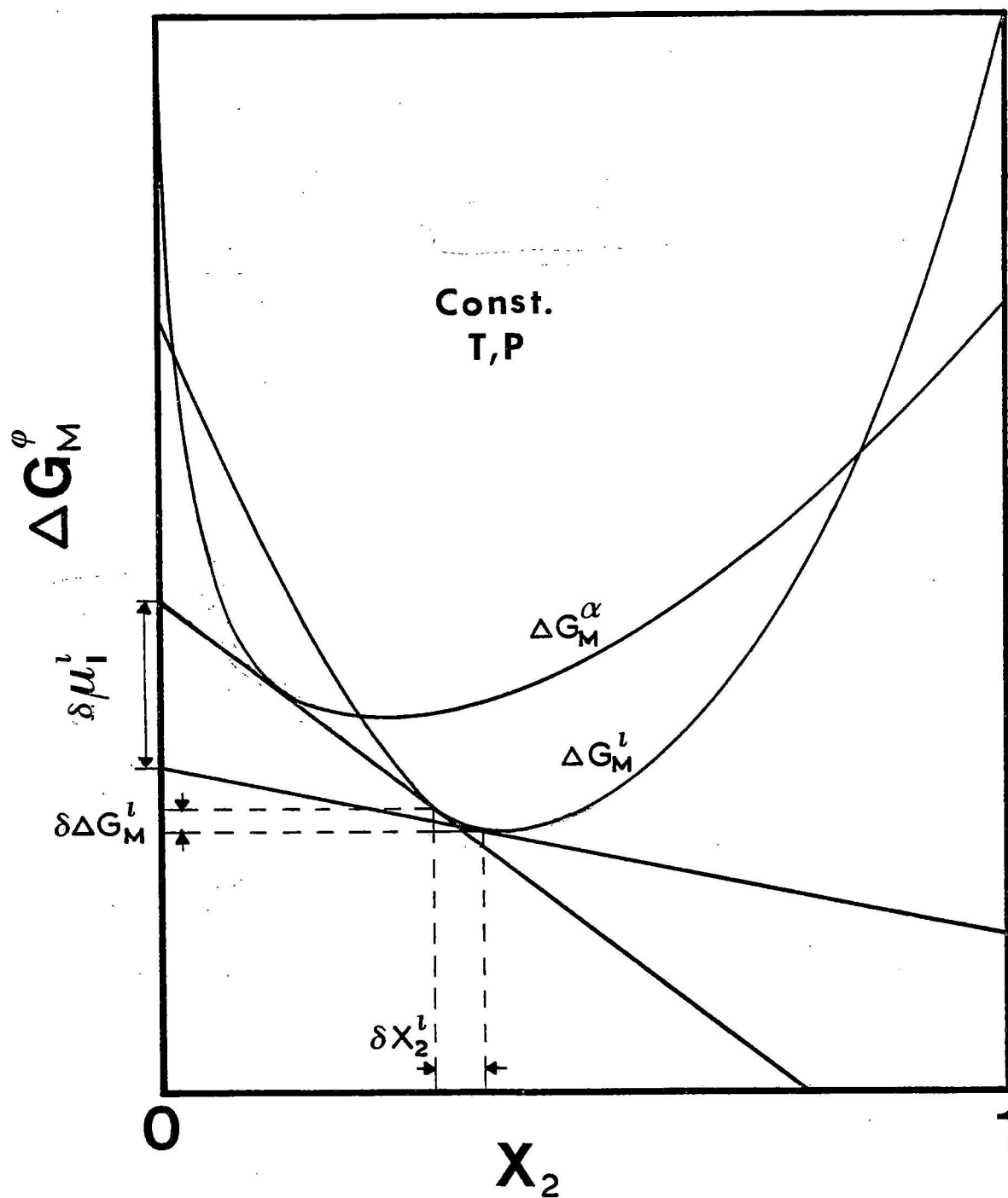


Figure 4.3 - Schematic representation of the chemical potential and the integral molar free energy of a binary system (Const. T, P)

The efficiency of the calculations is important and can become the limiting factor in calculations of the equilibrium in the multi-component system because each additional component adds one dimension to the field of stability of the coexisting phases (see Section 4.2). In the present study, an efficient technique was also necessary because of the large number of calculations needed in the modelling of the phase diagrams (Chapter 6).

In general, as the number of phases is increased, it becomes increasingly difficult to determine an approximate solution (starting point) for the minimization procedure. Extrapolation techniques and the Taylor expansion approximation of the difference in the Gibbs energy between neighboring equilibrium states are unwieldy for the equilibrium of three or more coexisting phases. The method of equality of chemical potentials employing the Newton-Raphson technique offers a simpler approach. The limitation is the large number of derivatives that are needed in Equations (4.21) and in Equation (4.17) when a model of the integral molar properties of mixing is employed (Chapter 6). However, computer languages are now available which are capable of generating automatically the exact derivatives of any function with respect to a given variable (65). Computer programs are also available to solve a large system of non-linear equations in which the Jacobian is approximated numerically. Moreover, it was found in the present study that the solution to Equations (4.16) was possible in the binary, ternary and quaternary systems by taking the Jacobian of a first-order approximation of the function $E(X)$ in Equation (4.21). This corresponds to approximating the function ΔG_m

(Chapter 6) as a simpler algebraic model (e.g. in terms of a binary regular solution model) in Equations (4.17) and (4.21), while retaining the original expression of the vector $E(X)$ for the multi-component system in Equation (4.20).

The sequence of compositions of the equilibrium between two phases in binary and ternary systems calculated by each method were compared: the extrapolation and minimization method of Chochol and application of the Newton-Rhapson technique to solve Equations (4.16) employing the aforementioned approximation of the Jacobian. The minimization method was found always to diverge when one of the compositions of the alpha and the beta phase boundaries approached a minimum, shown schematically in Figure 4.1. This was not the case with the other method. In addition, the number of iterations to convergence to the solution of each tie-line of the L-equilibrium in the Fe-Mn-C and Fe-Cr-C ternary systems was of the order of one hundred times larger for the former than for the latter method.

The method of equal chemical potentials employing the Newton-Rhapson technique was applied in the present study. Schematic diagrams indicating the relationship between the degree of freedom of Equations (4.16) and the dimensions of the composition fields of the equilibrium between two and between three phases in the Fe-Cr-Mn-Ni-C system are presented in the next sections.

4.2. Spatial Representation

The alloy phase diagram is essentially a map which locates, in composition-temperature space, the equilibrium fields of stability of the single and the coexisting phases, and which portrays the composition

relationship among coexisting phases as a function of temperature. Portrayal of the phase equilibria employ three types of geometric constructions:

1. Constructions representing the domain of the composition variable (concentration simplexes);
2. Constructions representing the composition relationship among coexisting phases (hyperconodes);
3. Constructions delineating fields of stability (continua).

Each of these types of constructions and their application to the portrayal of the phase equilibria of the Fe-Cr-Mn-Ni-C system are discussed briefly in the following sections.

4.2.1. The Concentration Simplex

Composition is represented in Euclidian space as an N-dimensional vector $P(X_i^o)$. However, only those vectors which satisfy two conditions can actually represent the composition of an N-component system:

$$\sum_{i=1}^N X_i^o = 1 \quad (4.23)$$

$$0 \leq X_i^o \leq 1 \quad i = 1, N \quad (4.24)$$

These conditions indicate that the sum of the mole fraction of each component in the alloy system must be unity and that the mole fraction cannot exceed unity nor be less than zero. To satisfy these conditions, P must lie in an (N-1) dimensional concentration simplex (66).

The ends of the set of mutually orthogonal unit vectors are the vertices of the simplex (67). The ends of the set of all other vectors

satisfying Equations (4.23) and (4.24) form a continuum in the simplex known as the composition field or representative points of the alloy system at a specified temperature and pressure (Figure 4.4). The vector can be expanded to include temperature and pressure as well as composition; viz. (67);

$$P(x_i^{\circ}, T, P)$$

In general, all simplexes representing the domain of the composition variables of the N-component system are (N-1) dimensional polyhedra. The polyhedra increase their dimension by one for each component added to the system. Consequently, the concentration simplex is bounded by simplexes of lower dimension, their number equal to the total number of combinations of the N components taken J at a time:

$$C_J^N = \frac{N!}{(J)!(N-J)!} \quad (4.25)$$

the composition field of the Fe-Cr-Mn-Ni-C quinary system is an equalateral pentahedroid. The projection of the 4-dimensional hypervolume into 2-dimensional space is shown in Figure (4.5) (68).

The pentahedroid is bounded by:

$$C_4^5 = 5 \text{ quaternary hypersurfaces (equilateral tetrahedra)}$$

$$C_3^5 = 10 \text{ ternary surfaces (equilateral triangles)}$$

$$C_2^5 = 10 \text{ binary edges (lines)}$$

$$C_1^5 = 5 \text{ unary vertices (points)}$$

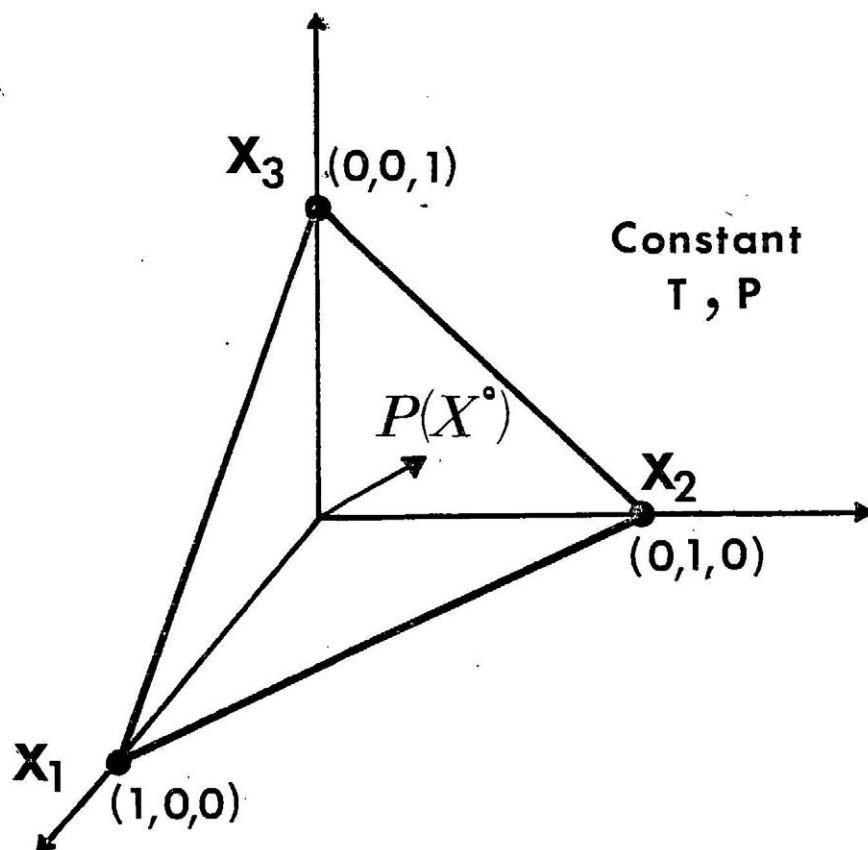


Figure 4.4 - The concentration simplex for a three-component system (Const. T,P)

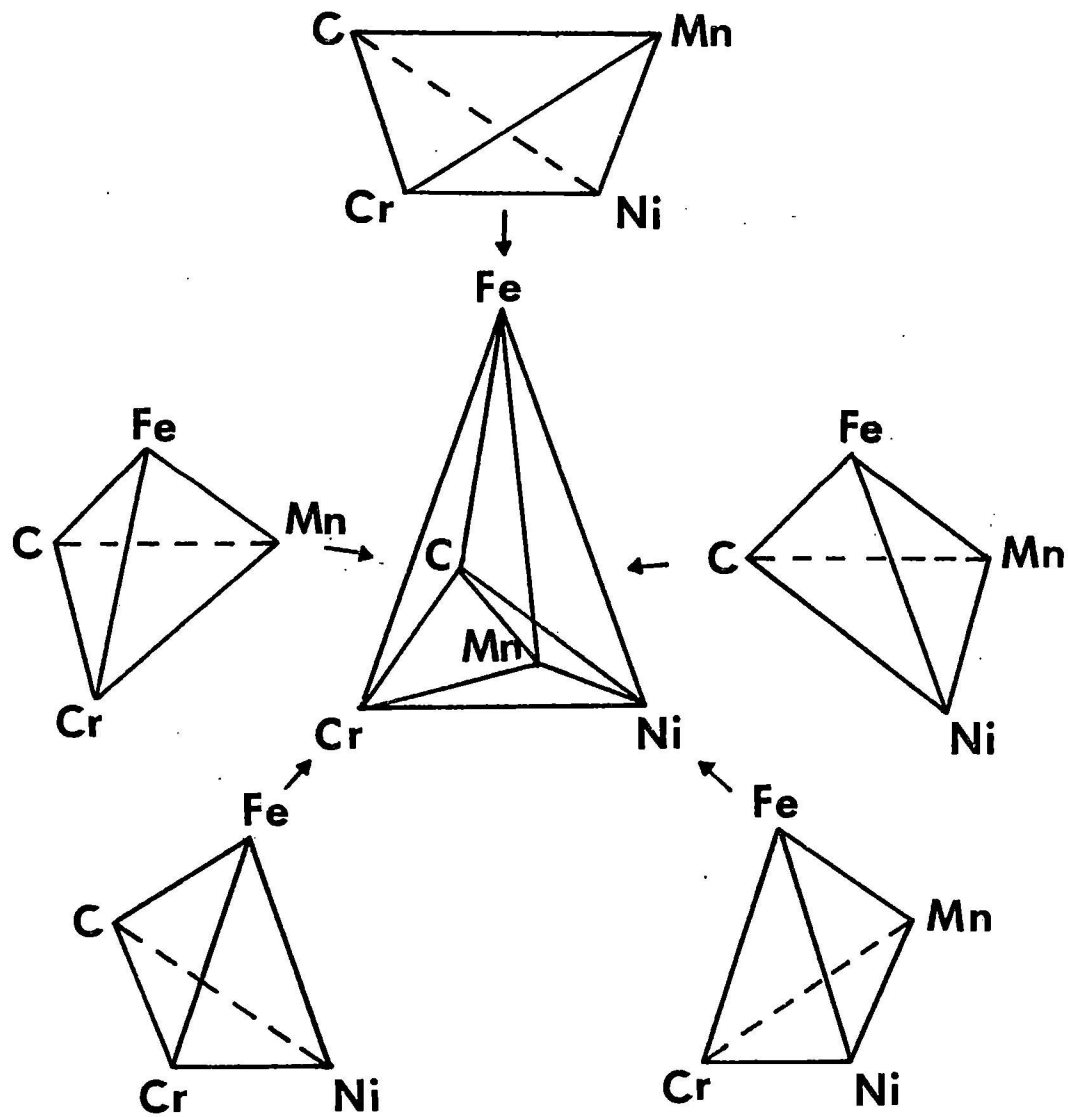


Figure 4.5 - The concentration simplexes of the Fe-Cr-Mn-Ni-C system
(Const. T,P)

4.2.2. The Hyperconode

Multicomponent alloy systems exhibit over a temperature and composition range at least two and not more than $(N+1)$ stable phases. The individual phases are always characterized by the differences in the long range ordering of the atoms in solution and usually by differences in composition. As noted in Section 4.1.1, the conditions of equilibrium dictate that of the many possible combinations of coexisting phases, only the most stable energetically should exist at each specific temperature, pressure and total composition. The composition relationship of each component (X_1^ϕ) among stable phases ($\phi=1,R$) at a specified temperature and pressure is represented spacially by a phase simplex or complex referred to as the hyperconode by Landeau (67). The hierarchy of hyperconodes in the quinary system are shown schematically in Figure 4.6. The hyperconode is a tie-line (conode) for the two-phase equilibrium, a tie-triangle for the three-phase equilibrium,* a tie-tetrahedron for the four-phase equilibrium, a 3-D complex with five vertices for the five-phase equilibrium and a 5-D complex with six vertices for the six-phase equilibrium (69). It is important to note that the tie-triangles and higher-order hyperconodes are actually defined by a set of tie-lines.

In the composition and temperature region investigated in the iron rich Fe-Cr-Mn-Ni-C system, two kinds of equilibria are observed: the equilibrium between the liquid and delta phases and between the liquid and the gamma phases and the equilibrium among all three phase (L+ δ + γ). Consequently only the tie-line and the tie-triangle are employed.

*For binary systems, the hyperconode designating the three-phase equilibrium is a "tri-triangle" with no altitude and is a phase complex.

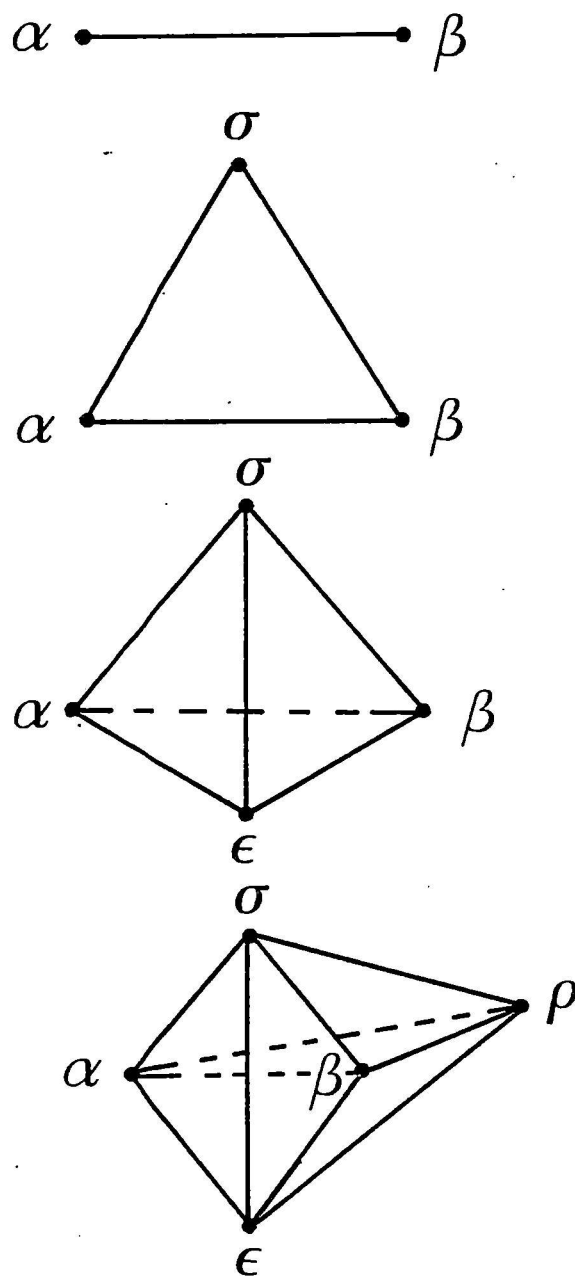


Figure 4.6 - The hyperconodes (phase simplexes) of the multi-component system

4.2.3. The Continuum

The hyperconode is the structural unit from which the field of stability of coexisting phases is constructed. A field is traced out in composition-temperature space by a continuum of the hyperconode. The field can be a point, line, surface, volume or hypervolume depending on the number of components of the system at a given temperature and pressure. The number of dimensions of the field is determined by the following relationship:

$$D = F + (P - 1) \quad (4.23)$$

where D is the dimensionality of the field, F is the degrees of freedom and P is the degree of hyperconode (number of coexisting phases). The criterion which designates the degree of freedom of the independent variables which define the field is the Gibbs phase rule, Equation (4.18). This rule provides the basis of the stepwise procedure to calculate the sequence of tie-lines and tie-triangles in the iron-rich Fe-Cr-Mn-Ni-C system to be discussed in the following section.

Topological rules for the positioning of phase boundaries through experimental points are discussed by Meijering and by Rhines (70, 69). These rules have a basis in the thermodynamic requirements of equilibrium of the stable phases in the alloy system (Section 4.1) and are not dealt with presently since the phase equilibria in the Fe-Cr-Mn-Ni-C system are calculated from the thermodynamic conditions of equilibrium.

4.2.3.1. The Ternary System

The Gibbs phase rule, Equation (4.18) applied to the equilibrium between two phases in the ternary system (Constant T, P) designates one degree of freedom. Accordingly, the field of stability of the equilibrium has two dimensions in the concentration simplex (Gibbs triangle). Any one of the independent variables must be fixed in order that the equilibrium can be calculated by the method of equal chemical potentials. This is shown schematically in Figure 4.7. The continuum of tie-lines between the liquid and solid phases trace out the liquidus and the solidus.

The equilibrium between three phases in the ternary system (constant T, P) has no degrees of freedom according to the phase rule. Consequently, there exists only one tie-triangle of the L- δ - γ equilibrium at each temperature (1 atm pressure). The vertices of the tie-triangles touch the single-phase fields of the δ , γ and L phases and trace out lines of two-fold saturation with temperature. The lines of two-fold saturation of liquid phase saturated with respect to the δ and γ phases and of δ phases saturated with respect to the L and γ phases are shown schematically in Figure 4.8. The peritectic reaction $L + \delta \rightleftharpoons L + \delta + \gamma$ is the ribbed surface traced out by the L- δ tie-lines of the L- δ - γ tie-triangles.

4.2.3.2. The Quaternary System

Application of the phase rule and Equation (4.23) to the equilibrium between two phases of the four-component system (constant T,P) indicates that the field of stability has three-dimensions in the composition tetrahedron. Accordingly, a tie-line is calculated for specific values of two of the independent variables, as shown in Figure 4.9. A continuum of

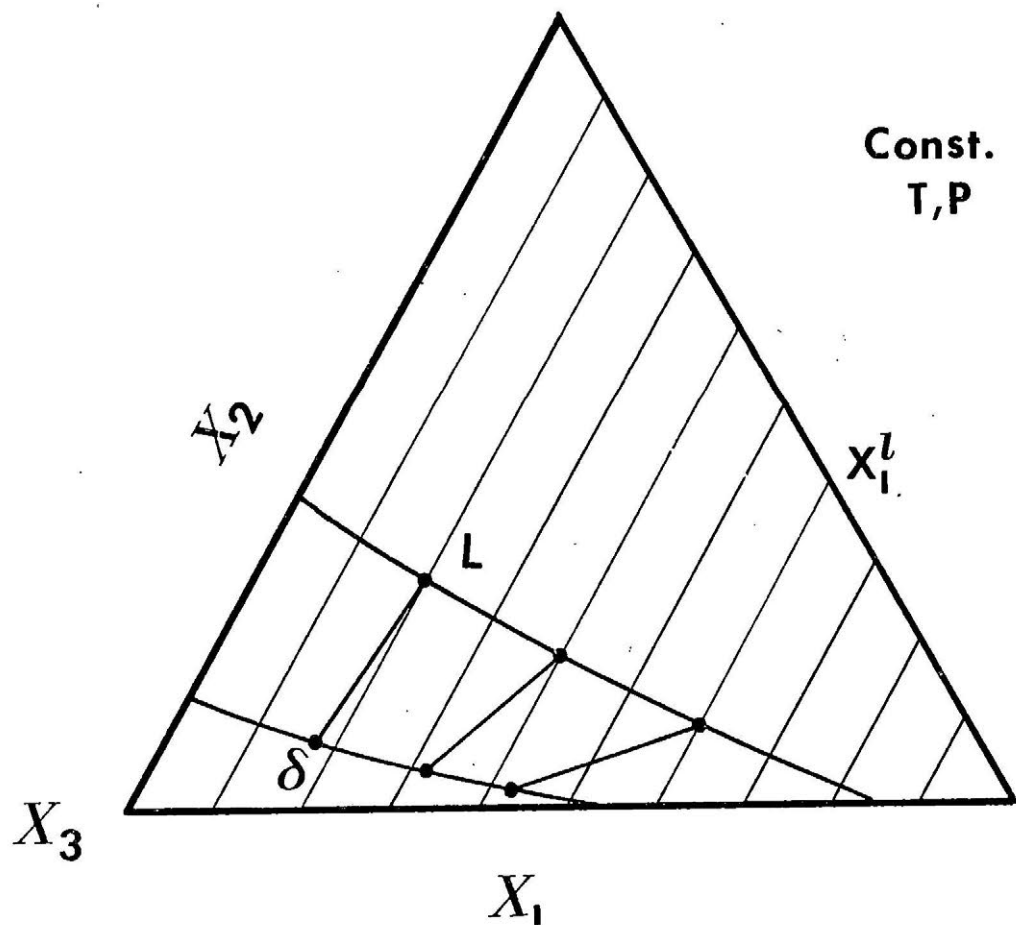


Figure 4.7 - Schematic representation of the procedure to calculate the continuum of tie-lines of the equilibrium between two phases in a ternary system (Const. T, P)

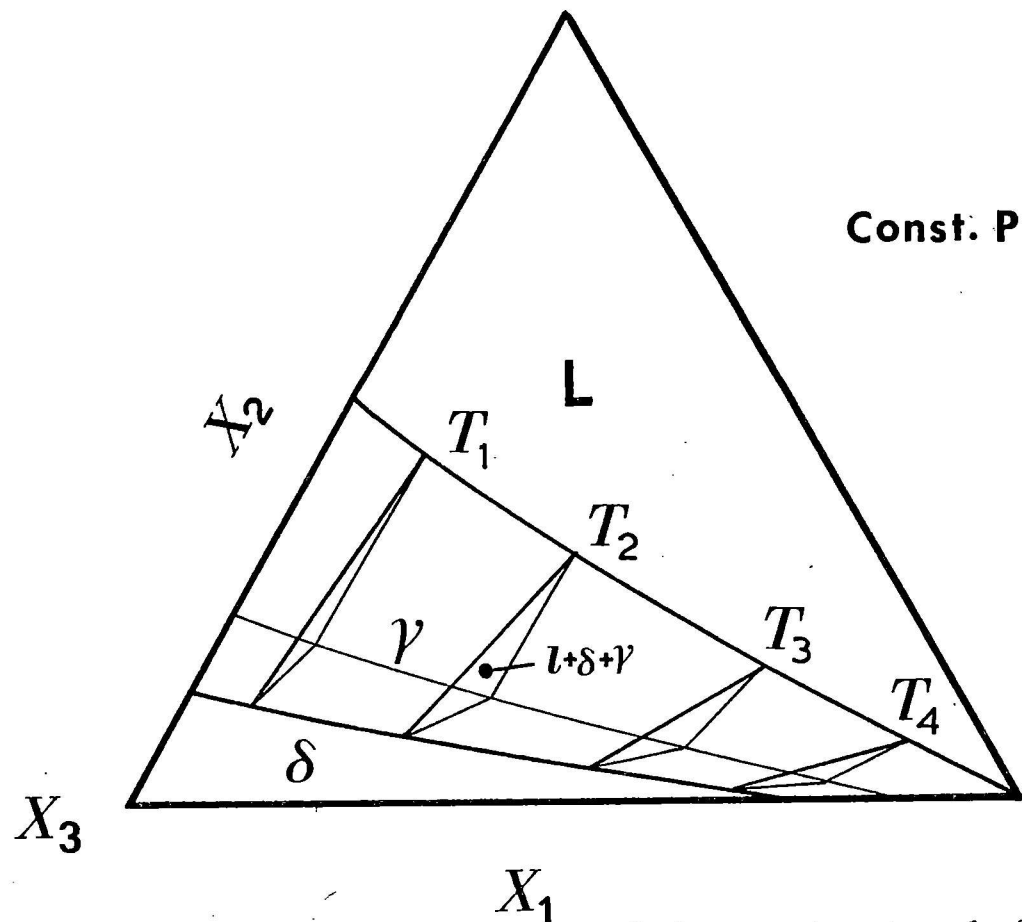


Figure 4.8 - Schematic representation of the procedure to calculate the continuum of tie-triangles of the equilibrium among three phases in a ternary system (Const. T,P)

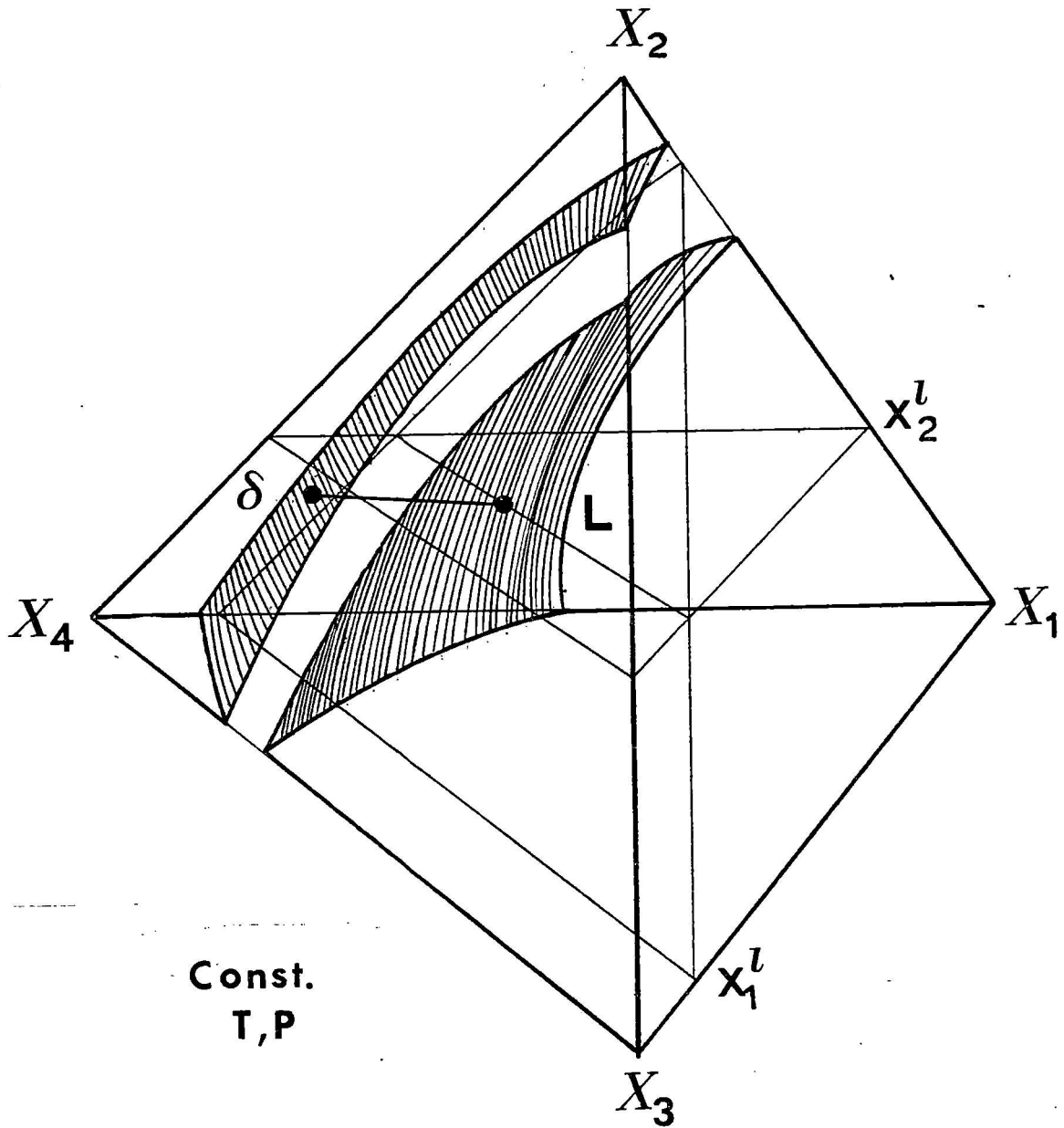


Figure 4.8 - Schematic representation of the procedure to calculate the continuum of tie-lines of the equilibrium between two phases in the quaternary system (Const. T,P)

tie-lines which trace out the phase boundaries of the field is generated by shifting the planes of constant X_1^ϕ to cover the entire composition field. As a consequence, the liquidus and solidus are surfaces in the quaternary system (constant T and P).

The equilibrium among the liquid, delta and gamma phases is, according to the phase rule, a ribbed volume (at constant T and P). The equilibrium is a hyper-volume in temperature - composition space. Solution to the system of Equations (4.16) for the case of equilibrium between three phases is possible when one of the composition variables is held constant at a specified temperature and pressure. This is in accord with Figure 4.10 which indicates that only one vertex of only one out of an infinite number of tie-triangles lies on the plane of constant composition. It is noted that the lines of two-fold saturation of the L- δ - γ equilibrium in the ternary systems become planes of two-fold saturation when the constraint on the temperature variable is relaxed.

4.2.3.3. The Quinary system

The equilibrium between two phases and the equilibrium between three phases in the quinary system has two and three degrees of freedom, respectively. However, the ends of the tie-lines and the vertices of the tie-triangle now connect hyper-volumes which are the domains of the single-phase fields. The liquidus and solidus are the hyper-surfaces or volumes of the liquid and solid single-phase fields as depicted in Figure 4.11.

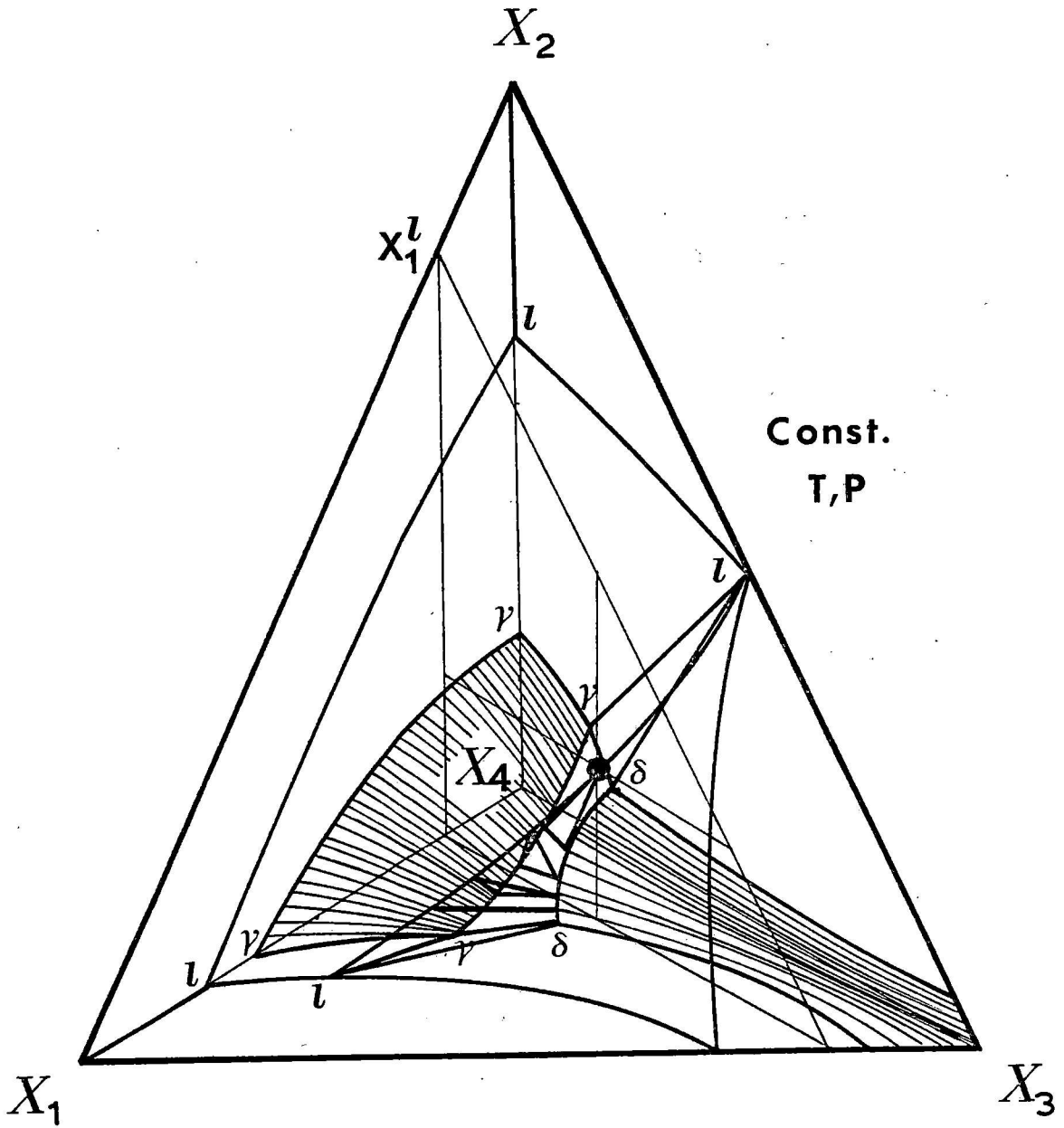


Figure 4.10 - Schematic representation of the procedure to calculate the continuum of tie-triangles of the equilibrium among three phases in a quaternary system (Const. T, P)

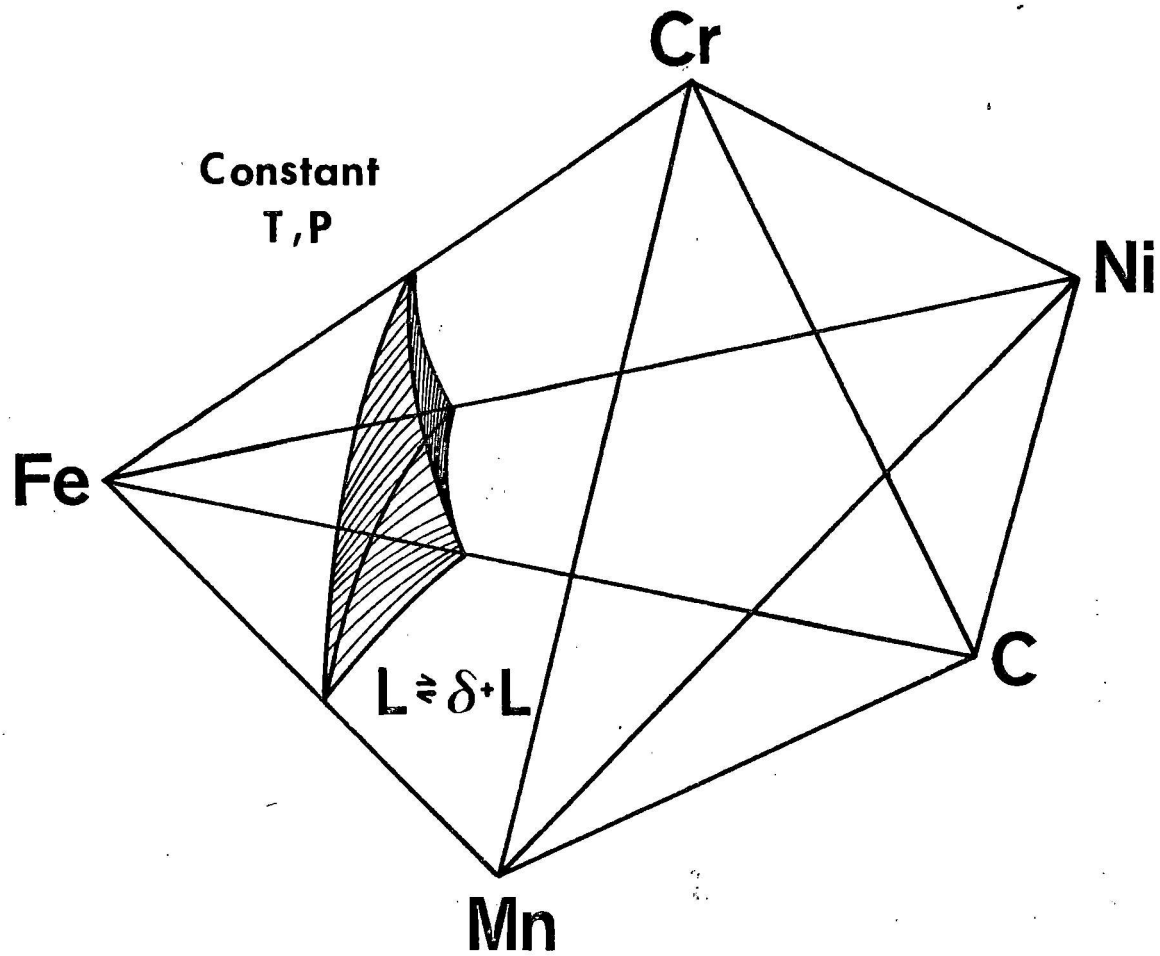


Figure 11 - Schematic representation of the liquidus (volume) of the quinary system projected into two-dimensional space (Const. T,P)

4.2.4. Method of Projection

Complete portrayal in two-dimensions of the phase equilibria of the higher order systems is impossible when the number of independent variables of the system exceeds two. Nonetheless, important aspects of each equilibrium could be examined in a sequence of plots each at a specified value of one or more of the independent variables, or in terms of ratios of the independent composition variables. Alternatively, the equilibrium can be projected onto the limiting sub-systems. This is a logical procedure since the phase equilibrium is actually represented by composition vectors which are the resultant of the base vectors of the system.

Two classes of projection methods are the perspective projection and the parallel projection methods, reviewed by Prince (66). In the perspective projection methods, the representative points of the equilibrium are projected from lines radiating from a vertex of the polyhedron. In parallel projection methods, the projection can be either parallel to one edge or orthogonal to one of its faces ($N > 3$). Polythermal projection specifically includes the temperature variable. Portrayal of the tie-lines, tie-triangles and phase boundaries of the sub-systems of the iron rich Fe-Cr-Mn-Ni-C system in Chapter 7 employ the polythermal orthogonal projection method.

CHAPTER 5

EXPERIMENTAL

It is recalled (Chapter 2) that the composition-temperature field in which coexisting solution phases are stable is defined by a continuum of tie-lines. The liquidus and solidus of an alloy system are mapped out by the composition and temperature co-ordinates of tie-lines joining the liquid and solid single-phase fields. Each tie-line dictates the compositions of conjugate liquid and solid phases at a specified temperature and total composition of the alloy system.

Experiments were conducted to determine the composition and temperature of the solid phase in equilibrium with a liquid phase of specified composition. An equilibrium couple was made by directional solidification of solid phase from an alloy melt. The couples were quenched, sectioned and analyzed chemically to reveal the compositions of the coexisting phases. Differential thermal analysis was then employed to measure the temperature coordinate of the liquidus at the composition of the conjugate liquid phase.

5.1. Differential Thermal Analysis

DTA is a method of determining the temperature of a phase change by recording the change in the rate of heating or cooling of a sample material relative to the temperature of a reference material. The measurement of the temperature of the thermal arrest recorded at the onset of solidification pinpoints the liquidus temperature of the alloy system of a specified composition.

5.1.1. Materials

Alloys were prepared from Ferrovac-E iron, Io-chrome, electrolytic manganese and nickel, and spectrographic graphite. Compositions (w/o) of impurities in the metals are listed below:

Iron

	C	Co	Cr	Cu	Mn	Mo
Min.	0.005	0.006	0.006	0.006	0.0005	0.001
Max.	0.010	0.005	0.01	0.01	0.001	0.01
	N	O(tot.)	P	S	Si	Ni
Min	0.0002	0.0002	0.002	0.003	0.006	0.02
Max	0.00085	0.003	0.003	0.005	0.006	0.02

Chromium

0.001 O 0.005 O₂ 0.0005 N₂ 0.001 S 99.99 + Cr.

Nickel

0.001 Cu 0.001 Mg 0.01 Si 0.01 Mn 99.9 + Ni

Manganese

99.99 + Mn

5.1.2. Apparatus

The DTA assembly is shown in Figure (5.1). The sample and reference materials (approximately 20 grams each) were contained in Coors alumina crucibles (99.8% purity, 19 mm O.D. x 25 mm). The reference material was copper. The sample and reference crucibles were housed in an alumina chamber which, in turn, was encased by an inductively-heated graphite susceptor. Approximately 6 KVA at 10 kilohertz was required to

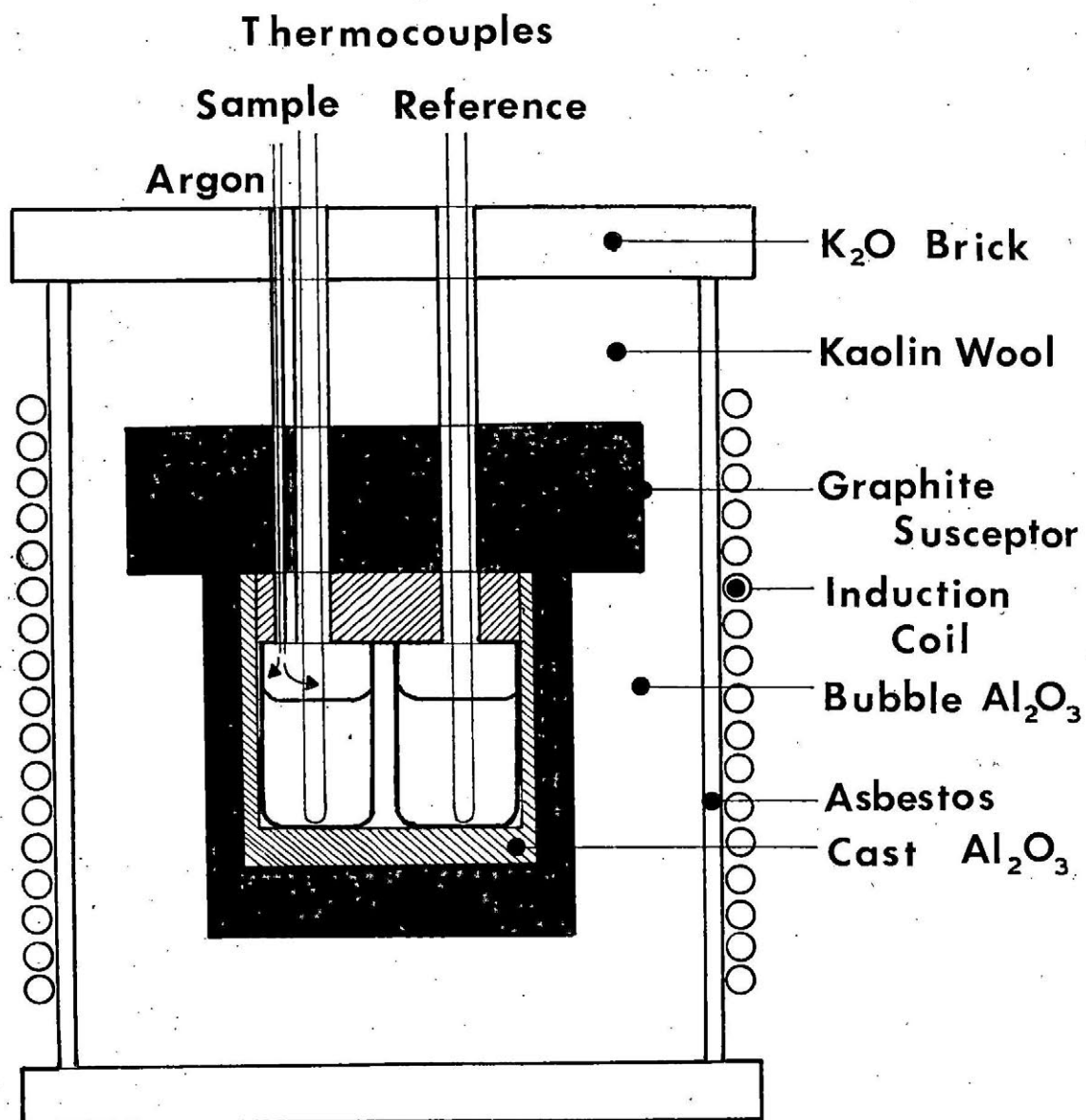


Figure 5.1 - The Experimental apparatus for DTA

heat the chamber to 1550°C.

An inert atmosphere was maintained over the melt by a steady flow of argon (50 PPM O₂). It was found that a flow rate of argon greater than 100 cm³/min was essential to protect the melt from contamination by carbon from the graphite susceptor.

Temperatures were measured by means of Pt/Pt - Pt/10 Rh thermocouples (0.01 in. dia.). The thermocouples were protected by closed-end Coors alumina sheaths (99.8% purity) and placed in direct contact with the melt, with the tip positioned at the bottom of the crucible. The depth of the metal bath with the thermocouple immersed in it ranged from 15 mm to 20 mm. Branches from the positive terminal of the sample and reference thermocouple were paired to indicate the temperature difference between the sample and reference. The temperature of the sample was taken to be the temperature of the system.

The thermocouples were calibrated against the melting points of Fe, Ni and Ag. Under standard experimental conditions, the following melting points were reproducible to within ± 1 °C*:

Element	Meas. EMF (Mv)	Meas. Temp.(°C)	Accepted ⁽⁵⁾ Temp.(°C)	Correction, (°C)
Fe	15.985	1534	1538	4
Ni	14.985	1451	1455	4
Ag	9.115	959	961	2

*

International Practical Temperature Scale of 1968.

5.1.3. Procedure

In a typical experiment, a charge of iron was melted and its melting point measured. This temperature was used to calibrate the system; consequently, all data refer to the melting point of pure iron, which is taken as 1538°C.* After the melting point of iron was established, the sample was remelted and an addition made to obtain an alloy of specified composition. The freezing point depression relative to the melting point of the iron sample was measured after each addition. Furnace controls were set to maintain a cooling rate of about 10°C/min through the expected arrest temperature.

5.1.4. Sources of Experimental Error

Sources of experimental error encountered in the DTA experiments are identified below:

1. Incomplete dissolution of the alloying elements.
2. Contamination of the melt by oxygen and carbon.
3. Vaporization of alloying elements.
4. Thermal gradients in the sample and reference.
5. Non-uniformity of composition in the melt.
6. Errors in the identification of the arrest temperature.

Items (1) through (3) were checked by chemical analysis of the sample. Compositions of some of the ingots from DTA experiments on ternary systems are listed in Table I.

A superheat of fifty degrees was necessary to insure complete dissolution of chromium and carbon, which were added in their elemental forms.

* A calculation of the freezing point depression due to impurities in the iron is given in the Appendix.

Table 5.1. Calculated additions and corresponding chemical analyses of DTA ingots

	Fe - Cr - C System				Fe - Ni - C System	
	Cr	C	O	Cu	Ni	C
Cal.	15.9	0.13	0.004	0.01	8.0	0.74
Anal.	-	0.14	0.005	-	7.9	0.75
Cal.	22.1	0.08	0.004	0.01	12.0	0.55
Anal.	-	0.09	0.007	-	11.8	0.55
Cal.	13.8	0.44	0.004	0.01	18.0	0.09
Anal.	13.6	0.44	-	0.03	17.6	0.10
Cal.	12.0	0.62	0.004	0.01	18.0	0.24
Anal.	11.8	0.61	-	-	17.6	0.25
Cal.	12.1	0.55	0.004	0.01		
Anal.	11.8	0.56	-	-		
	Fe - Mn - C System		Fe - Cr - Ni System			
	Mn	C	Cr	Ni	C	
Cal.	3.8	0.32	14.1	8.8	<0.01	
Anal.	3.6	0.33	14.1	8.8	0.01	
Cal.	5.0	0.58	9.8	14.0	<0.01	
Anal.	4.4	0.60	9.6	13.8	0.01	
Cal.	5.0	0.49	6.0	17.9	<0.01	
Anal.	4.7	0.51	6.0	17.7	0.01	

The analyses of carbon are in good agreement with the composition calculated from additions of carbon to the melt. This was substantiated by the agreement of $\pm 1/2^\circ\text{C}$ between the measured and accepted liquidus of the iron rich Fe-C system (9).

Loss of manganese due to vaporization was found to be significant. Repeated measurements of the freezing point depression of a sample of "constant" manganese content have shown the measured temperature to increase about $1/3$ to $1/2^\circ\text{C}$ during each cycle. Consequently, experiments with manganese as an alloying element were limited to three cycles of melting and freezing.

A crucial assumption for the practical use of DTA is that the thermal gradients present in the sample and reference are negligible. Thermal gradients along the axis of the thermocouple result in a temperature being measured that is lower than the actual temperature of the system. The thermocouple positioned off-center is found to affect adversely the shape of the thermalgram, probably due to thermal gradients present in the sample. However, freezing points of an alloy of specified composition were found to be reproducible to $\pm 1/2^\circ\text{C}$ independent of the mass of the alloy (10 to 25 grams) when the thermocouple was positioned at the center of the melt.

The thermocouple sheath was used to stir the melt. The induction field provided additional stirring. Uniform composition in the melt was insured relatively quickly, as the measurement of the temperature of the liquidus of specified composition were found to be reproducible within one cycle of melting and freezing.

Points on the liquidus were determined solely from thermalgrams recorded on cooling. Figure 5.2 is a schematic diagram of thermalgrams depicting a typical sequence of freezing points recorded after additions of constituents were made to form an alloy in the system Fe-C-Mn-Cr. T_S is the temperature arrest recorded at the onset of solidification. ΔT_L is the temperature difference ($1538^\circ\text{C} - T_L$) and ΔT_P is the temperature difference ($1538^\circ\text{C} - T_P$) where T_L and T_P are assumed to be the temperatures of the liquidus transformation ($L \rightarrow L + \delta$) and ($L \rightarrow L + \gamma$) and the peritectic transformation ($L + \delta \rightarrow L + \delta + \gamma$), respectively. The temperature difference $T_S - T_L$ is the degree of supercooling. When a small amount of aluminum (0.05 w/o) was added to deoxidize the melt to form small alumina particles, the degree of supercooling did not exceed 5°C . The maximum temperature recorded during solidification T_L was observed over a period of approximately 30 seconds. This was probably due to the relatively adiabatic conditions of the DTA chamber. In addition, the maximum temperature T_L was not found to vary with cooling rate. These characteristics of the thermalgram obviated the need to define an accepted transformation temperature based on extrapolation as is usually done (10). Consistent with the work of Hume-Rothery, the thermal arrest on freezing was found to be $1-2^\circ\text{C}$ lower than on melting. This error and a calculated error of $2 \frac{1}{2}^\circ\text{C}$ due to presence of impurities in the Ferrovac iron (Appendix B) account for the discrepancy between the measured and accepted melting point of iron of 4°C . The random error in the measurement of the temperature of the liquidus by DTA is estimated to be $\pm 1^\circ\text{C}$.

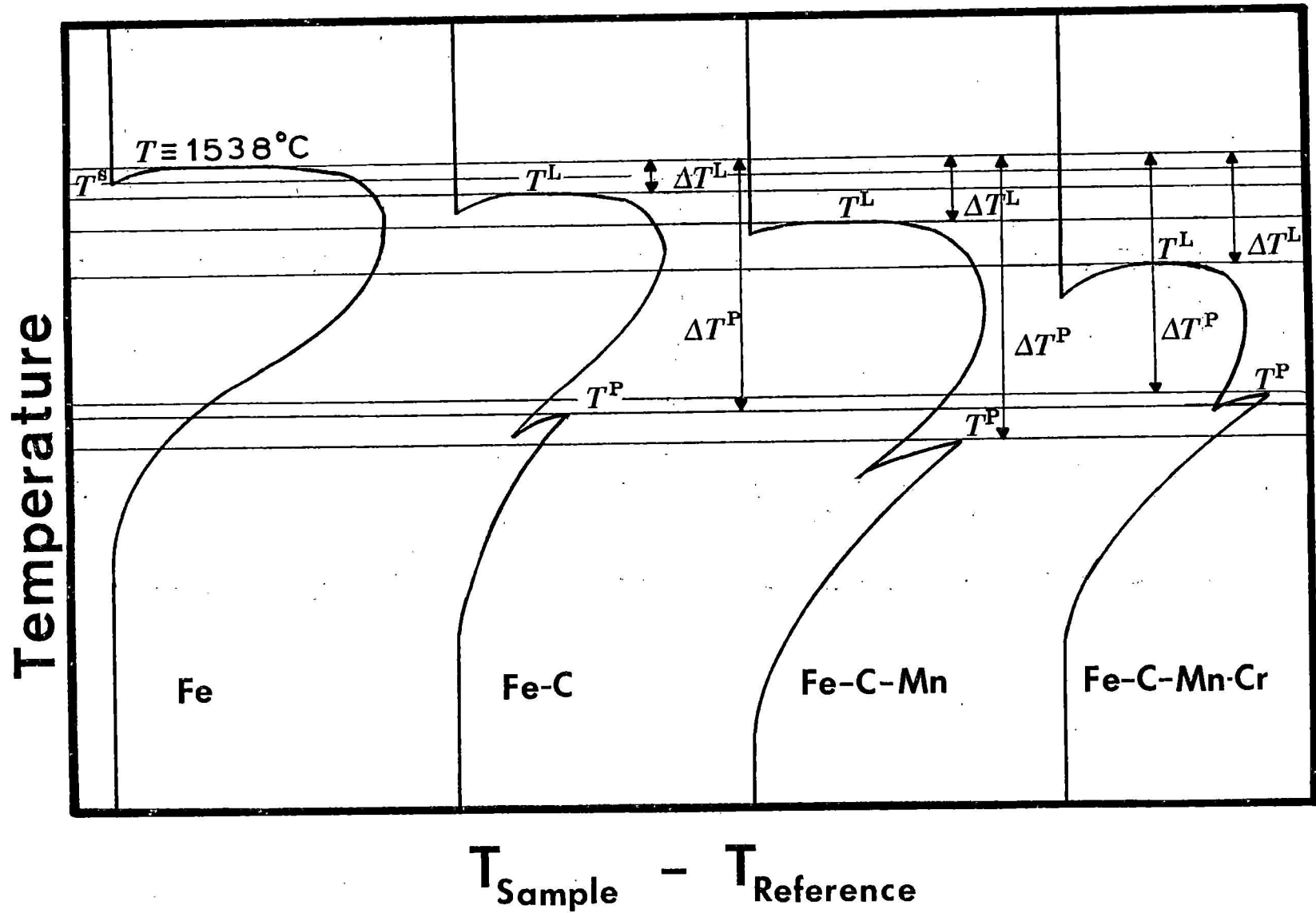


Figure 5.2 - Schematic diagram of the sequence of thermalgrams of the freezing points of Fe and the alloys Fe-C, Fe-C-Mn and Fe-C-Mn-Cr

5.2. Equilibrium Couples

An equilibrium couple was made by solidifying a solid phase from the alloy melt. Under conditions of high thermal gradient G to solidification rate R , the solidification front is planar (71). The ratio is estimated to be approximately 10^5 °C-sec. over the composition region investigated in the ternary and quaternary systems.

5.2.1. Materials

Alloys were prepared from the same stock of materials that was used in the DTA experiments (Section 5.1.1).

5.2.2. Apparatus

The apparatus designed for directional solidification of an alloy melt is shown in Figure (5.3). The melt was contained in a Coors cast alumina crucible (99.8% purity, 13 mm I.D. x 150 mm). The crucible was housed in a graphite susceptor, which was inductively heated. A steady flow of Argon gas of about $100 \text{ cm}^3/\text{min}$ was maintained over the melt. A screw assembly (rotated by hand) enabled the crucible to be lowered with respect to the graphite susceptor. This was attached to the bottom of the induction coil frame.

5.2.3. Procedure

The apparatus employed was essentially the same as was used by Chochol, but the procedure was quite different (13).

Approximately 70 grams of Ferrovac E rod and alloying elements were placed in the crucible, with the iron rod positioned at the bottom. It was necessary to preheat to 500°C for 30 minutes to drive out water vapor that may have been present in the materials. The materials were

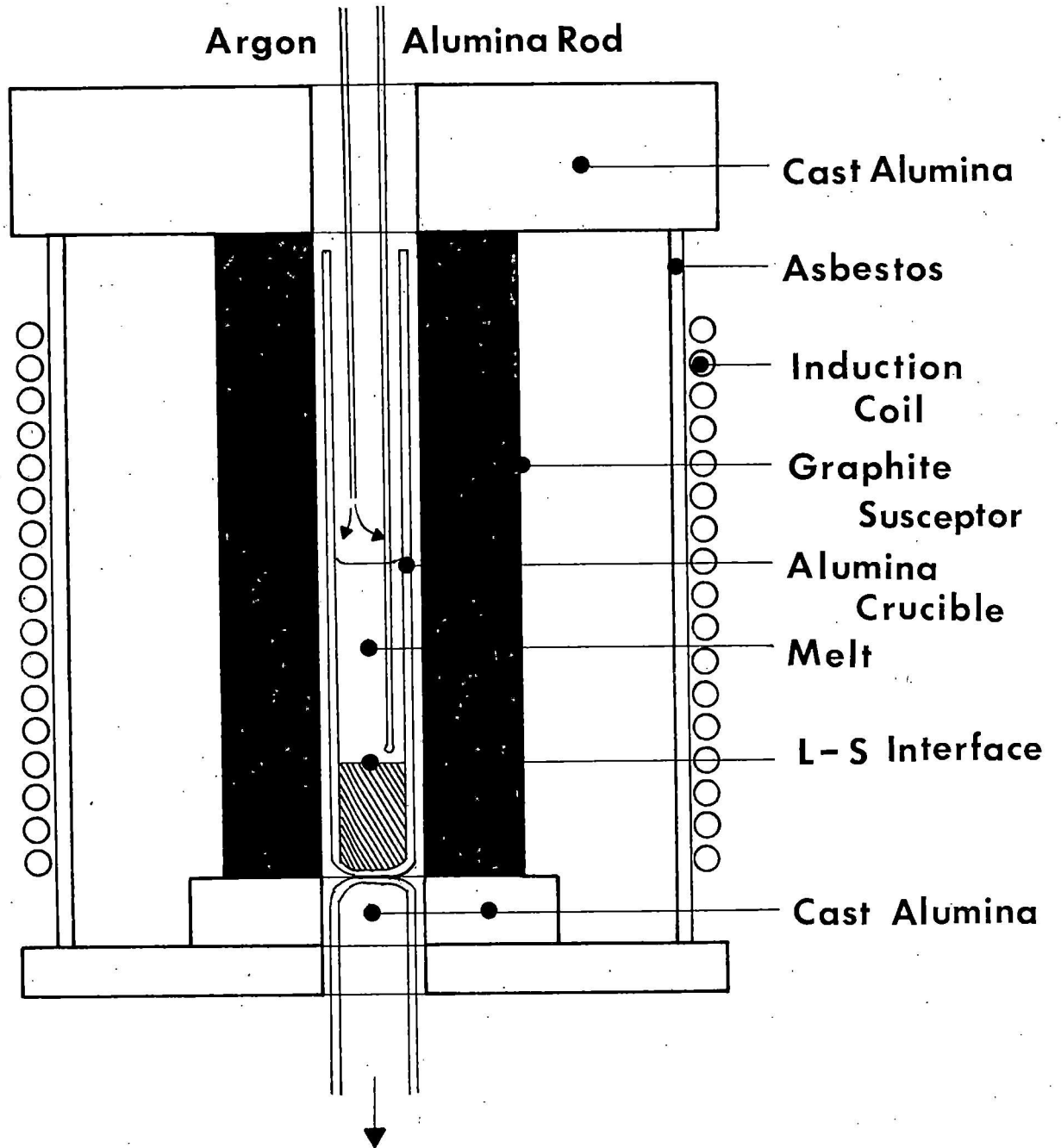


Figure 5.3 - The experimental apparatus for the directional solidification of alloy melts

melted and then stirred with an alumina rod (2 mm dia.) to insure uniform composition. The crucible was then lowered in the induction coil to initiate solidification at the bottom of the crucible. After freezing a base of one cm thick, withdrawal was stopped for a period of thirty minutes. During this period, the melt was stirred thoroughly to remove excess solute in the vicinity of the solidification front. The melt was again withdrawn in increments of two mm, with the interface held stationary for thirty minutes after each increment to insure a plane-front separation between the liquid and solid phases and to allow sufficient time for the equilibration of carbon in the increment with respect to the liquid phase. During the period in which the solidification front was stationary, the melt was stirred to maintain a uniform composition. The position of the front was measured with the alumina rod. A thermal gradient of approximately $50^{\circ}\text{C}/\text{cm}$ was maintained across the solidification front at all times.

The procedure was repeated until a depth of approximately two cm of solid phase was grown from the melt. The total mass of the ingot was chosen so that the total amount of liquid phase at the completion of the experiment was at least five times the total mass of the solid phase solidified as small increments (base not included). With this ratio of masses, the composition of the liquid phase was found to remain essentially unchanged during solidification of the increments of solid phase.

At the completion of the experiment, the crucible was withdrawn from the susceptor and cooled rapidly in a quenching device designed by Chochol (13). The objective of this device was to establish the

primary resistance to heat removal at the crucible-air interface, which, in turn, would establish a near-uniform temperature across the diameter of the ingot during quenching. Metallographic inspection of the quenched liquid phase revealed columnar grains, which were of uniform size in the longitudinal direction of the ingot. Figures (5.4A and 5.4B) show the interface between quenched liquid and pre-solid phase and the microstructure of the quenched liquid phase and pre-solid phase (at the base of the ingot), respectively.

The ingot was sliced into specimens (1 1/2 mm thick) with a diamond saw (1/2 mm thick). The specimens (three to each side of the interface) were analyzed subsequently for C, Cr, Mn, Ni, S, P and Al with a high energy emission spectrograph. Partitioning of the impurities S, P and Al was also observed in all ingots and was used to help delineate the position of the liquid-solid phase interface. The absolute accuracy of the analyses of carbon (w/o) is:

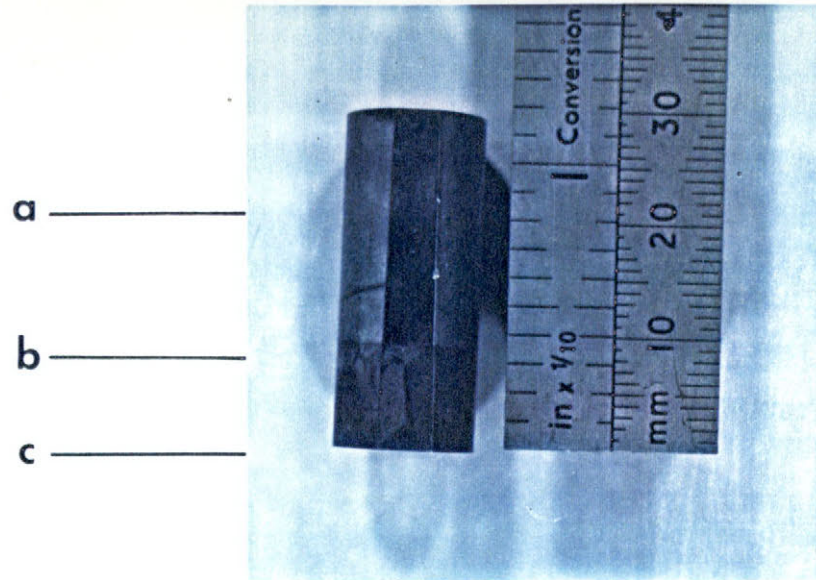
$$\pm 0.01 \quad 0.00 < X_c < 0.20$$

$$\pm 0.02 \quad 0.20 < X_c < 0.60$$

$$\pm 0.03 \quad 0.60 < X_c < 1.00$$

The relative accuracy of carbon is ± 0.01 w/o at all levels. Consequently, the difference in the analyses of the composition of the specimens of liquid and solid phases of each ingot is not in error more than ± 0.01 w/o C. The absolute accuracy of Cr, Mn and Ni is $\pm 5\%$ of the total composition of each element in the specimen. The relative accuracy of the alloying metals is ± 0.1 w/o at all levels.

A



B

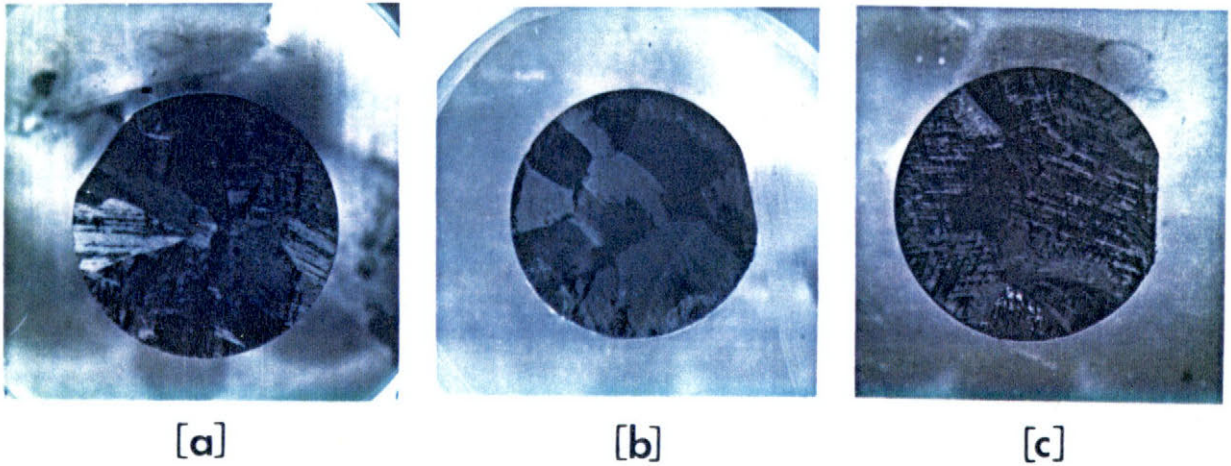


Figure 5.4 - Photographs of an etched ingot exhibiting the interface between the quenched pre-solid gamma and liquid phases (A). The microstructure of the cross-section of the ingot at positions a, b and c are also shown (B) (6% Nital etch).

5.2.4. Source of Experimental Error

Sources of experimental error encountered in the formation of equilibrium couples are identified below.

1. Non-equilibrium conditions at the liquid-solid phase interface.
2. Non-uniform liquid composition.
3. Instability of the liquid-solid phase interface.
4. Entrapment of liquid phase in the solid phase during solidification.
5. Error in the identification of the conjugate compositions.

Two non-equilibrium conditions may occur at the liquid-solid phase interface of a solidification front: (1) precipitation of a metastable phase and (2) precipitation of an equilibrium phase of non-equilibrium composition. Both conditions have been observed to occur in alloys solidified at high solidification rates (72,73). The solidification rate employed in the growth of the solid phase in the present experiment is well under the range where departures from equilibrium may occur (57).

However, it is pointed out that formation of a metastable phase may occur at low solidification rates when a solute boundary layer is present in the vicinity of the solidifying front. A case in point is the precipitation of a metastable carbide from a liquid phase at a composition near that of saturation with respect to the carbide. Fortunately, carbides were not observed in the high-carbon specimens of pre-solid phase (Sodium Picrate etch).

The presence of a solute boundary layer adjacent to the solidification front of an alloy having a segregation ratio less than unity

$(X_i^{\text{solidus}}/X_i^{\text{liquidus}} < 1)$ will result in the solid phase forming at a solute composition in excess of that which would be in equilibrium with the bulk liquid phase (71). Because of the difficulty of insuring that the composition of the liquid phase is uniform during solidification, the segregation ratio determined experimentally may be somewhat greater than is actually the case. This error would be most significant for the case of carbon partitioned between liquid and delta phase, since carbon dissolved in iron has a much smaller segregation ratio than the alloying metals.

A second problem related to the effect of a solute boundary layer on the composition of solid phase is the movement of the planar interface in response to small fluctuations of heat input. Chochol applied a relatively large thermal gradient in the vicinity of the liquid-solid phase interface; the gradient was as high as 200°C/cm. As a high thermal gradient may displace the chemical equilibrium across the liquid-solid phase interface, the gradient was kept below 50°C/cm in the present experiment. However, with the smaller thermal gradient, the position of the liquid solid phase interface was found to be more responsive to fluctuations of heat input and was more difficult to monitor. The interface of the equilibrium couples of alloys of high chromium content were the most difficult to monitor since the chromium component of the slope of the liquidus (and solidus) with temperature is small relative to the other components and, in fact, approaches zero at 20% Cr in the Fe-Cr system.

Liquid phase trapped in the solid phase during solidification can also complicate measurement of the solidus composition. Lack of symmetry

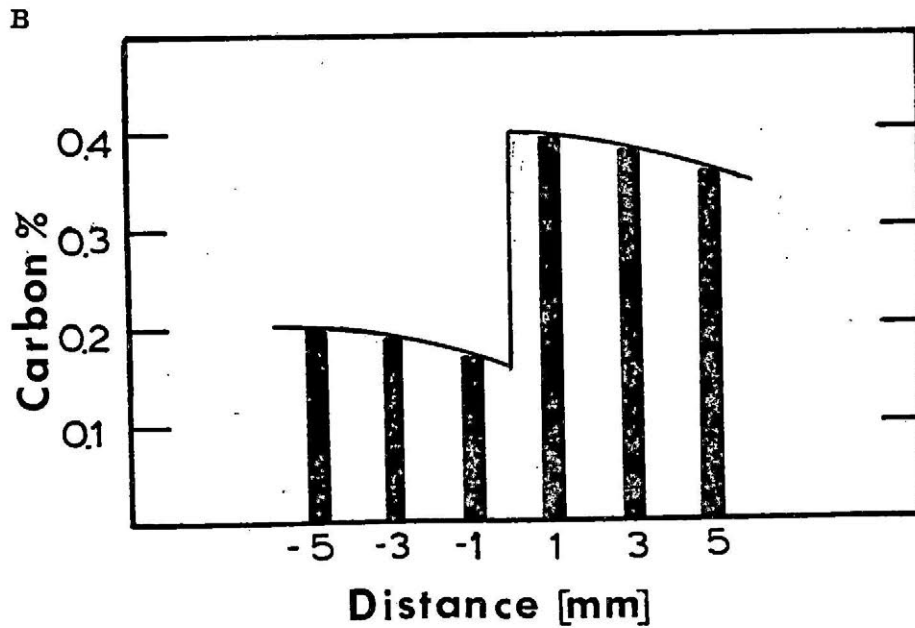
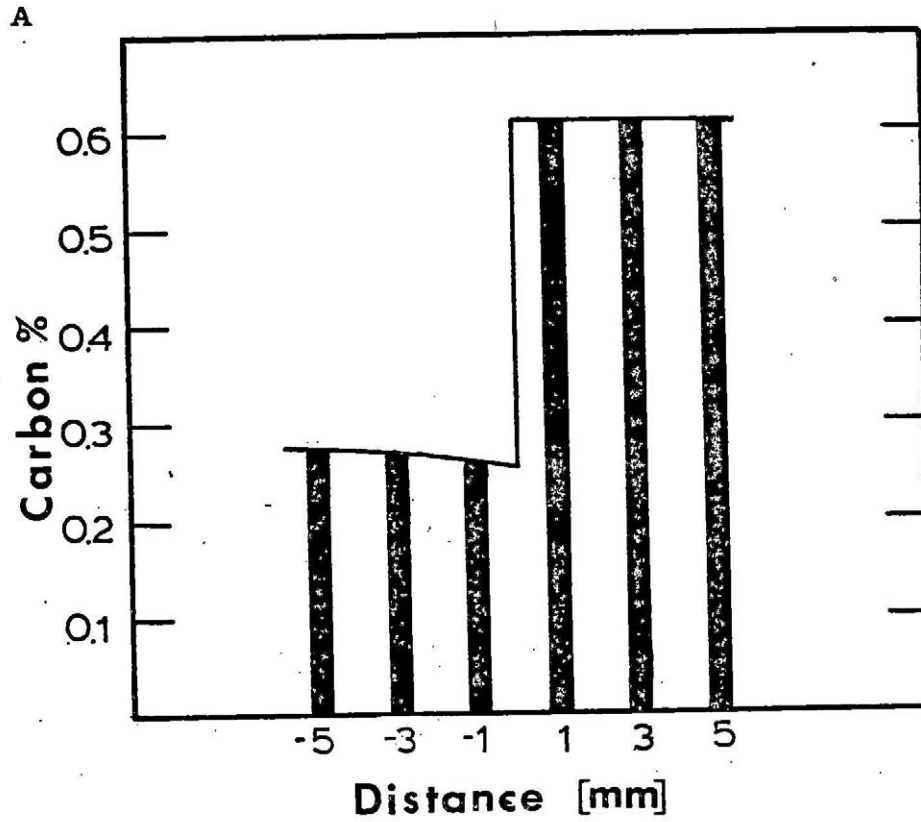


Figure 5.5A and B - Schematic drawings of two types of composition profiles observed in the quenched equilibrium couples (only carbon composition shown)

of temperature with respect to the center of the melt can cause an uneven solidification front, which, in turn, may cause liquid phase to become trapped in relatively large, isolated pools. During periods in which the solidification rate is unsteady, the solidification front may be cellular or even dendritic and liquid phase may also become trapped in small amounts between cells and dendrites. However, either situation would not be expected to have occurred in all of the pre-solid phase specimens of the ingot. Composition profiles of the pre-solid phase specimens were observed to be generally uniform and evidence of solidification shrinkage in the pre-solid phase portion of the ingot was not observed.

Vaporization of manganese occurred at a rate of about 0.5% hour, when present in the melt. However the interface was not observed to grow in response to depletion of manganese in the liquid phase. The solidus of the alloy systems containing manganese may be in error by as much as 0.3 w/o Mn.

Figures 5.5A and 5.5B show two types of composition profiles observed in the ingots. The profiles that were generally flat required little or no extrapolation to estimate the compositions of the phases at the liquid-solid phase interface. However, some ingots exhibited steeper composition profiles. Those were extrapolated the equivalent of one specimen thickness (1 1/2 mm) as shown in Figure (8.6B). The maximum error in the identification of the composition of conjugate phases is ± 0.02 w/o for carbon and ± 0.10 w/o for the alloying metals.

CHAPTER 6

THERMODYNAMIC MODELING OF PHASE DIAGRAMS

Alloy phase diagrams are obtained from two classes of experiments. One class of experiments is the direct measurement of the relationship between composition and temperature which define the field of stability of a group of phases coexisting at equilibrium. Methods such as differential thermal analysis and equilibrium couples can be employed to determine the temperature of a phase boundary at a selected composition and the corresponding composition of each of the phases in equilibrium.

The phase diagram which results from analysis of this class of experiments is expressed mathematically as (6.0).

$$T = f(M_p) \quad (6.1)$$

T is the temperature associated with the concentration matrix

$$M = \left\| \left\| X_{ij} \right\| \right\| \quad \begin{array}{l} i = 2, 3 \dots N \\ j = 1, 2 \dots R \end{array} \quad (6.2)$$

where N and R are the total number of components and coexisting phases of the alloy system at a constant pressure, respectively.

The other class of experiments is the measurement of thermochemical properties of the alloy system by such means as calorimetry, vapor pressure, equilibration with other phases and electromotive force. The activity of at least one component in each solution phase is measured within the temperature and composition field of stability of the single phase. The activity data can usually be expressed as an algebraic

function of the independent composition and temperature variables. Expressions of the activities of the other components are derived by applying the Gibbs-Duhem relationship. Alternatively, the activity each component is expressed in terms of an algebraic model of the integral molar free energy of mixing of the solution phase. In either case, the differences of standard states of the pure components must also be known in order that the equations governing chemical equilibrium can be solved to obtain the concentration matrix associated with the phase equilibrium (Chapter 4). At equilibrium, the Gibbs free energy of the system of coexisting phases is expressed mathematically as

$$G_s = f(T, \mathbf{M})_p \quad (6.3)$$

Equation (6.3) is readily transformed to Equation (6.1), which implies that the phase diagram determined from the two classes of experiments should, in principle, be consistent. However, inconsistencies arise from the fact that experimental errors encountered in each class of experiments are inherently different. Moreover, the sensitivity of the calculated phase diagram to errors in the measurement and mathematical representation of the thermochemical properties of a phase varies with composition and temperature and with the magnitude of the difference of the Gibbs energies of the coexisting phases (74). Coupling of thermochemical and phase diagram measurements is important to assess the consistency of both types of thermodynamic measurements.

In the present study, mathematical methods were applied to the phase diagram measurements of the Fe-Cr-Mn-Ni-C system to achieve two objectives:

1. Mathematically predict the experimental results.
2. Determine the magnitude of the thermodynamic interaction of each of the solution phases in the alloy system.

Both objectives were accomplished with thermodynamic modeling of the phase diagram measurements.* With the aid of suitable mathematical and computer techniques, parameters in a model of integral molar free energy of mixing were estimated from the measurements of phase boundaries and tie-lines. This approach has the benefit of condensing the enormous amount of phase diagram measurements of the Fe-Cr-Mn-Ni-C system into a few parameters. In addition, the ability of the thermodynamic model to predict the experimental quantities permitted interpolation and extrapolation in the composition region investigated to within the experimental accuracy and set an upper limit on number of experiments needed on the phase diagram.

A criterion was developed to assess the effect of the number and accuracy of the experimental quantities on the statistical significance of parameters in the model under consideration. The same criterion can be used to assess the ability of various models to predict a set of experimental quantities of a given accuracy .

* Surfaces of saturation can also be modeled with the use of simplex methods or regression analysis (68). However tie-lines between two solution phases cannot be predicted with such models.

This chapter begins with a discussion of the model of the molar Gibbs energy assumed for the liquid and solid solution phases of the iron-rich Fe-Cr-Mn-Ni-C system. Methods to obtain parameters in thermodynamic models from experimental data on phase equilibria are reviewed. Finally the method which was selected for the present analysis is discussed in detail.

6.1. The Integral Molar Free Energy

The major Gibbs energy of mixing a solution phase ϕ at constant pressure is described mathematically as follows:

$$\Delta G_{\mathbf{M}}^{\phi} = \sum_{i=1}^N \mu_i^{\circ\phi} X_i^{\phi} + RT \sum_{i=1}^N X_i^{\phi} \ln X_i^{\phi} + \Delta G_{\mathbf{M}}^{\mathbf{E},\phi} \quad (6.4)$$

where $\mu_i^{\circ\phi}$ is the standard chemical potential of pure component i

X_i^{ϕ} is the mole fraction of component i in phase ϕ

R is the Universal Gas Constant

T is the temperature

N is the number of components

$\Delta G_{\mathbf{M}}^{\mathbf{E},\phi}$ is the excess molar Gibbs energy of mixing of phase ϕ

6.1.1. Interaction Models of Solution Phases

Interaction models which describe mathematically the thermodynamic properties of mixing of the solution phases of alloy systems ($\Delta G_{\mathbf{M}}^{\mathbf{E},\phi}$) range between two extremes: those based on statistical thermodynamics and those which are strictly empirical. An excellent review by Ansara gives a detailed description of various interaction models (60). A very brief description is given here.

Models of the thermodynamic interaction among unlike atoms in a solution phase have been derived upon consideration of bond energies and ordering of atoms in solution. The simplest model that describes departure from ideal solution behavior is the quasi-chemical model employing the regular solution assumption of no excess entropy of mixing. This model is usually termed a "regular solution model." It has one parameter which is assumed to be a measure of the difference in bonding energies between a solution of unlike atoms and a mechanical mixture of unlike atoms. Since no ordering is assumed, the parameter is not a function of temperature. A "quasi-regular" or "sub-regular" solution model is also a one parameter model in which a temperature dependence is assumed.(25).The competitive action of different neighboring atoms towards a central atom is considered in more sophisticated models. In particular, the central atoms model takes into account the vibrational as well as the configurational contribution to the excess thermodynamic properties (27). The model has been applied successfully on interstitial solutions of carbon in alloyed iron (30). With such models, relatively few parameters are needed to represent important but often subtle differences in the behavior of solutions.

Another class of models utilizes power series of a function to represent the excess thermodynamic properties. Analytical expressions of this type have been developed by Margules, Wilson and recently by Pelton (75). The order of expansion; i.e., the minimum number of parameters, is determined in accordance with the desired statistical fit of the data. However, it is noted that some functions may not adequately represent the thermodynamic interaction of a phase over a specified

composition range, regardless of the order of expansion. A case in point is the inability of known power series expansions to represent the locally strong interactions of liquid phase saturated with respect to stable stoichiometric compounds in the iron-sulfur system (76).

The interactions among components in the limiting subsystems of the multicomponent system are weighted according to geometric position in the multicomponent concentration simplex in a third class of models. However, the mathematical forms of these models do not reduce to the expression of ideal solution behavior. Such models are termed "empirical geometric models" and include the Bonnier equation, the Toop equation, the Kohler equation, the Colinet equation and the Muggianu equation.

6.1.1.1. Selection of a Solution Model

Modeling of a multicomponent system begins logically with analysis of the limiting sub-systems. Two extremes can be taken in the selection of interaction model:

1. Consideration of different models for each solution phase in each alloy sub-system.
2. Consideration of a generalized model for the solution phases of the entire multicomponent system.

The model which best represents the thermodynamic interaction of a particular phase may differ for each alloy sub-system in which the phase is stable. Furthermore, it may not be possible to represent subtle differences in the behavior of the solution phases of a particular alloy

system with one model. On the other hand, a single interaction model may be adequate to represent the thermodynamic interactions of each of the solution phases in the alloy systems. In the modeling of phase diagrams, the criterion to assess the model(s) chosen for the coexisting solution phases is the discrepancy between the calculated and experimental phase diagram. If the discrepancy is within the experimental error of the experimental phase diagram at all points in the composition field investigated, then the model employed is judged acceptable.

Obviously, the latter approach is simpler. The N-component system is bounded by C_J^N ($J = 1, 2 \dots N-1$) sub-systems of J components (concentration simplexes) where C_J^N is the total number of combinations of N taken J at a time; viz,

$$C_J^N = \frac{N!}{(N-J)!(J)!} \quad (6.5)$$

Consequently, the number of alloy systems which would employ the same model would increase as N is increased. and, in the computation of the phase diagram, only the parameters would be different among the systems having the same number of components. The total number of sub-systems which comprise the N-component system is

$$\sum_{j=1}^N C_J^N = 2^N - 1 \quad (6.6)$$

For the extreme, but unlikely situation where a different model is chosen for a particular phase in each of the sub-systems, the number of models

considered would be enormous as N is increased and computation of the phase diagrams cumbersome.

To reduce the complexity of the computer calculations of the ternary and higher order systems, one interaction model was assumed for all solution phases investigated in each of the sub-systems of the Fe-Cr-Mn-Ni-C system.

6.1.1.2. The Quasi-Regular Solution Model

The ten binary sub-systems of the Fe-Cr-Mn-Ni-C system have been calculated by Kaufman and agreement with the experimental phase diagrams in the literature is reasonable.* The solution phases were modeled with the quasi-regular solution model; consequently, the hypothesis was made in the present study that a generalized quasi-regular solution model can accommodate the thermodynamic interactions of all the sub-system of interest in the Fe-Cr-Mn-Ni-C system. This is generally the case as shown in the chapter on discussion of results (Chapter 8).

The quasi-regular solution model of the thermodynamic interactions of N components in phase ϕ is given by the following expression.

$$\Delta G_{\mathbf{M}}^{E,\phi} = \sum_{n_1=1}^N \cdots \sum_{\substack{n_i=1 \\ n_1 \neq n_i \neq n_J}}^N \cdots \sum_{n_J=J}^N \left[\frac{[\prod_{i=1}^J X_{n_i}] [\sum_{i=1}^J X_{n_i} \theta_{n_i}^{(1,2,\dots,J)}]}{[\sum_{i=1}^J X_{n_i}]} \right]$$

$\theta_{n_i}^{(1,2,\dots,J)}$ are the parameters associated with the interaction among J components and X_{n_i} is the mole fraction of component n_i in phase ϕ in the N-component system.

* See Chapter 2 for references.

The quasi-regular solution model of the quinary system is:

$$\Delta G_M^{E,\varphi} =$$

$$\begin{aligned} & \frac{X_1 X_2}{X_1 + X_2} [X_1 \theta_1^{(1,2)} + X_2 \theta_2^{(1,2)}] + \frac{X_1 X_3}{X_1 + X_3} [X_1 \theta_1^{(1,3)} + X_3 \theta_3^{(1,3)}] \\ & + \frac{X_1 X_4}{X_1 + X_4} [X_1 \theta_1^{(1,4)} + X_4 \theta_4^{(1,4)}] + \frac{X_1 X_5}{X_1 + X_5} [X_1 \theta_1^{(1,5)} + X_5 \theta_5^{(1,5)}] \\ & + \frac{X_2 X_5}{X_2 + X_5} [X_2 \theta_1^{(2,5)} + X_5 \theta_4^{(2,5)}] + \frac{X_3 X_5}{X_3 + X_5} [X_3 \theta_3^{(3,5)} + X_5 \theta_5^{(3,5)}] \\ & + \frac{X_4 X_5}{X_4 + X_5} [X_4 \theta_4^{(4,5)} + X_5 \theta_5^{(4,5)}] + \frac{X_2 X_3}{X_2 + X_3} [X_2 \theta_2^{(2,3)} + X_3 \theta_3^{(2,3)}] \\ & + \frac{X_2 X_4}{X_2 + X_4} [X_2 \theta_2^{(2,4)} + X_4 \theta_4^{(2,4)}] + \frac{X_3 X_4}{X_3 + X_4} [X_3 \theta_3^{(3,4)} + X_4 \theta_4^{(3,4)}] \\ & + \frac{X_1 X_2 X_3}{X_1 + X_2 + X_3} [X_1 \theta_1^{(1,2,3)} + X_2 \theta_2^{(1,2,3)} + X_3 \theta_3^{(1,2,3)}] \\ & + \frac{X_1 X_2 X_4}{X_1 + X_2 + X_4} [X_1 \theta_1^{(1,2,4)} + X_2 \theta_2^{(1,2,4)} + X_4 \theta_4^{(1,2,4)}] \\ & + \frac{X_1 X_2 X_5}{X_1 + X_2 + X_5} [X_1 \theta_1^{(1,2,5)} + X_2 \theta_2^{(1,2,5)} + X_5 \theta_5^{(1,2,5)}] \\ & + \frac{X_1 X_3 X_4}{X_1 + X_3 + X_4} [X_1 \theta_1^{(1,3,4)} + X_3 \theta_3^{(1,3,4)} + X_4 \theta_4^{(1,3,4)}] \\ & + \frac{X_1 X_4 X_5}{X_1 + X_4 + X_5} [X_1 \theta_1^{(1,4,5)} + X_4 \theta_4^{(1,4,5)} + X_5 \theta_5^{(1,4,5)}] \end{aligned}$$

(C ont.)

$$\begin{aligned}
& + \frac{X_1 X_3 X_5}{X_1 + X_3 + X_5} \left[X_1 \theta_1^{(1,3,5)} + X_3 \theta_3^{(1,3,5)} + X_5 \theta_5^{(1,3,5)} \right] \\
& + \frac{X_2 X_3 X_4}{X_2 + X_3 + X_4} \left[X_2 \theta_2^{(2,3,4)} + X_3 \theta_3^{(2,3,4)} + X_4 \theta_4^{(2,3,4)} \right] \\
& + \frac{X_2 X_3 X_5}{X_2 + X_3 + X_5} \left[X_2 \theta_2^{(2,3,5)} + X_3 \theta_3^{(2,3,5)} + X_5 \theta_5^{(2,3,5)} \right] \\
& + \frac{X_2 X_4 X_5}{X_2 + X_4 + X_5} \left[X_2 \theta_2^{(2,3,4)} + X_4 \theta_4^{(2,3,4)} + X_5 \theta_5^{(2,3,4)} \right] \\
& + \frac{X_3 X_4 X_5}{X_3 + X_4 + X_5} \left[X_3 \theta_3^{(3,4,5)} + X_4 \theta_4^{(3,4,5)} + X_5 \theta_5^{(3,4,5)} \right] \\
& + \frac{X_1 X_2 X_3 X_4}{X_1 + X_2 + X_3 + X_4} \left[X_1 \theta_1^{(1,2,3,4)} + X_2 \theta_2^{(1,2,3,4)} + X_3 \theta_3^{(1,2,3,4)} + X_4 \theta_4^{(1,2,3,4)} \right] \\
& + \frac{X_1 X_2 X_3 X_5}{X_1 + X_2 + X_3 + X_5} \left[X_1 \theta_1^{(1,2,3,5)} + X_2 \theta_2^{(1,2,3,5)} + X_3 \theta_3^{(1,2,3,5)} + X_5 \theta_5^{(1,2,3,5)} \right] \\
& + \frac{X_1 X_2 X_4 X_5}{X_1 + X_2 + X_4 + X_5} \left[X_1 \theta_1^{(1,2,4,5)} + X_2 \theta_2^{(1,2,4,5)} + X_4 \theta_4^{(1,2,4,5)} + X_5 \theta_5^{(1,2,4,5)} \right] \\
& + \frac{X_1 X_3 X_4 X_5}{X_1 + X_3 + X_4 + X_5} \left[X_1 \theta_1^{(1,3,4,5)} + X_3 \theta_3^{(1,3,4,5)} + X_4 \theta_4^{(1,3,4,5)} + X_5 \theta_5^{(1,3,4,5)} \right] \\
& + \frac{X_2 X_3 X_4 X_5}{X_2 + X_3 + X_4 + X_5} \left[X_2 \theta_2^{(2,3,4,5)} + X_3 \theta_3^{(2,3,4,5)} + X_4 \theta_4^{(2,3,4,5)} + X_5 \theta_5^{(2,3,4,5)} \right] \\
& + \frac{X_1 X_2 X_3 X_4 X_5}{X_1 + X_2 + X_3 + X_4 + X_5} \left[X_1 \theta_1^{(1,2,3,4,5)} + X_2 \theta_2^{(1,2,3,4,5)} \right. \\
& \quad \left. + X_3 \theta_3^{(1,2,3,4,5)} + X_4 \theta_4^{(1,2,3,4,5)} + X_5 \theta_5^{(1,2,3,4,5)} \right]
\end{aligned}$$

Equation (5.6) is a generalization of the model proposed by Kaufman for binary and ternary alloy systems and extended by Chochol to quaternary systems (25,13). The parameter $\theta_{n_i}^{(1,2\dots J)}$ is independent of composition but may assume a linear temperature dependence:

$$\theta_{n_i}^{(1,2\dots J)} = a_{n_i}^{(1,2\dots J)} + b_{n_i}^{(1,2\dots J)} \times T \quad (6.9)$$

It is seen from Equation (6.5) that the interaction among J components is modelled with J parameters. Thus the total number of parameters in the model for a solution phase is

$$Q = \sum_{J=2}^N J C_J^N \quad (6.10)$$

For a quinary system, $Q = 75$.

To determine the parameters for each phase ϕ , one begins with an investigation of the binary systems, then the ternary systems and so on. For example, investigation of each of the five quaternary sub-systems involves, for each phase ϕ , the evaluation of four parameters, with twenty-four parameters in the model having been determined from prior investigation of the binary and ternary systems which comprise each quaternary system.

Equation (6.7) has several convenient properties. If the parameters are set equal and independent of temperature, Equation (6.7) is reduced to the regular solution model of the interactions among J components:

$$\Delta G^{E,\phi} \approx \theta(1,2,\dots,J) \prod_{i=1}^J X_i \quad (6.11)$$

The regular solution model is justified over a specified composition and temperature range by the criterion that the calculated differs from the experimental phase diagram within the experimental accuracy of the phase diagram. This assumption has reduced greatly the number of parameters to be evaluated in the model of the solution phases in the Fe-Cr-Mn-Ni-C system.

6.2. Methods to Determine Thermodynamic Parameters from Phase Diagrams

The equations governing chemical equilibrium of alloy systems are transcendental and non-linear in the independent variables. But, more importantly, the solution matrix is implicit. This fact prevents the evaluation of parameters from a regression on the solution matrix.

Nonetheless, it is theoretically possible to apply mathematical methods to determine parameters in the model of the integral free energy of a system of coexisting phases from experimental knowledge of compositions and temperatures of the equilibrium. I chose to consider the case of equilibrium between two solution phases.

A distinction is made between a hypothetical case in which the experimental tie-lines, the model of thermodynamic interactions of each phase, and the relative phase stabilities are known exactly, and the more realistic case in which there is some error in the experimental determination of the tie-lines and choice of the interaction model. In the hypothetical case, the system of equations of equal chemical potentials

is in fact, a mathematical function of m independent parameter variables and n independent composition and temperature variables. However, in order that the solution matrix agrees with the concentration matrix of the experimental tie-lines, each of the m parameter variables must assume a specific value.* Conversely, the m parameters could be calculated by resolving a system of m independent equations which are, in fact, the system of equations of equal chemical potentials in which the composition and temperature independent variables assume m specific values. Since the two phase equilibrium is a continuum ($J > 1$) there are more than m specific values of the n composition and temperature variables from which to choose.

From the above analysis, several points become evident. The parameters evaluated from the tie-lines determined experimentally may assume a range of values if: (1) there is uncertainty in the experimental data, (2) the model is not suitable or (3) both the data and the model are in error. That is, as the error in the experimental data or in the model is increased to such magnitude that each parameter assumes a value which differs significantly for each group of m experimental tie-lines selected, the system of equations becomes "overdeterminant" and the calculated parameters are no longer meaningful.

*The parameters assuming a range of values would imply uncertainty in the model or would imply that thermodynamic behavior of a solution could be modeled exactly with more than one model, which is an absurdity!

Tiller has proposed a method to obtain thermodynamic parameters from data on two-phase equilibria in binary alloy systems (77-79). The method involves a series expansion of a function of the chemical potential in both composition and temperature. By selection of coefficients in the expansion, a number of interaction models were considered; among them, the regular solution, quasi-regular solution and the Margules models. The number of tie-lines selected (each at a different temperature) is equal to the degrees of freedom of the resulting set of equations.

Another method, applicable to the present study, has already been mentioned. The parameters $(1, 2, \dots, J)$ in Equation (6.11) may be evaluated by solving the system of Equation (4.16) in which the P independent parameter variables are evaluated as a function of P tie-lines determined experimentally.* If many experimental tie-lines are available, the parameters are evaluated from more than one set of P tie-lines and the average value and standard deviation of each parameter determined.

The discrepancy between calculated and experimental tie-lines suggests several indirect methods to obtain the thermodynamic parameters. Two procedures have been developed on the basis of minimization of the discrepancy with respect to the parameter variables in the model. Tiller has employed a linear program to obtain thermodynamic parameters from the simultaneous analysis of tie-lines and thermochemical data of binary systems (81). The objective function is defined in terms of the

* For two-phase equilibrium Equation (6.11) assumed as a model for each phase, would require $P=2xJ$ parameters to be determined.

discrepancy between experimental and calculated tie-lines. The thermochemical data occur in constraint equations. Nishizawa et al. have applied this procedure on two-phase equilibria in ternary systems (81). The second method, attributed to Sillem, has been applied by Uhrenius on ternary and quaternary two-phase equilibria (82, 83). This method consists of searching for parameters that minimize the square of the discrepancy between calculated and experimental tie-lines. To aid in the search, the mathematical relationship between the square of the discrepancy and the P parameters is approximated by a P-dimensional paraboloid. The minimum of the paraboloid is taken as the "best-set" parameters.

The first two methods are restrictive on two accounts. Application of either of these methods to modeling of tie-lines in multicomponent systems requires a specific number of tie-lines. But, more importantly, both methods have the disadvantage that the experimental tie-line must be known with respect to all components and that the composition of both phases must be known to the same level of accuracy.

The third and fourth methods have the advantage that parameters are evaluated on the basis of the accuracy of the composition of both phases of the tie-lines. In addition, the parameters are based on only one phase boundary for the case when surfaces of saturation but not the tie-lines are available, or based on only one component of the tie-lines which may be known more precisely. These methods, furthermore, are easily adopted to modeling of other types of hypercomodes where data may be available; e.g., tie-triangles of the peritectic volume. Parameters

of the model of a solution phase common to several equilibria can be evaluated from the simultaneous analysis of each equilibrium. In short, the third and fourth methods are more adapted to the realities of the phase diagram determined experimentally.

The fourth method was employed in the present study so that the parameters evaluated from analysis of tie-lines could be compared to parameters obtained from thermochemical measurements reported in the literature. In addition, the means to establish the statistical significance of the parameters are well defined in this method.

6.2.1. Optimization Procedure

The error-square sum U' is defined as a measure of the discrepancy between a set of experimental and calculated quantities:

$$U' = \sum_i^M \sum_j^R \sum_k^{J-1} W'_{ijk} [X_{ijk}^{Exp} - X_{ijk}^{Cal}]^2 \quad (6.12)$$

where

J is the number of components of the subsystem,
($J = 2, 3, \dots, N$)

R designates the phase boundaries

M is the total number of measured quantities

W'_{ijk} is the weighting factor

X_{ijk}^{Exp} is the measured quantity

X_{ijk}^{Cal} is the element of the solution matrix corresponding to
 X_{ijk}^{Exp} in the concentration matrix.

The quantity X_{ijk}^{Cal} is an implicit function of the parameters, consequently, U' is also an implicit function of the parameters. The procedure is to search for the parameters that give the global minimum of U' . Mathematically, this corresponds to:

$$\left. \frac{\partial U'}{\partial \theta^r} \right|_{\substack{j=1,2,\dots,P \\ r \neq j}} = 0 \quad (6.13)$$

In order that minimum of the error-square sum be unique; that is, that the evaluated parameters define a global minimum, the following conditions hold:

1. The functional relationship between experimental and calculated quantities is correct.
2. Experimental errors are random and follow a Gaussian distribution.
3. The weighting factor W_{ijk} is a measure of the inherent experimental accuracy of the set of experimental quantities.

Violation of these conditions can cause the error-square sum to exhibit several minima, or at the extreme, valleys in which the minimum cannot be distinguished with respect to each parameter. This is usually the case if the functional relationship is incorrect, in which case, the parameters are not independent. Differences among phase diagrams of an alloy system calculated from different interaction models of the solution phases, i.e., different functional relationships, are usually on the order of the experimental error. In this case, the error-square sum can be used as a criterion to assess different interaction models.

In the modelling of experimental data in general, condition (1) is usually assumed because of its simplicity. However, Beers has pointed out that there is no statistical means by which random error could be distinguished from systematic error (84). To determine the extent of systematic error in the present study, the results were checked against those obtained by other investigators when available (Chapter 7).

Condition (3) is important when the compositions of the experimental quantities have been determined at different levels of accuracy. The accuracy at which a phase diagram is known can itself depend on composition and temperature. The rationale by which the weighting factor is defined is based on a statistical analysis of the experimental quantities and is developed in the next section.

6.2.1.1. Calculation of the Weighting Factor

The solution matrix to the system of Equations (4.16) is a hyperconode (tie-line, tie-triangle, etc.) at a constant temperature and pressure; that is, temperature and pressure are not considered variable during convergence to the solution. Consequently, in the comparison of calculated and measured quantities, errors in the measurement are treated only as an error in the composition variable at each temperature. This is illustrated schematically in Figure (6.1) for the case of equilibrium between two phases.

Equilibrium between two phases at constant T and P consists of two phase boundaries joined by at least one tie-line. In the analysis of the weighting factor, the phase boundaries are considered separately.

The "calculated" isotherm in Figure (6.1) is an implicit function

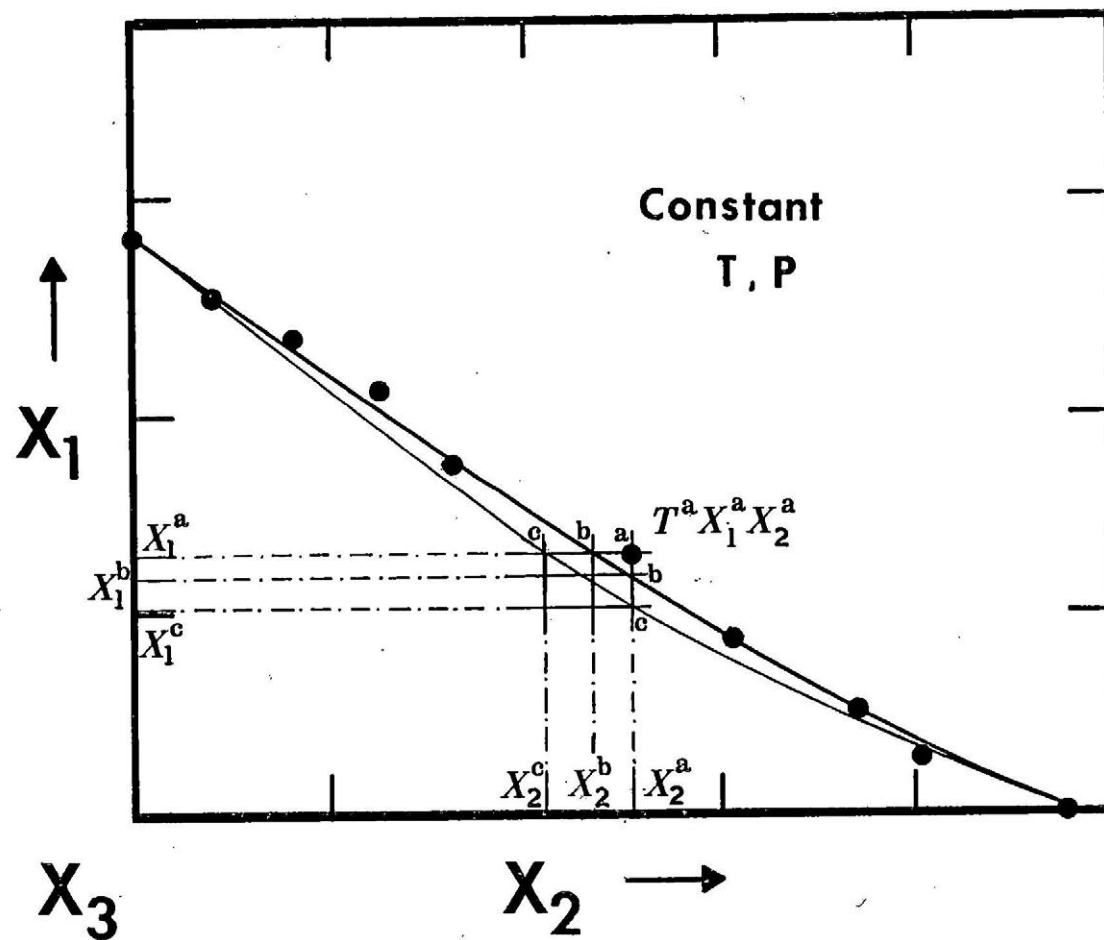


Figure 6.1 - The experimental and calculated isotherms of a surface of saturation in the ternary system X_1 - X_2 - X_3 at T_A

of the parameters of the model under consideration. The "true" isotherm is taken as the calculated isotherm which is the best fit of the experimental points measured at T_A . The discrepancies between the true isotherm at T_A and the measured point (T_A, X_1^A, X_2^A) are $X_1^A - X_1^B$ and $X_2^A - X_2^B$ for component 1 and 2 respectively. For ternary systems, the discrepancy of component ($k = 2,3$) averaged over M data points is:

$$\overline{\Delta D}_k = \frac{1}{M} \sum_{i=1}^M (X_{ik}^A - X_{ik}^B)^2 / (M-1) \quad (6.14)$$

For quaternary systems, $\overline{\Delta D}_k$ is taken as the maximum discrepancy between the data point and the phase boundary surface at T_A for each component, averaged over all data points at T_A . For data located on phase boundary J , the average weighting factor \overline{w}_{jk} is defined as the reciprocal of the square of the average discrepancy $\overline{\Delta D}_{jk}$

$$\overline{w}_{jk} \equiv \left(\frac{1}{\overline{\Delta D}_{jk}} \right) \quad \begin{array}{l} j = 1, R \\ k = 2, 3 \end{array} \quad (6.15)$$

\overline{w}_{jk} is a constant and since the position of the global minimum with respect to the parameters is independent of any constant multiplying itself, the weighting factor and the error-square sum is re-defined:

$$U \equiv \sum_{i=1}^M \sum_{j=1}^R \sum_{k=1}^{N-1} W_{jk} (X_{ijk}^{Cal} - X_{ijk}^{Exp})^2 \quad (6.16)$$

and

$$W_{jk} \equiv \frac{\overline{w}_{jk}}{\overline{w}_{j2} + \overline{w}_{j3}} \quad (6.17)$$

The problem still remains to select the quantity \bar{w}_{jk} since the true isotherm is not known a priori. This problem is circumvented for ternary systems by the following procedure: The quantity \bar{w}_{jk}' is defined

$$\bar{w}_{jk}' \equiv \left(\frac{M-1}{\sum_{i=1}^M \frac{A}{X_{ijk}} - X_{ijk}} \right)^2 = \left(\frac{M-1}{\sum_{i=1}^M \frac{\text{Exp}}{X_{ijk}} - X_{ijk}} \right)^2 \quad (6.18)$$

The assumption is made:

$$\frac{\bar{w}_{jk}}{\bar{w}_{j2} + \bar{w}_{j3}} = \frac{\bar{w}'_{jk}}{\bar{w}'_{j2} + \bar{w}'_{j3}} \quad (6.19)$$

which is equivalent to assuming that the "slope" of the calculated isotherm is in general nearly the same as the true isotherm T_A . This assumption was shown to be satisfactory by a perturbation analysis of the model.

6.2.1.2. Linear Functional Relationship

Sillén has applied a least square analysis on a linear functional relationship between measured and calculated quantities (82). From this analysis, he derived an analytic relationship between the error-square sum and parameters in a general linear equation. For this special case, U is found to be a quadratic function of the parameters. The procedure to determine the constants that describe the $U-\theta_r$ ($r=1,P$) surface is termed Pit-Mapping. The surface is a P -dimensional paraboloid described by the following expression:

$$U = C_0 + 2 \sum_{r=1}^P C_{0r} X_r + \sum_{r=1}^P \sum_{s=1}^P C_{rs} X_r X_s \quad (6.20)$$

where C_o , C_r and C_s are the constants that describe the paraboloid.

X_r is the deviation variable; i.e., the difference between the variable parameter θ_r and the approximate set (starting values) θ_r' .

The constants are evaluated from a set of equations determined from the specification of $(1/2)(P+1)(P+2)$ values of X_r in Equation (6.20). The minimum X_r^* is determined by solving the following system of equations:

$$\left. \frac{\partial U}{\partial X_r} \right|_{\substack{r \neq S \\ S=1,P}} = \sum_{S=1}^P \sum_{r=1}^P X_r C_{rs} + C_{or} = 0 \quad (6.21)$$

The solution is:

$$X_r^* = \frac{P}{\sum_{S=1}^P} \frac{P}{\sum_{r=1}^P} |C_{os}| |C_{rs}| |X| |C|^{-1} \quad (6.22)$$

where $|C|$ is the determinant of the constants C_{rs} and $|C_{rs}|$ is the sub-determinant corresponding to C_{rs} .

The best-set parameter is $\theta_r = X_r^* + \theta_r'$ ($r=1,P$). At the minimum (at $X_r = X_r^*$), the standard deviation of the measured quantities is defined as:

$$\sigma^2 (X_{ijk}^{\text{Exp}}) \equiv \frac{U_{\min}(X_r^*)}{M-P} \quad \begin{array}{l} i = 1, 2, \dots, M \\ j = 1, 2, \dots, R \\ k = 1, 2, \dots, J-1 \end{array} \quad (6.23)$$

where M is the number of measured quantities

R designates the phase boundaries

J is the number of components

P is the number of parameters

Sillén then defines a supercurve called the D-boundary, where

$$U_D = U_{\min} + \sigma^2(X_{ijk})$$

The standard deviation of the parameters is defined as the maximum difference between θ_r^* and the values θ_r which map out the D boundary:

$$\sigma(\theta_r^*) \equiv \left| \text{Max } \theta_r^P - \theta_r^* \right| \quad (6.24)$$

For the case of a linear functional relationship between the calculated and the measured quantities, it is found that

$$\sigma(\theta_r^*) = \sqrt{\frac{||C_{rr}|| U_{\min}}{||C|| (M-P)}} \quad (6.25)$$

Equation (6.25) is easily derived from Equation (6.20) to (6.23). Its simplicity is due principally to the quadratic dependency of U on θ_r . It is pointed out that $\sigma(X_r^*)$ is a function of only the second-order constants C_{rr} .

6.2.1.3. Non-linear Functional Relationship

For non-linear systems of equations, U may be a very complicated function of θ_r ; nonetheless, U can be expanded as a power series about the minimum:

$$* \quad \frac{\partial U}{\partial \theta_r} \Big|_{\substack{r \neq S \\ S=1,P}} = 0; \text{ hence, } \sum_r^P C_{rdr} = 0$$

$$U - U^* = \sum_r^P C_{rdr} + \sum_r^P \sum_s^P C_{rsdrds} + \sum_r^P \sum_s^P \sum_t^P C_{rst} drdsdt \quad (6.26)$$

where C_{rs} and C_{rst} are constants that describe the curvature of U at the minimum and dr is the deviation variable equal to $\theta_r - \theta_r^*$. For U close to the global minimum, the influence of the higher-order terms in Equation (6.26) is diminished; that is, near U_{\min} , $\langle dr ds dt \rangle / \langle dr ds \rangle$. Thus, for the initial set of parameters chosen close to the minimum, the curvature of the error surface could be described approximately by employing only the second-order terms. This assumption is equivalent to fitting the error surface to a P -dimensional paraboloid. The procedure, therefore, is to model the error-square sum, Equation (5.17), using the equation of a paraboloid, Equation (6.20). For the case of a linear functional relationship, the global minimum is found in one calculation; for the case of a system of non-linear functional relationships, the global minimum is approached iteratively by the substitution of improved estimates of the parameter θ_r^* in subsequent calculations. Convergence is defined by one of the following criteria at the n th iteration:

$$|U_n(\theta_{r,n-1}^*) - U_{n-1}^*(\theta_{r,n-2}^*)| \leq \epsilon \quad (6.21a)$$

$$|\theta_{r,n}^* - \theta_{r,n-1}^*| \leq \epsilon_r \quad (6.21b)$$

where ϵ and ϵ_r are specified residuals. At the n th iteration, the constants C_o , C_r and C_{rs} are re-evaluated in a closer vicinity to the global minimum. If the pit is observed to be skewed, the constants are evaluated at the D boundary so that the diameter of the paraboloid at U_D is the maximum width of the D boundary. Equation (6.25) is again solved

to obtain the standard deviations of the parameters.

In order that Equation (6.27) could be satisfied in the present study, the initial set of approximate parameters θ_r' had to be chosen in the vicinity of the minimum. An optimization procedure called "Direct Search" was developed to achieve this purpose.

6.2.1.4. . . . Direct Search

It is possible to map out the error surface as a function of parameters to reveal the approximate location of the global minimum. However, development of such a map covering all possible values of the parameters would be a lengthy procedure. Nonetheless, the approximate location of the global minimum could be reached by adjustment of the parameters (initially set to zero) in the direction of decreasing U . The basis for Direct Search is to compare directly the values of U for discrete changes in each of the parameters θ_r ($r=1,P$). For P parameters, U is evaluated at $(2P+1)$ test points:

$$U(\theta_r), U(\theta_r + \Delta\theta_r), U(\theta_r - \Delta\theta_r)$$

Of the $(2P+1)$ test points, the lowest value of U is selected and the parameters adjusted in the direction of the steepest descent. The optimization procedure moves at a "rate" specified by the increment $\Delta\theta_r$, hence, is best suited to reach the general vicinity of the global minimum from any location in the P -dimensional space. It is not suggested to actually find the global minimum since $\Delta\theta_r$ would need to be reduced considerably at each step near the minimum, resulting in a lengthy optimization procedure. Because there are no reasonable restrictions of

the maximum size if $\Delta\theta_r$. Direct Search is used to reach the minimum in few iterations, at which Equation (6.22), is applied to obtain the location of the minimum precisely.

CHAPTER 7RESULTS

The experimental results of the binary, ternary and quaternary systems are portrayed in this chapter. All temperatures (refer to the freezing point depression of pure iron ($\Delta T = 1538 - T$)). Figures 7.1 through 7.4 refer to the binary systems; Figures 7.5 through 7.19 refer to the ternary systems and figures 7.20 through 7.24 refer to the quaternary systems. Numerical listings of the experimental results are given in the appendix.

The results of the thermodynamic modeling are superimposed on each figure showing the experimental results. All calculated results in this chapter refer to the quasi-regular solution model. The relative phase stabilities assumed in the calculations and the parameters in this model are listed in Tables 7.1 through 7.4.

The regular solution simplification of the quasi-regular solution model, Equation (6.11), was assumed in the modelling of the interaction among three and among four components. This corresponds to the following equations stating the thermodynamic interaction among J components:

Binary Systems (J=2)

$$\Delta G_{ij}^{\phi, E} = \frac{X_i X_j (X_i \theta_i^{(i,j)} + X_j \phi_j^{(i,j)})}{X_i + X_j} \quad (7.1)$$

Ternary Systems (J=3)

$$\Delta G_{ijk}^{\phi, E} = X_i X_j X_k \theta^{(i,j,k)} \quad (7.2)$$

Quaternary Systems (J=4)

$$\Delta G_{i,j,k,l}^{\phi,E} = X_i X_j X_k X_l \theta^{(i,j,k,l)} \quad (7.3)$$

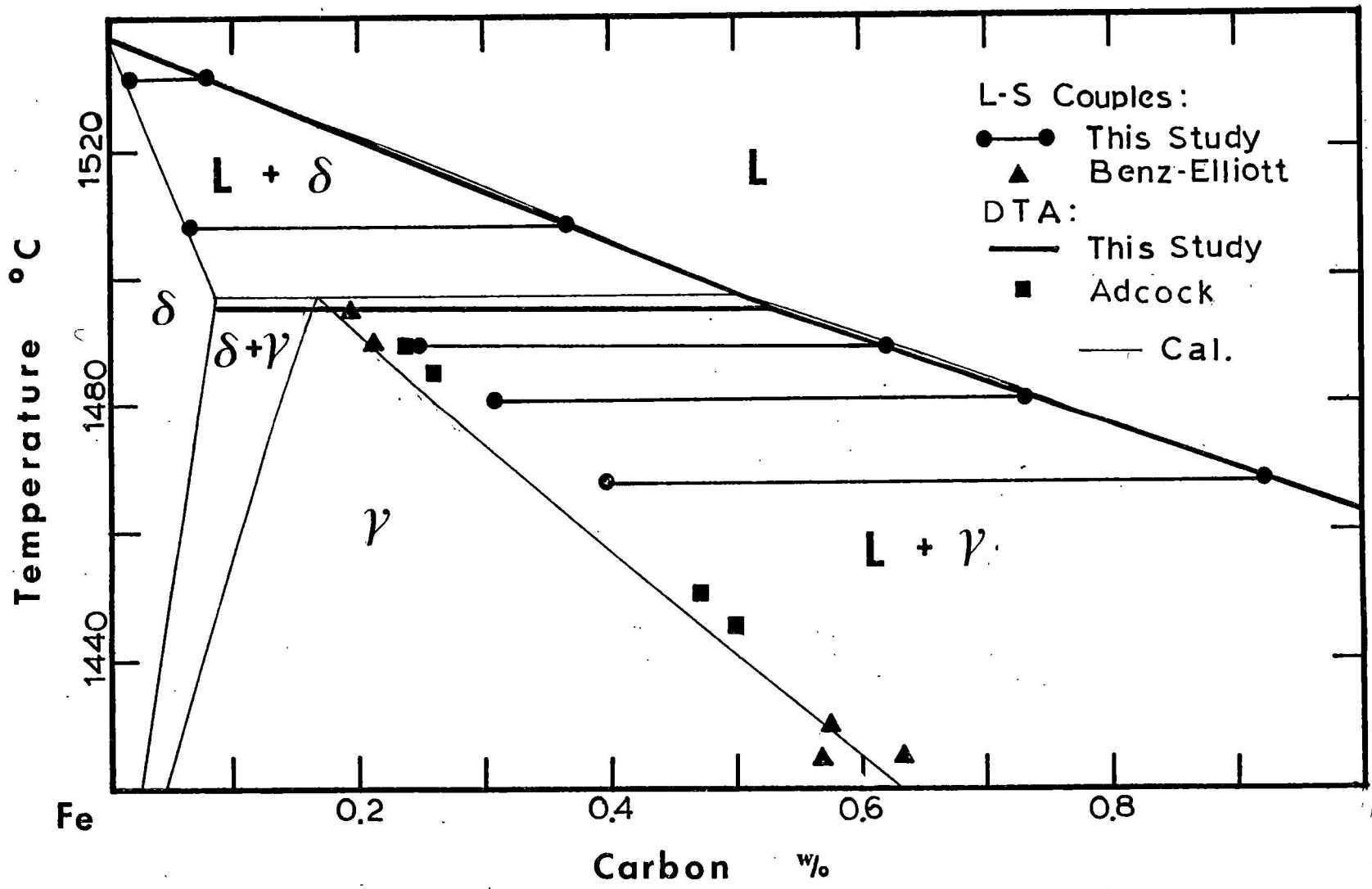


Figure 7.1 - The Fe-C system determined experimentally from equilibrium couples and DTA, and calculated by the model

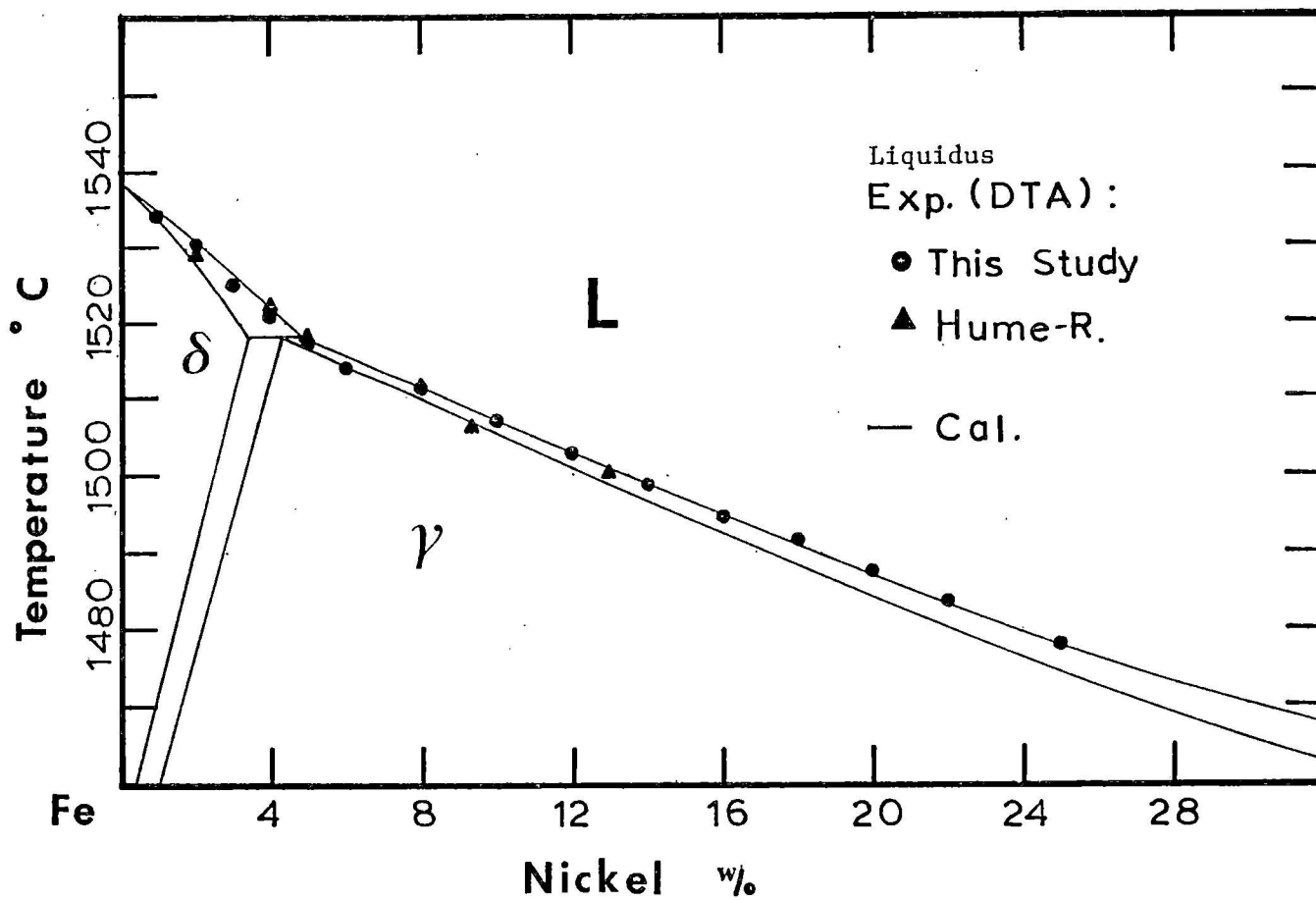


Figure 7.2 - The Fe-Ni system determined experimentally and by calculation

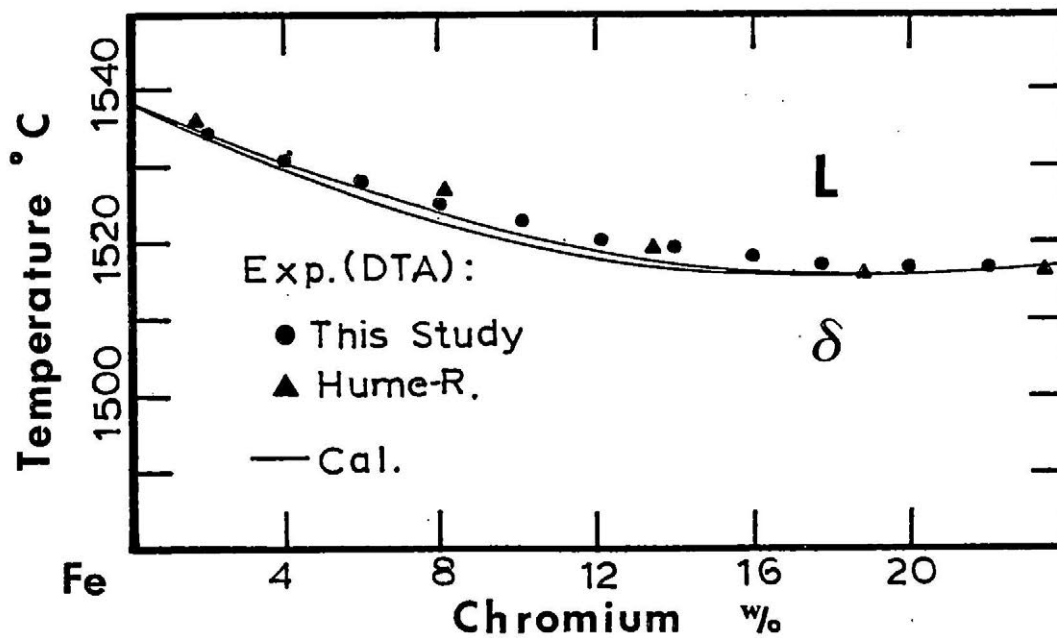
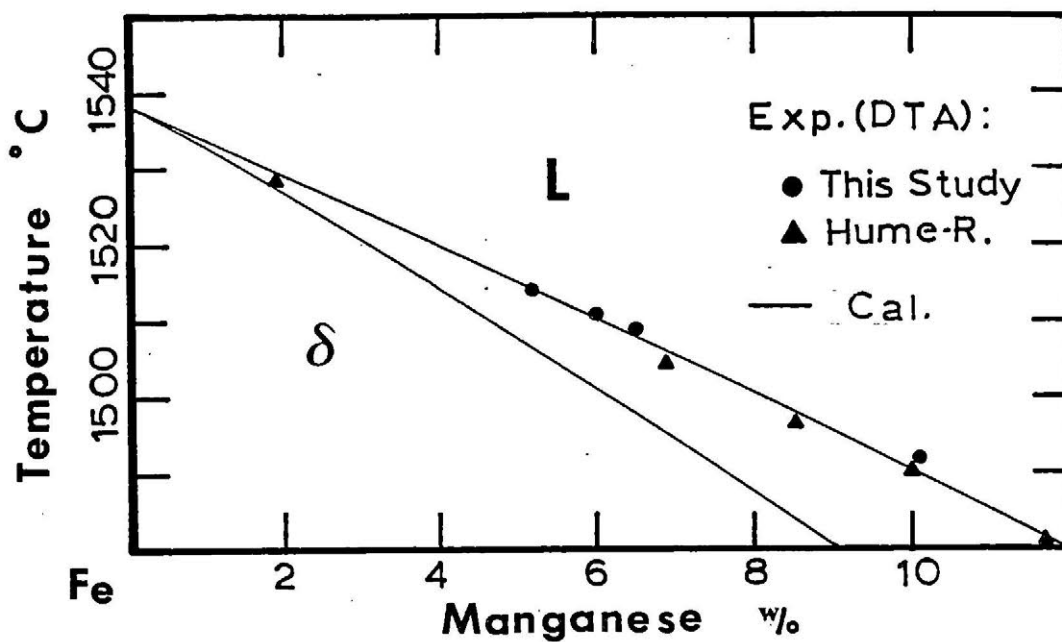


Figure 7.3 - The Fe-Mn and Fe-Cr systems determined experimentally and by calculation

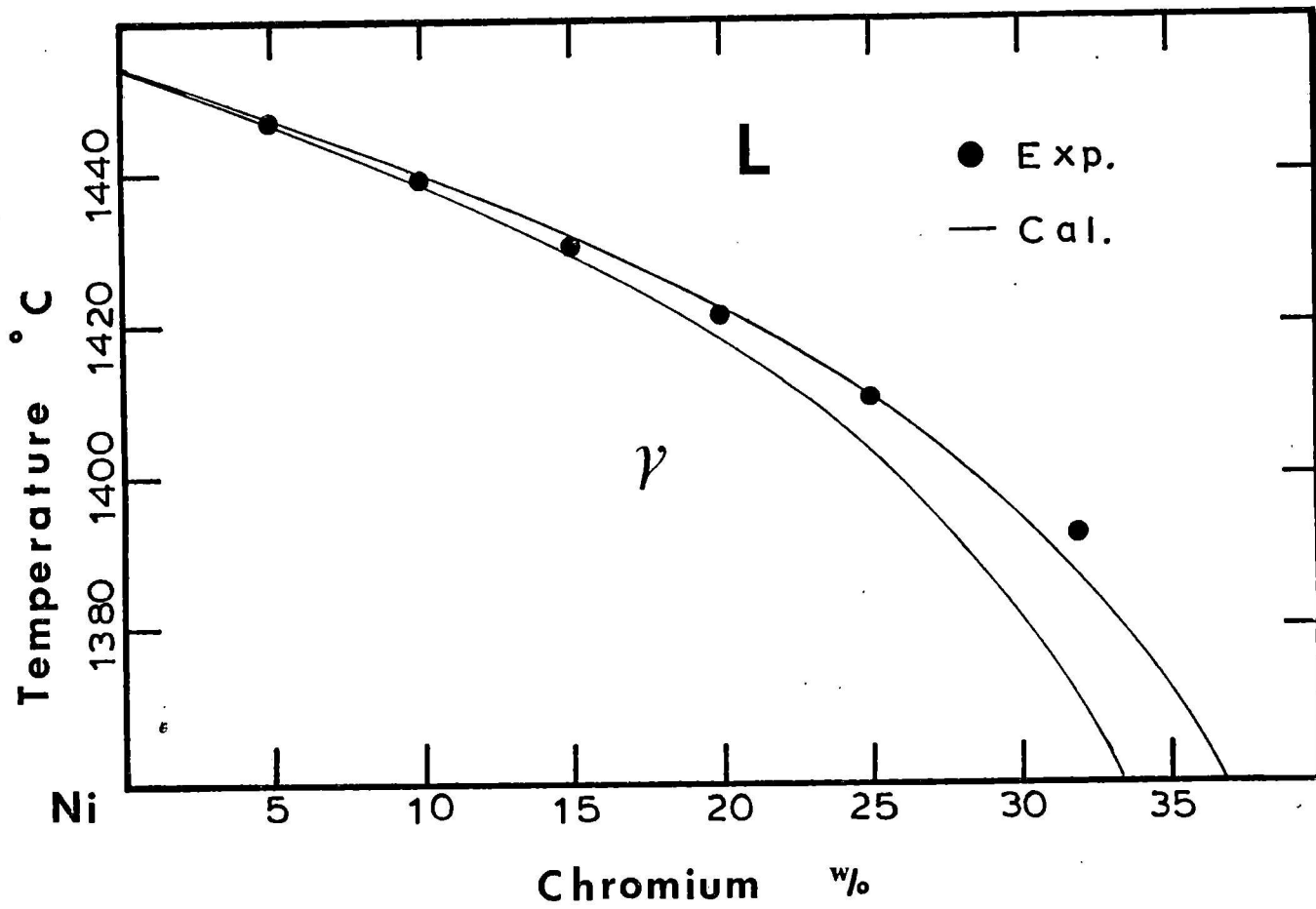


Figure 7.4 - The Ni-Cr system determined experimentally and by calculation

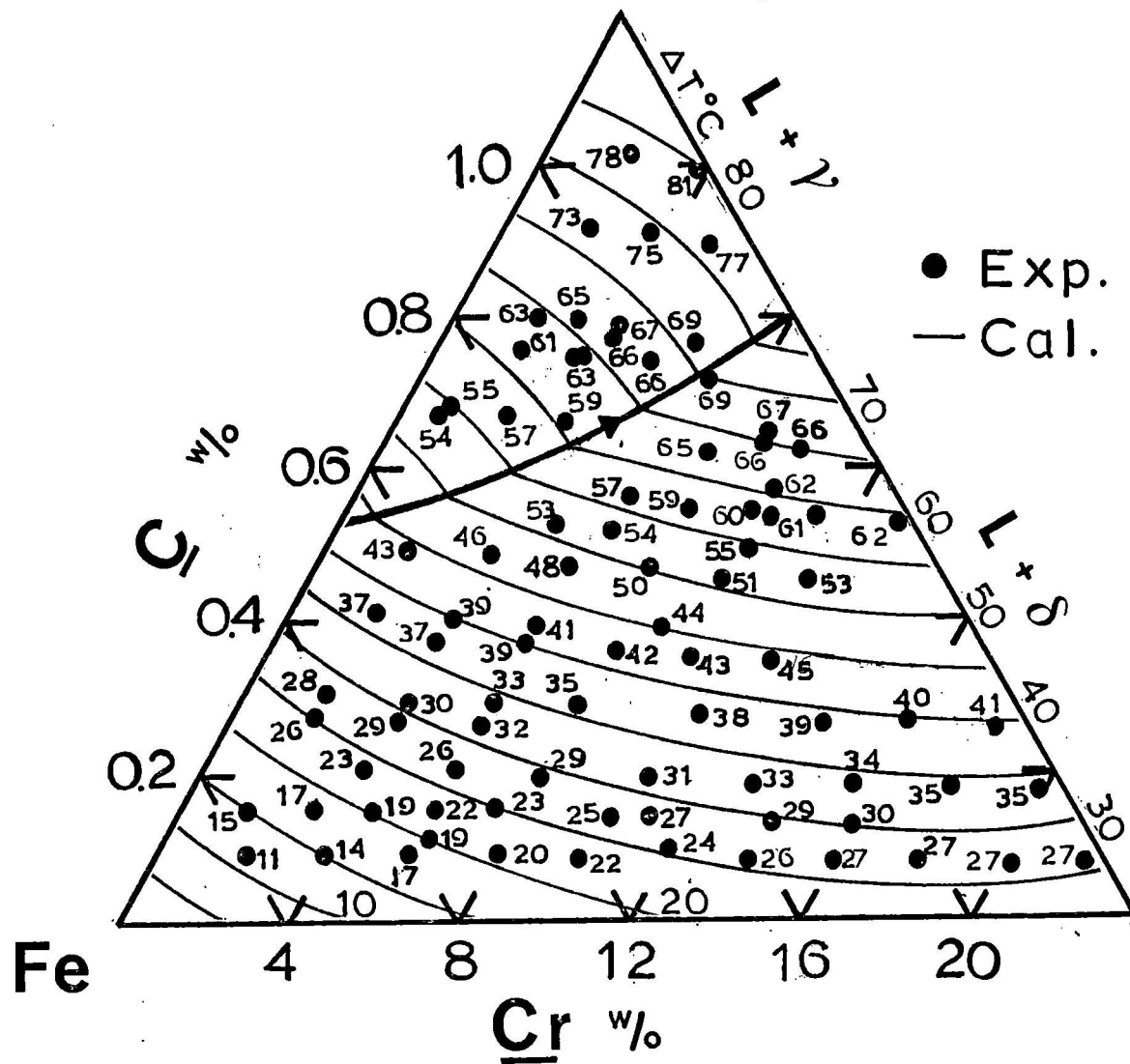


Figure 7.5 - The liquidus in the Fe-Cr-C system determined experimentally and by calculation

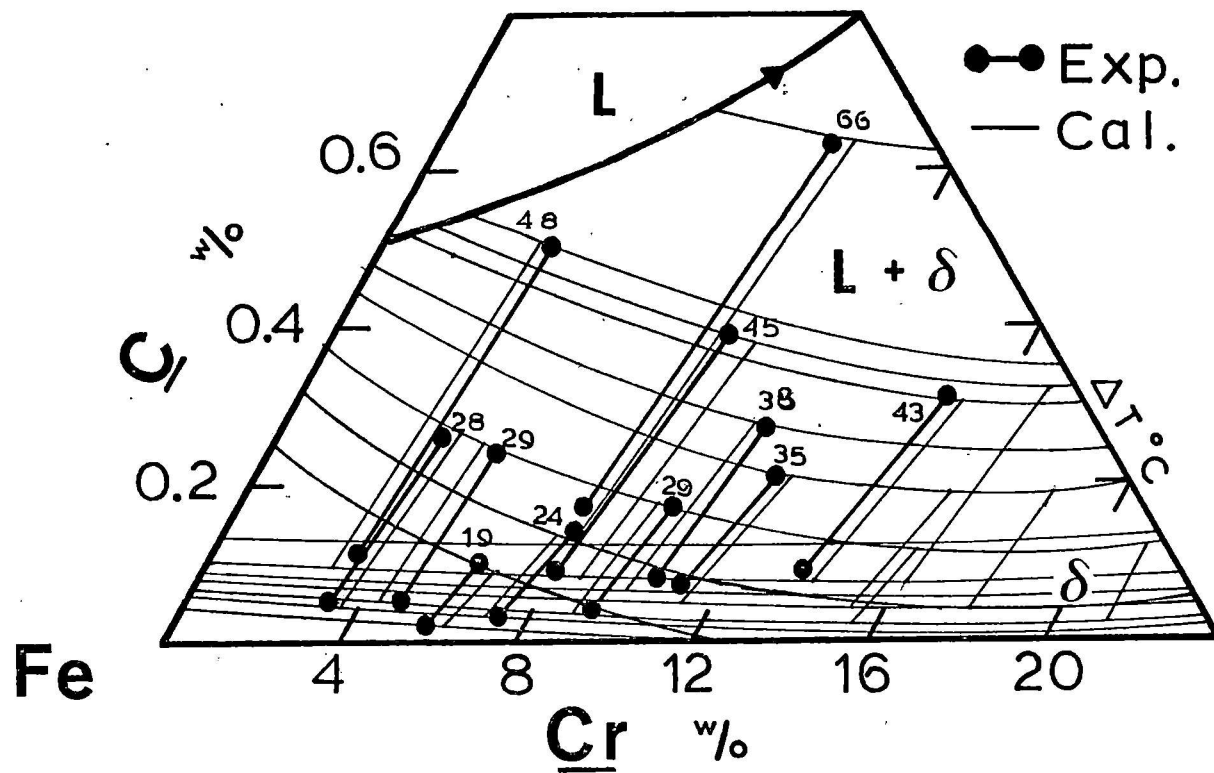


Figure 7.6 - The equilibrium between the liquid (L) and BCC (δ) phases in the Fe-Cr-C system determined experimentally and by calculation

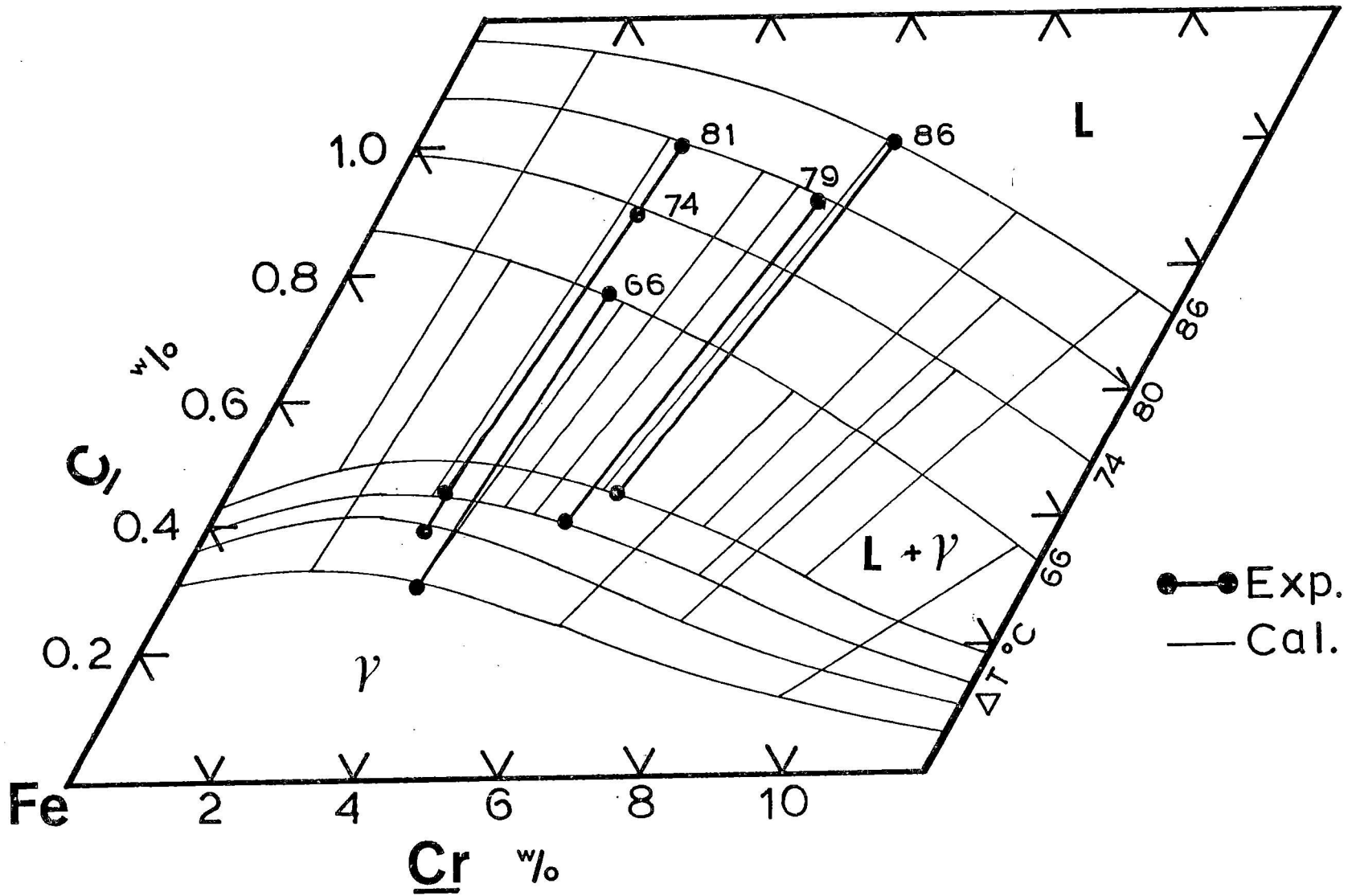


Figure 7.7 - The equilibrium between the liquid (L) and FCC (γ) phases in the Fe-Cr-C system determined experimentally and by calculation

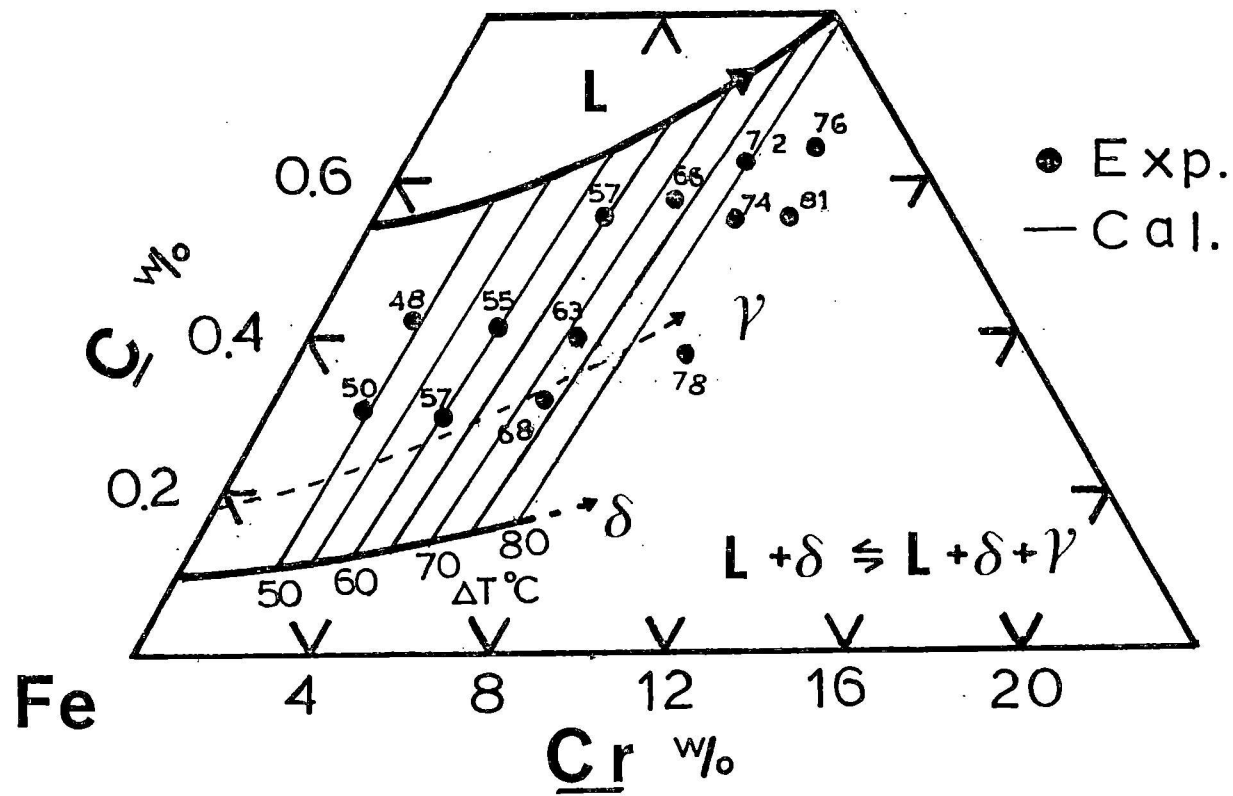


Figure 7.8 - The peritectic reaction in the Fe-Cr-C system determined experimentally and by calculation

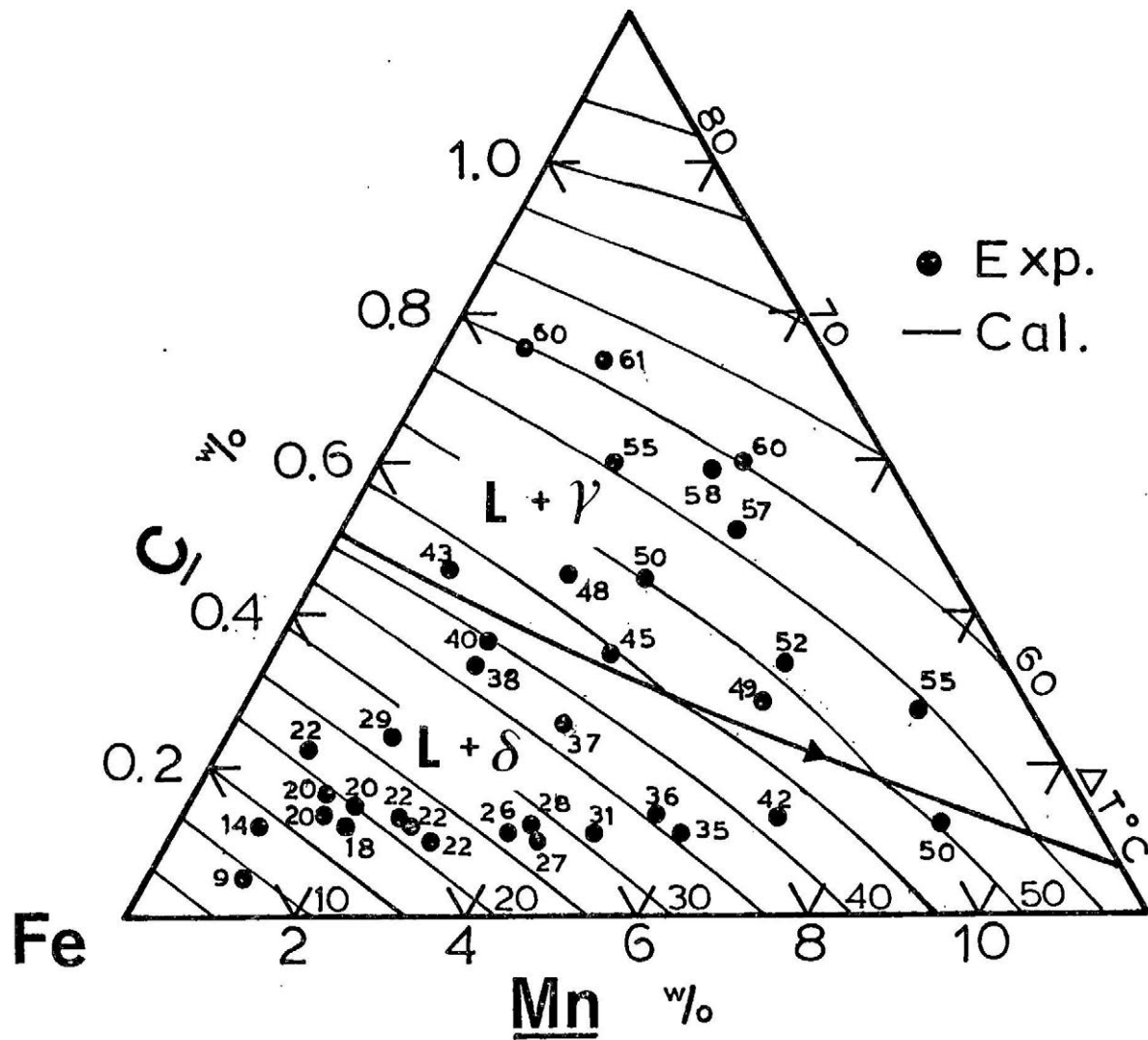


Figure 7.9 - The liquidus in the Fe-Mn-C system determined experimentally and by calculation

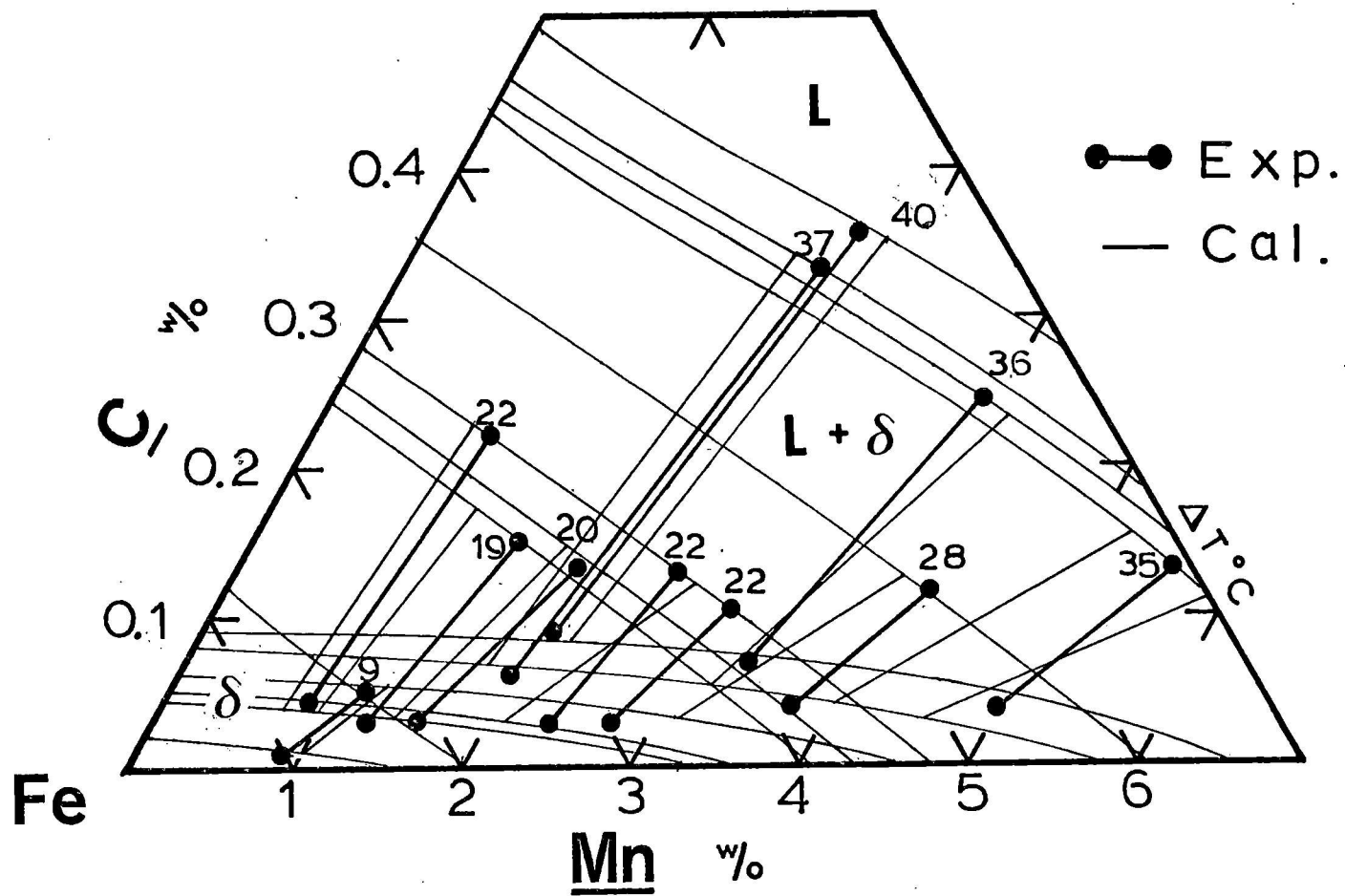


Figure 7.10 - The equilibrium between the liquid (L) and BCC (δ) phases in the Fe-Mn-C system determined experimentally and by calculation

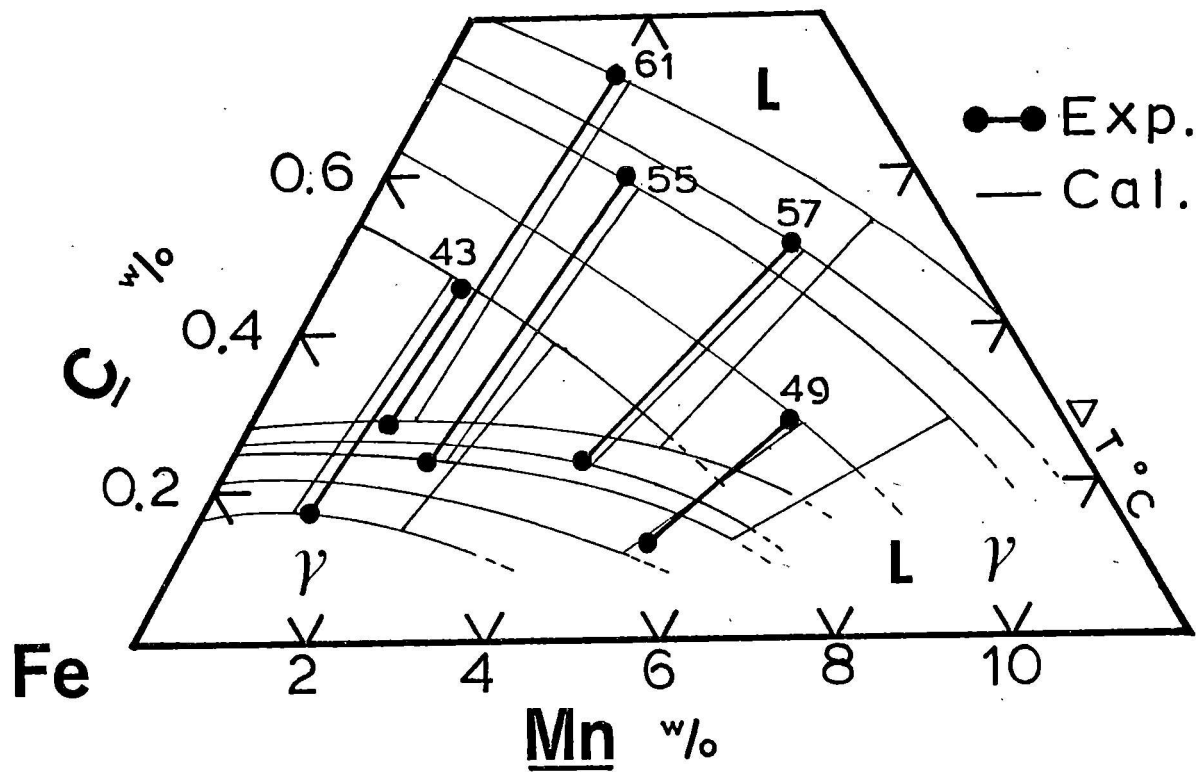


Figure 7.11 - The equilibrium between the liquid (L) and FCC (γ) phases in the Fe-Mn-C system determined experimentally and by calculation

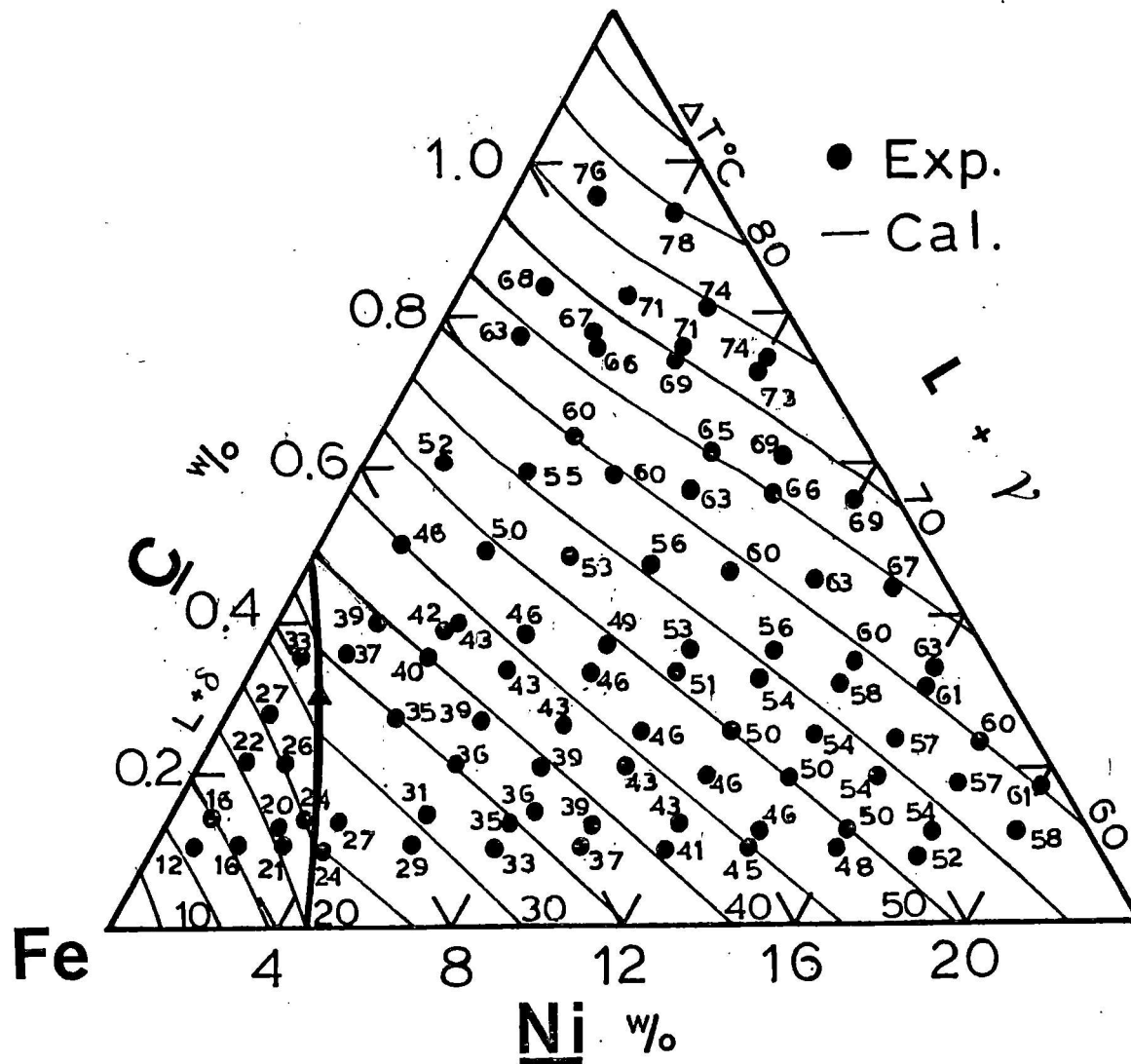


Figure 7.12 - The liquidus in the Fe-Ni-C system determined experimentally and by calculation

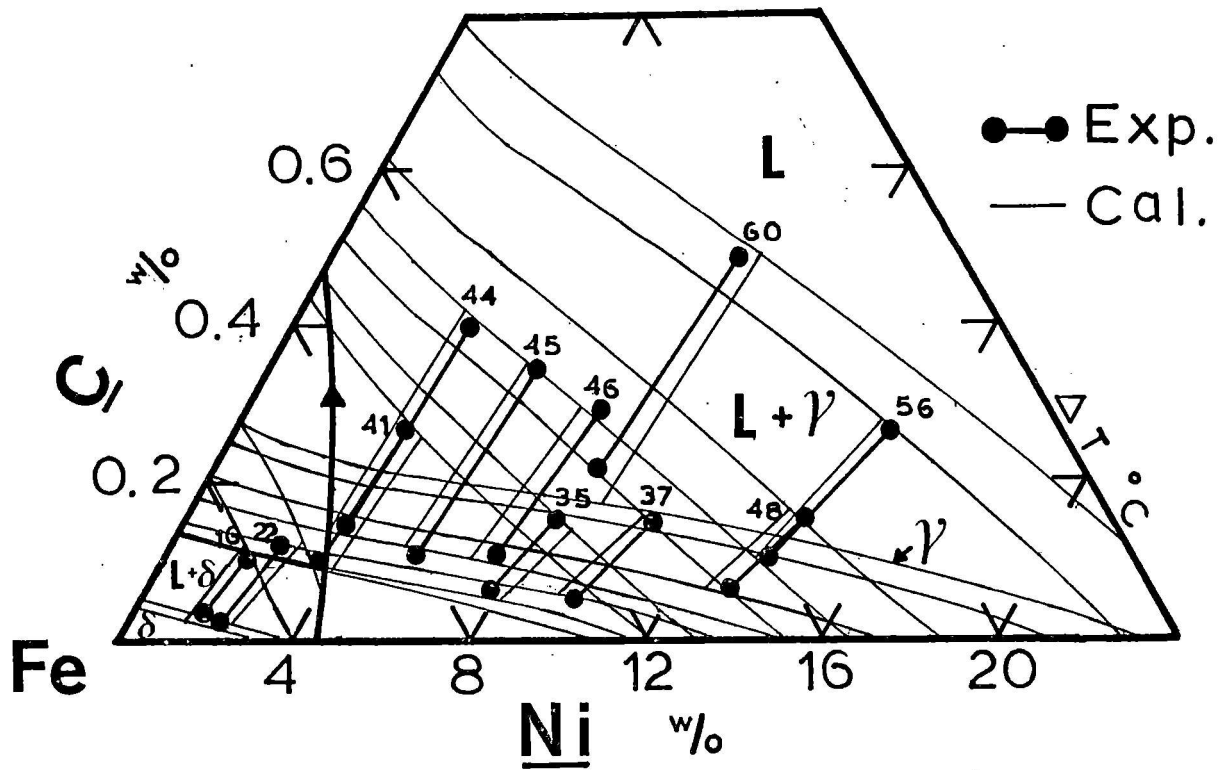


Figure 7.13 - The equilibrium between the liquid (L) and BCC (δ) phases and between the liquid and FCC (γ) phases in the Fe-Ni-C system determined experimentally and by calculation

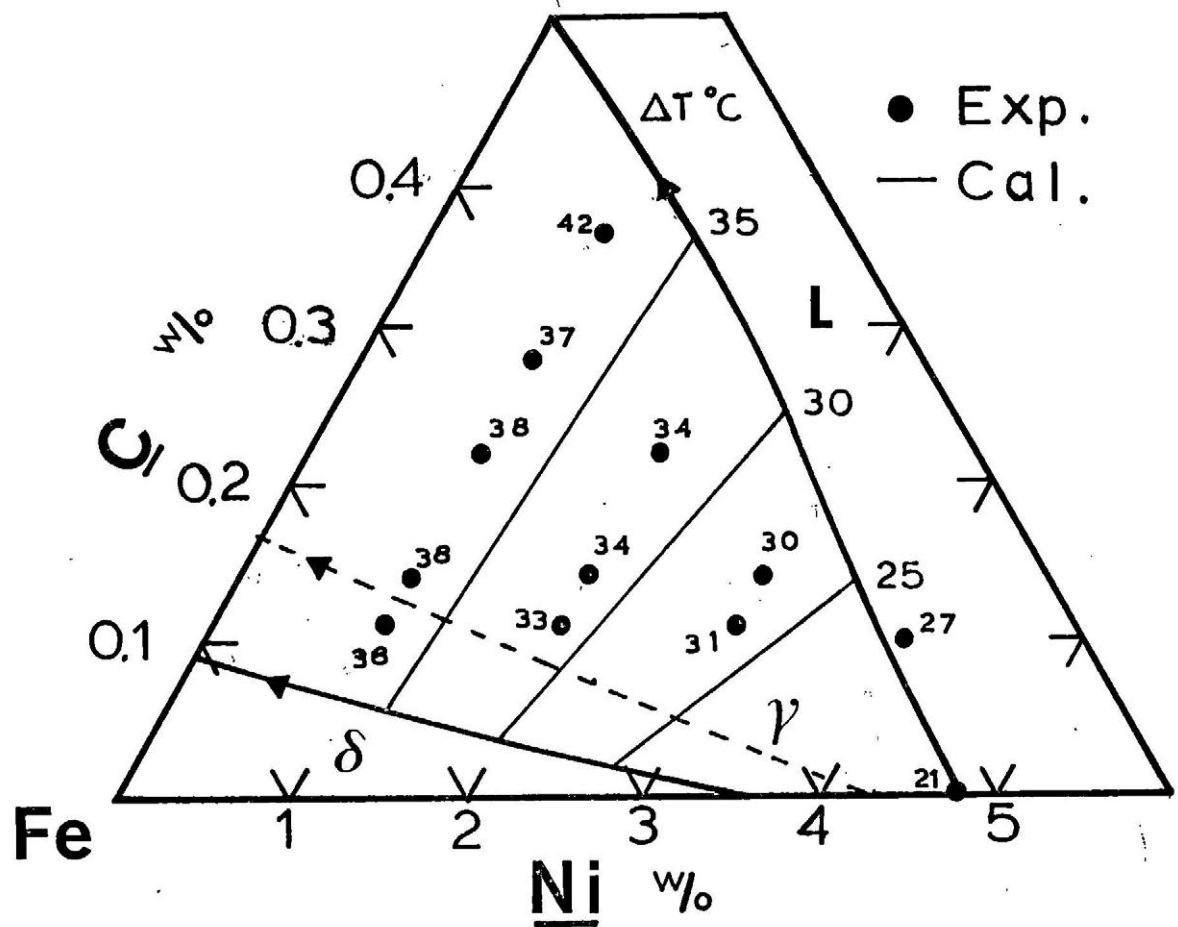


Figure 7.14 - The peritectic reaction $L + \delta \rightleftharpoons L + \gamma$ in the Fe-Ni-C system determined experimentally and by calculation

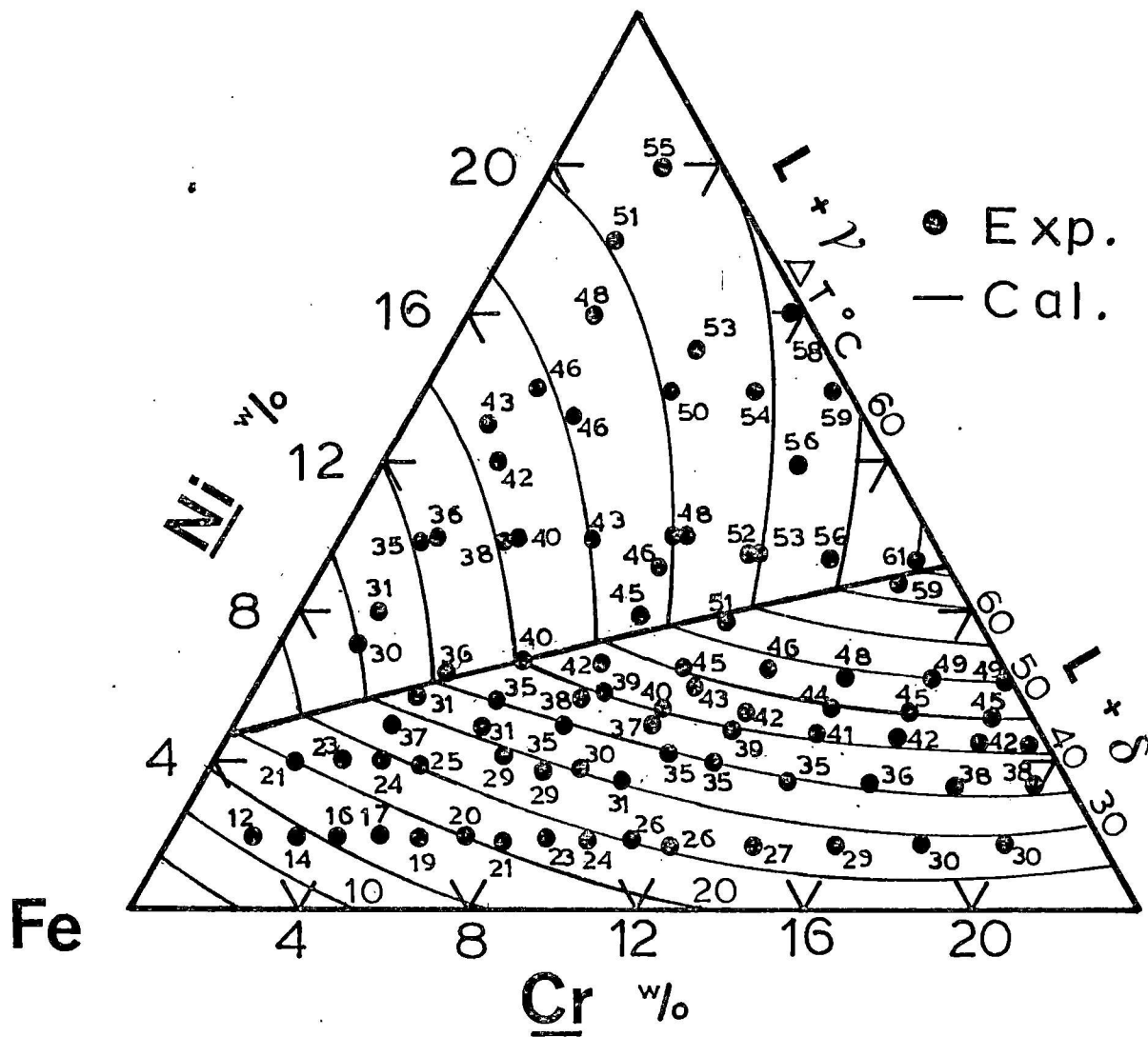


Figure 7.15 - The liquidus in the Fe-Cr-Ni system determined experimentally and by calculation

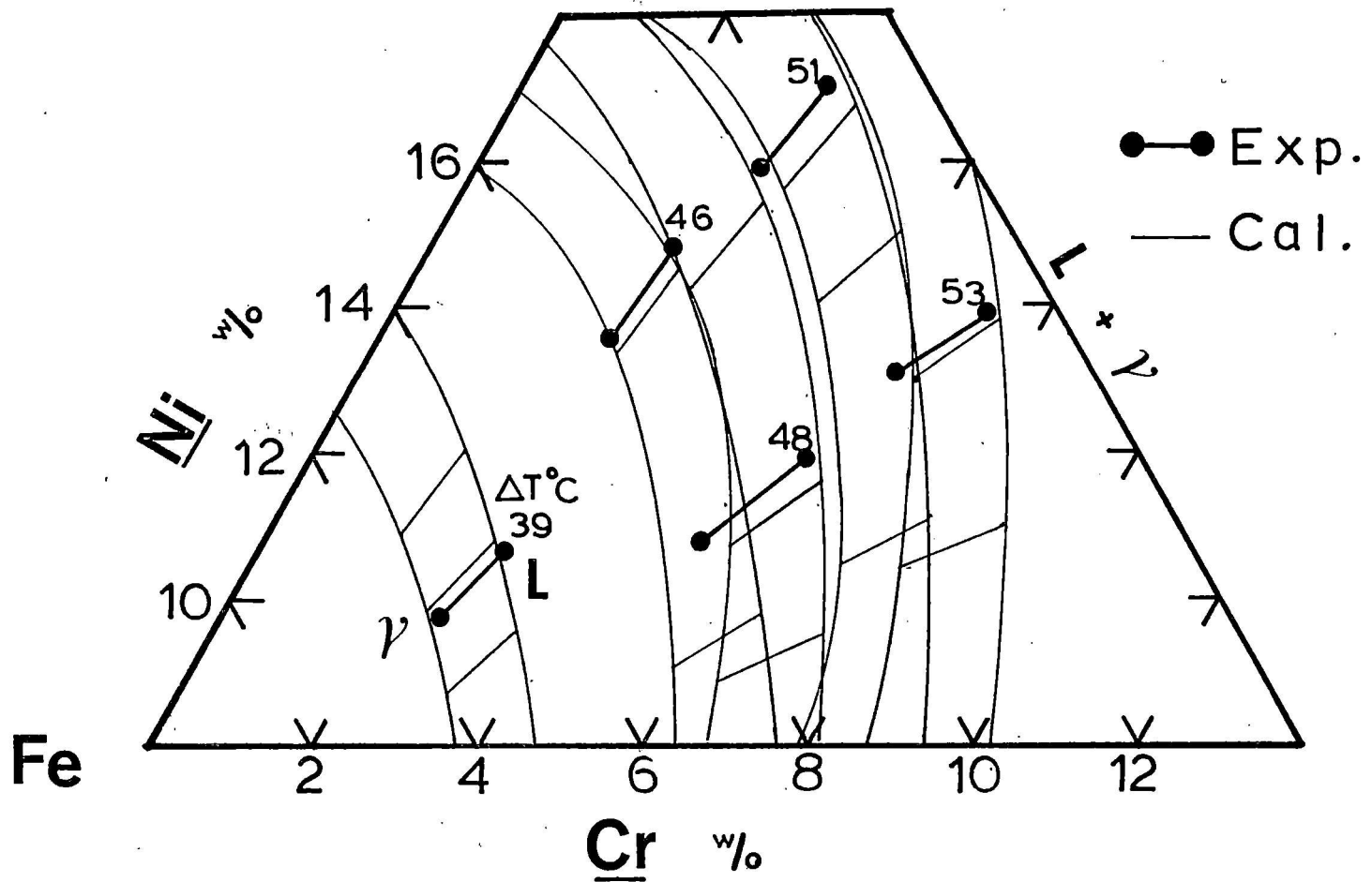


Figure 7.16 - The equilibrium between the liquid (L) and FCC (γ) phases in the Fe-Cr-Ni system determined experimentally and by calculation

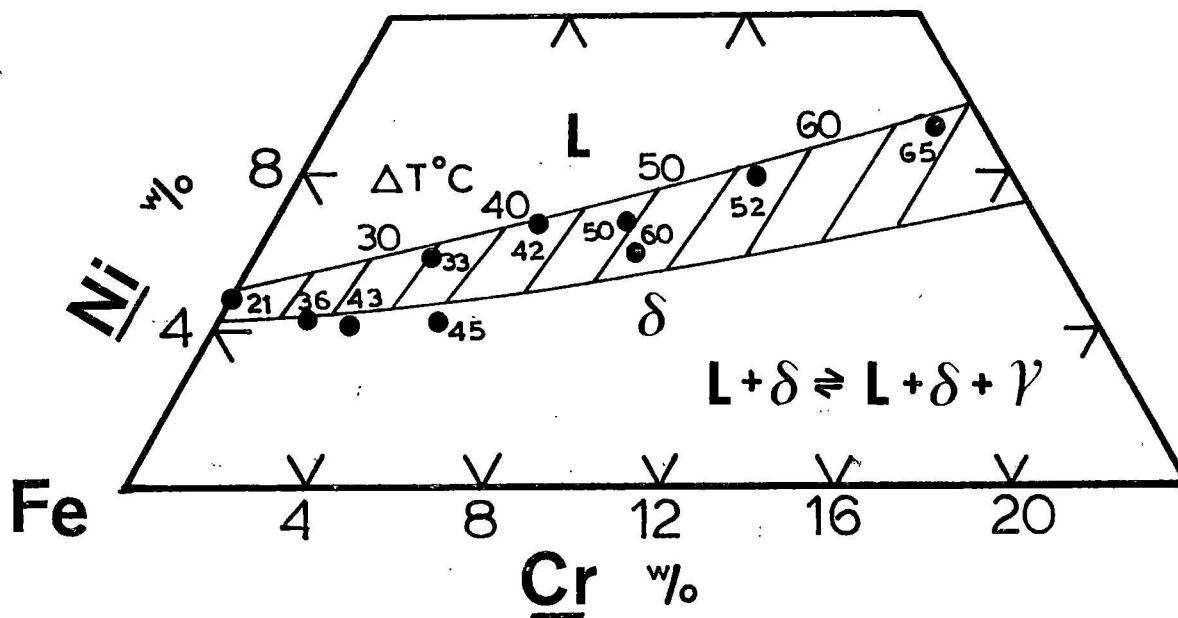


Figure 7.17 - The peritectic reaction in the Fe-Cr-Ni system determined experimentally and by calculation

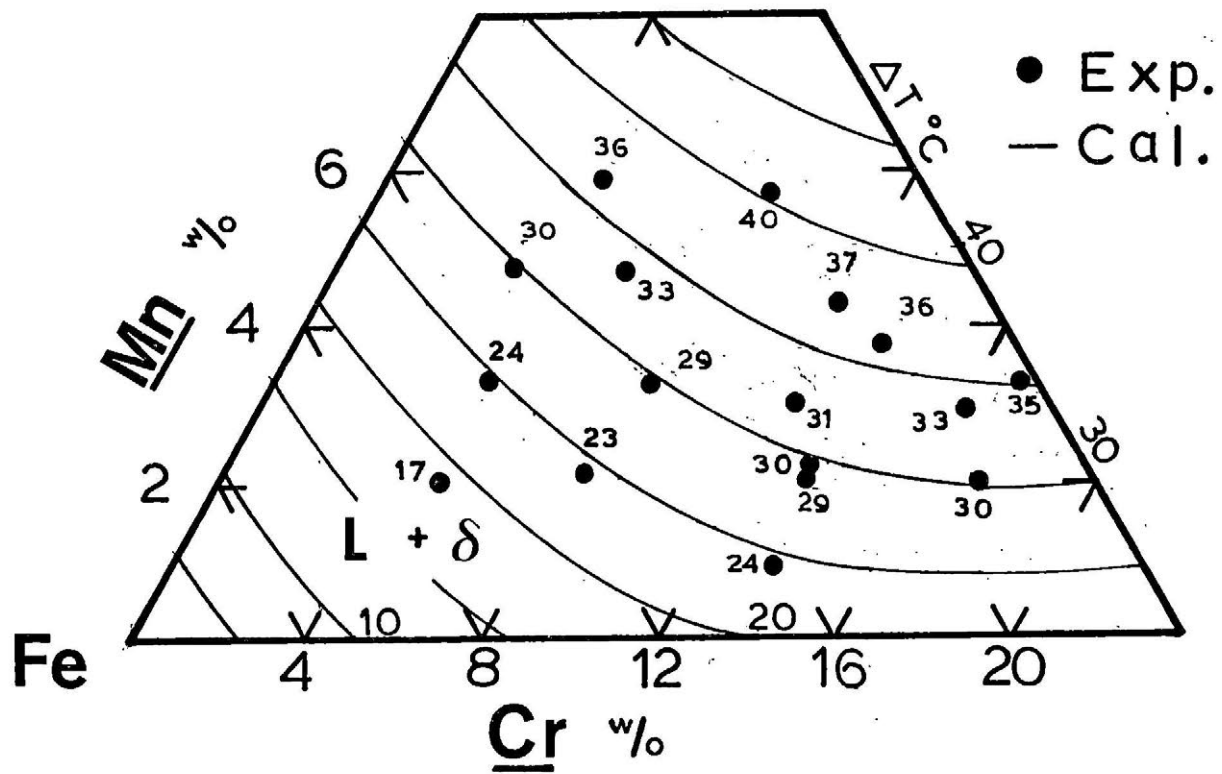


Figure 7.18 - The liquidus in the Fe-Cr-Mn system determined experimentally and by calculation

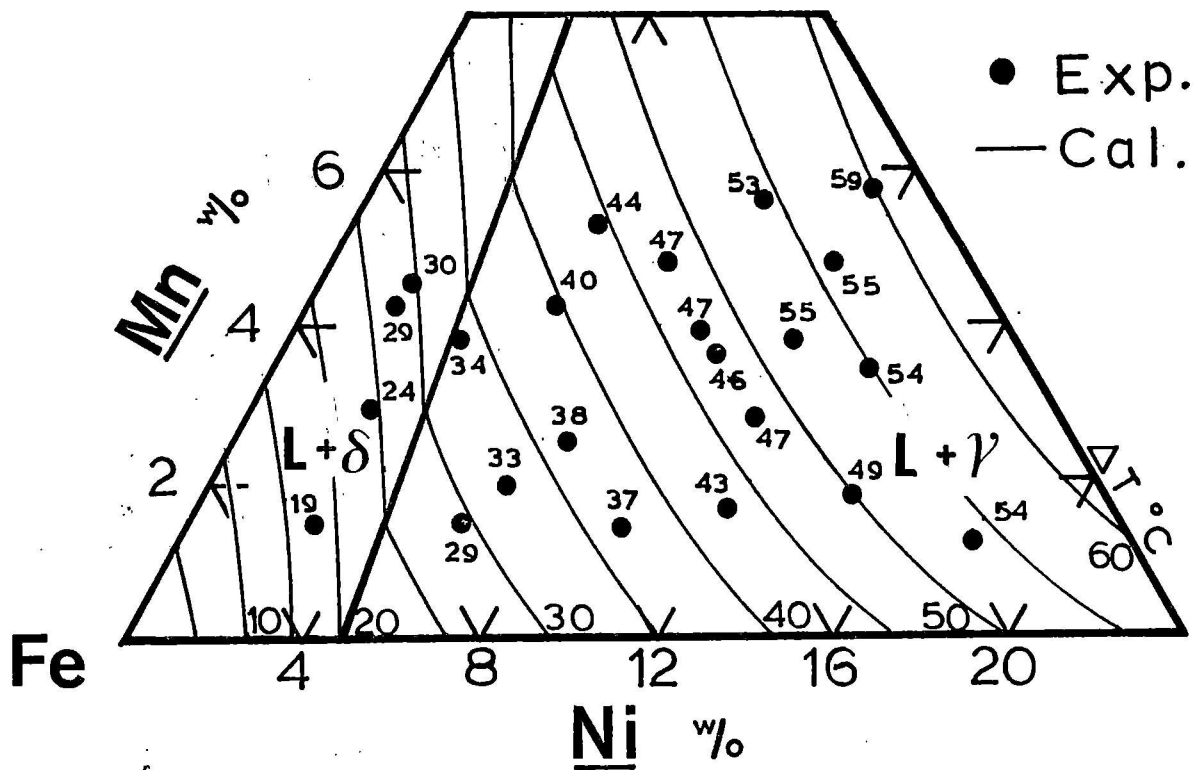


Figure 7.19 - The liquidus in the Fe-Mn-Ni system determined experimentally and by calculation

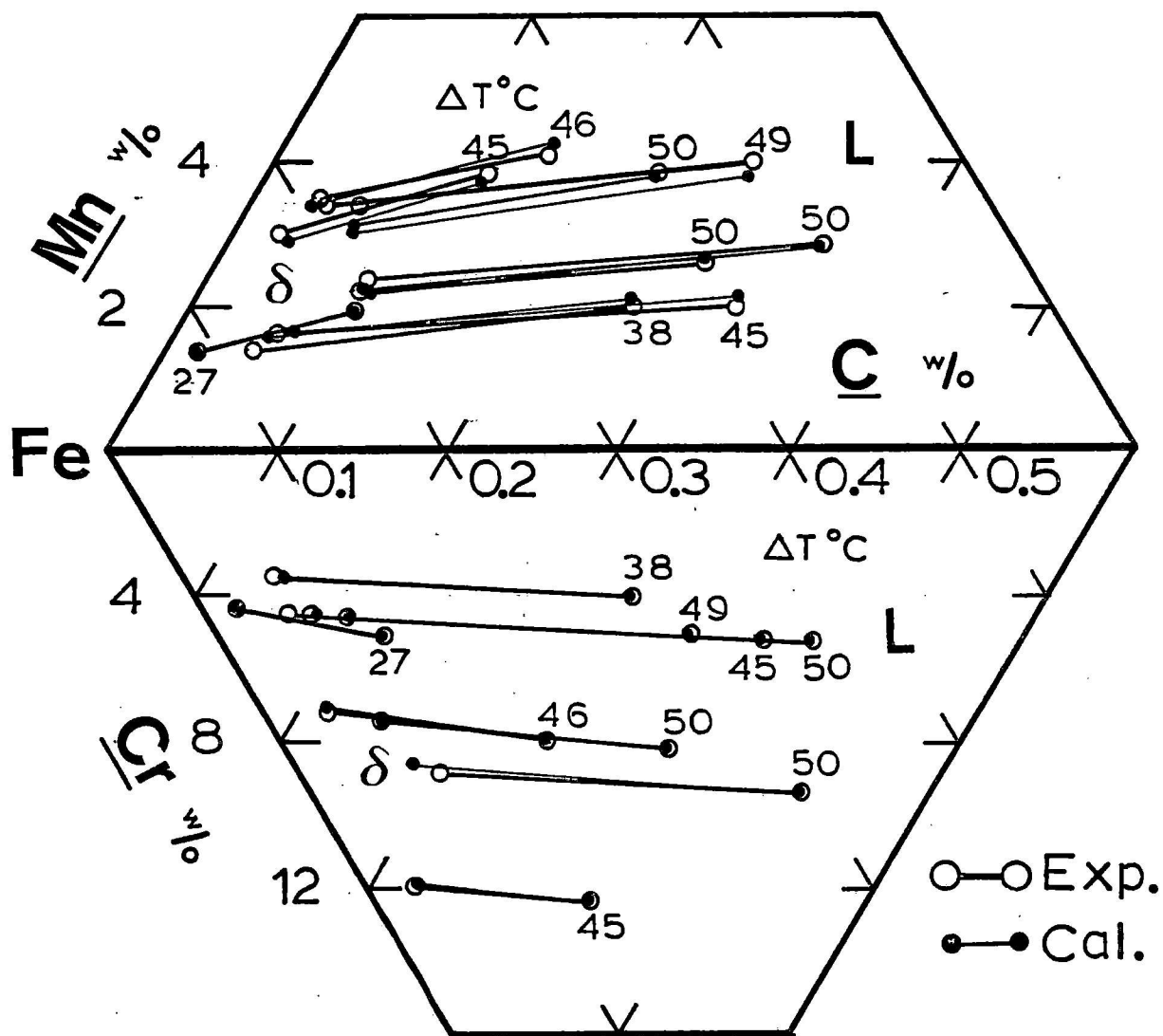


Figure 7.20 - The experimental and calculated tie-lines of the L- δ equilibrium in the Fe-Cr-Mn-C system projected (orthogonally) onto the Fe-Cr-C and Fe-Mn-C basal planes

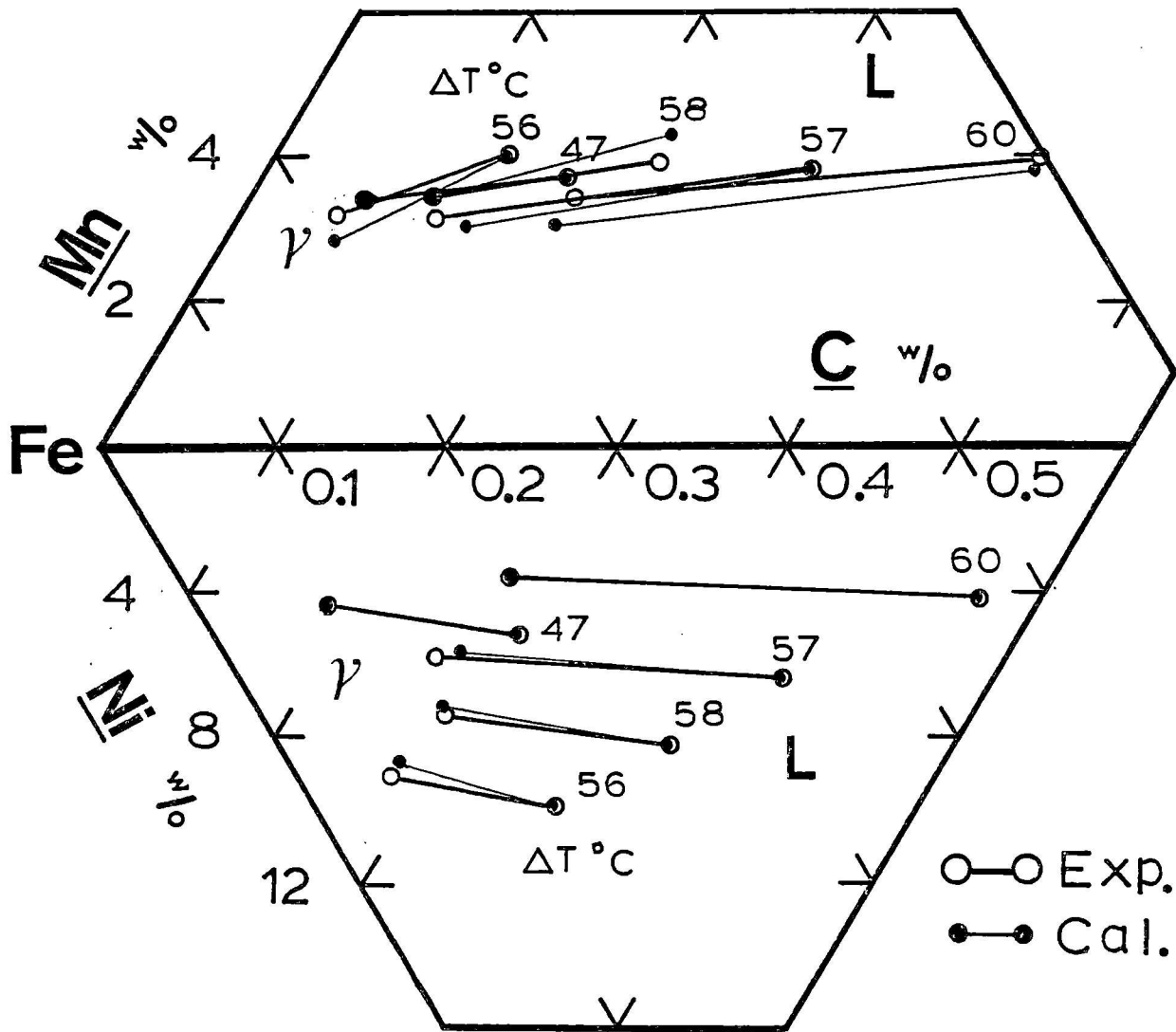


Figure 7.21 - The experimental and calculated tie-lines of the L- γ equilibrium in the Fe-Mn-Ni-C system projected (orthogonally) onto the Fe-Ni-C and Fe-Mn-C basal planes

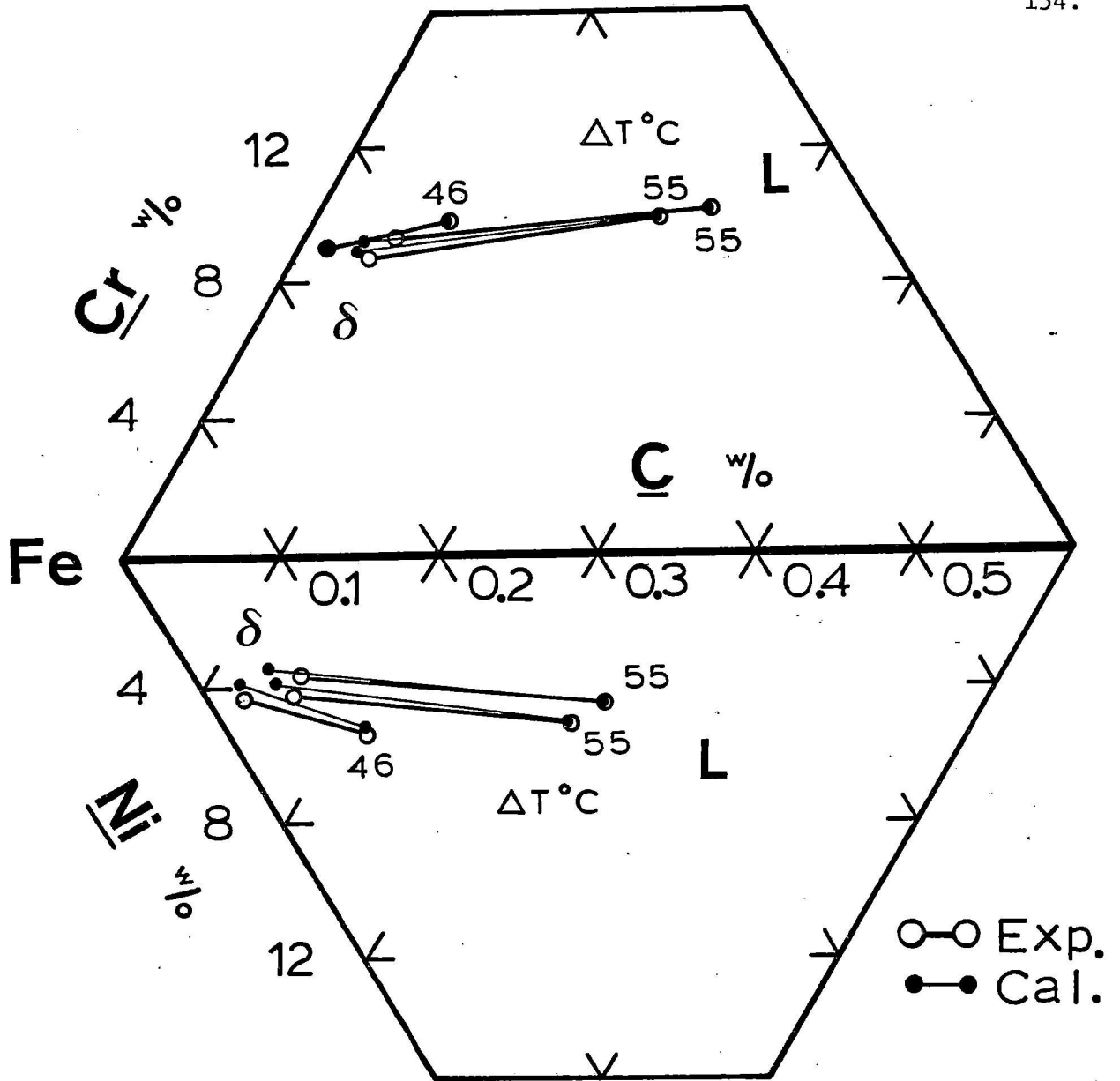


Figure 7.22 - The experimental and calculated tie-lines of the L/δ equilibrium in the Fe-Cr-Ni-C system projected (orthogonally) onto the Fe-Cr-C and Fe-Ni-C basal planes ($\theta^L(\text{FeCrNiC}) = 0$; $\theta^\delta(\text{FeCrNiC}) = 0$).

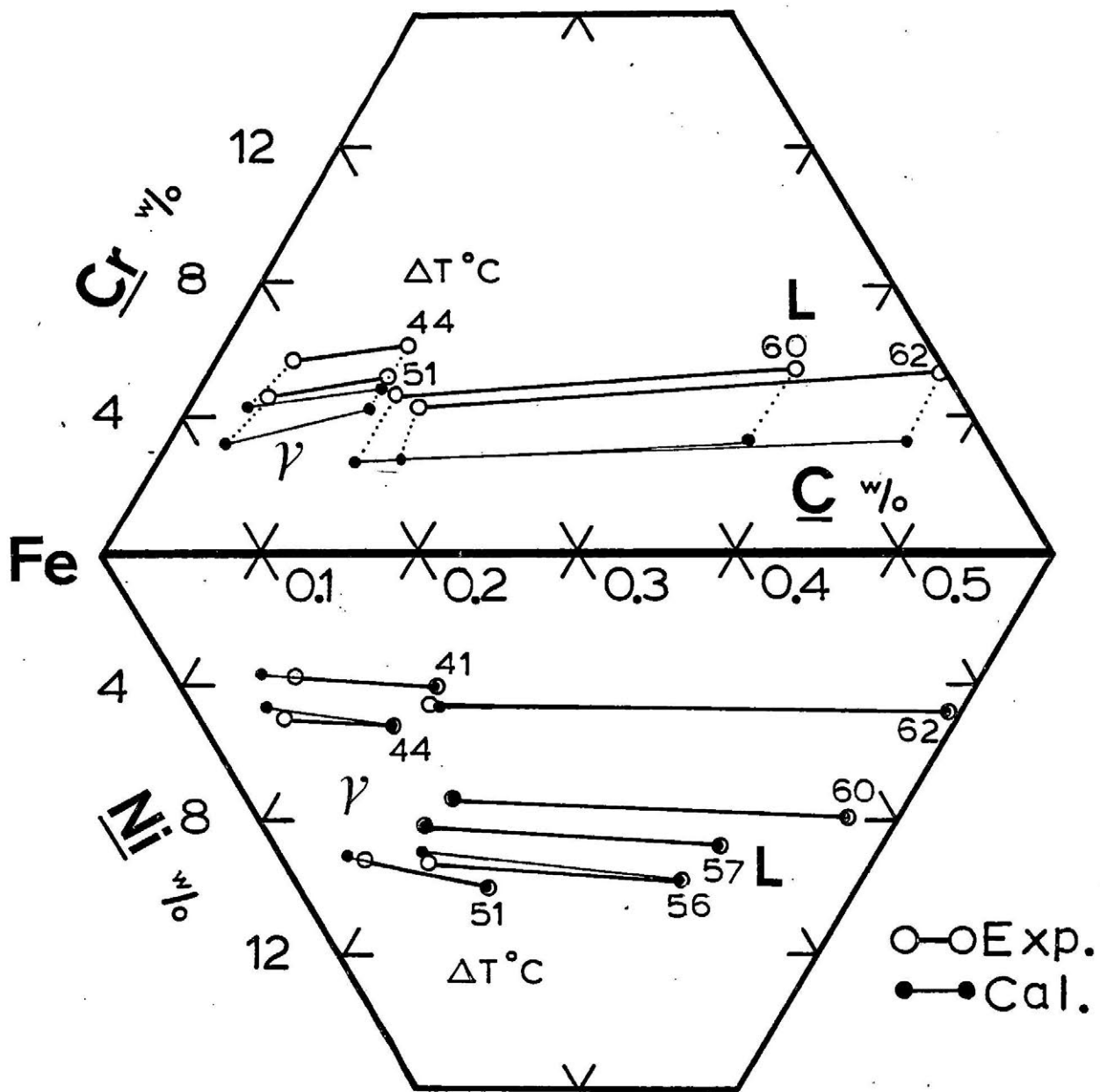


Figure 7.23 - The experimental and calculated tie-lines of the L- γ equilibrium in the Fe-Cr-Ni-C system projected (orthogonally) onto the Fe-Cr-C and Fe-Ni-C basal planes ($\theta^L_{(FeCrNiC)}$, $\theta^\gamma_{(FeCrNiC)}=0$)

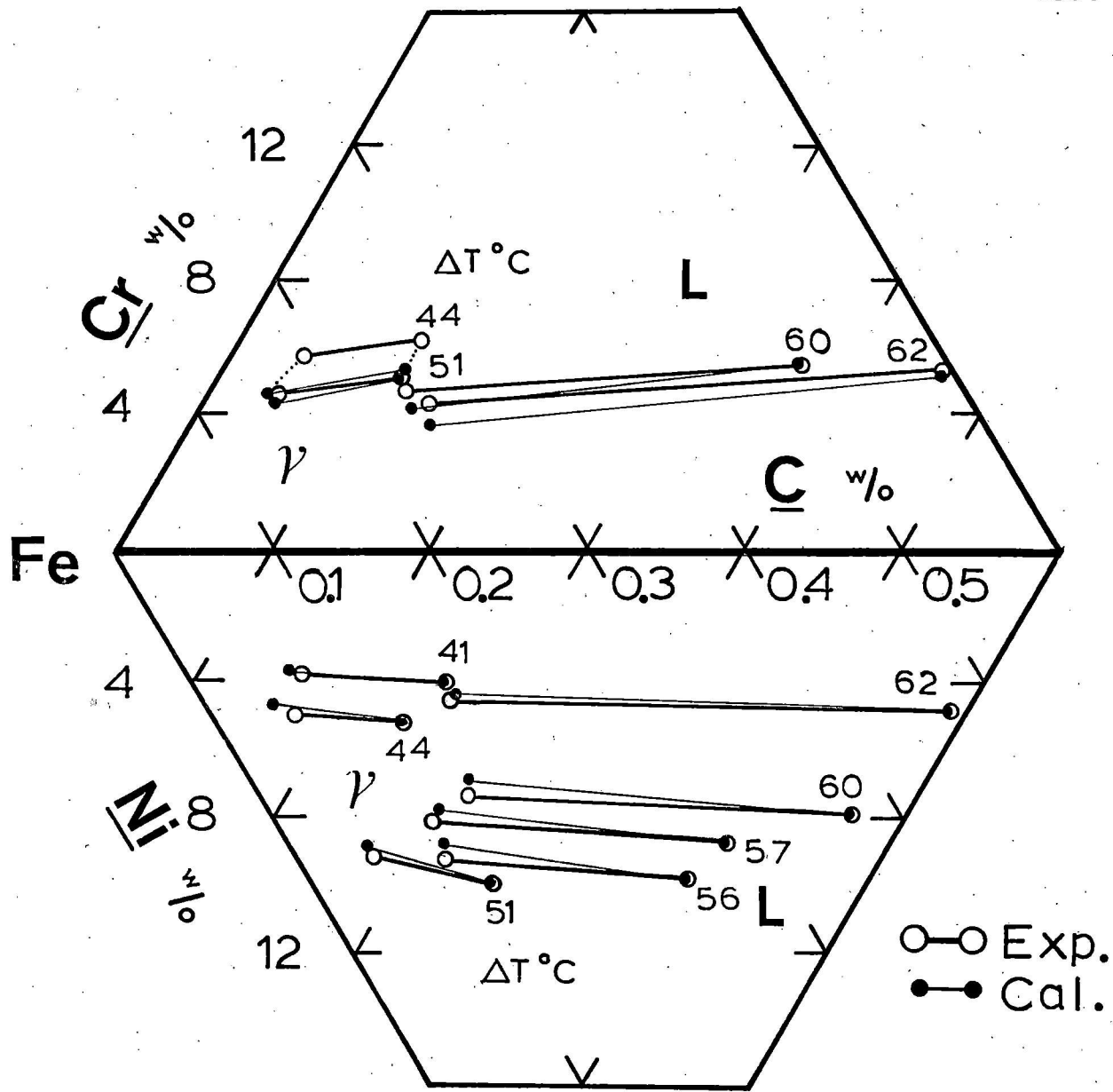


Figure 7.24 - The experimental and calculated tie-lines of the L/γ equilibrium in the Fe-Cr-Ni-C system projected (orthogonally) onto the Fe-Cr-C and Fe-Ni-C basal planes

$$(\theta^L_{FeCrNiC}) = -1000000; (\theta^{\gamma}_{FeCrNiC}) = -1400000$$

Table 7.1. Relative phase stabilities of the liquid and BCC and the liquid and FCC forms of the pure elements

$$\Delta G_i^{L \rightarrow \phi} \text{ (cal/mole)}$$

$i \rightarrow \phi$	δ	γ	References*
Fe	$-3300.0 + 1.822 T$	$-3527.0 + 1.957 T$	(7)
Cr	$-4050.0 + 1.900 T$	$+ 306.0 + 0.184 T$	(21), (22)
Mn	$-3500.0 + 2.300 T$	$-3905.0 + 2.600 T$	(54), (42)
Ni	$-3440.0 + 2.500 T$	$-4210.0 + 2.436 T$	{43}
C	$+7800.0 + 3.000 T$	$+5800.0 + 3.000 T$	(8)

* Parentheses indicate reference source of the parameter and brackets indicate reference source of the original parameter which was adjusted in this study.

Table 7.2. Binary interaction parameters in the quasi-regular solution model

System		Parameters		References*
i	j	θ_j^ϕ	θ_i^ϕ	
Fe	Cr			
	L	+5020 - 2.800 T	+4980 - 2.800 T	{41}
	δ	+6000 - 2.800 T	+6000 - 2.800 T	{41}
	γ	0 - -	0 - -	(22)
Fe	Mn			
	L	-5460 + 4.060 T	-4600 + 4.060 T	{54}
	δ	+1240 + 0.356 T	980 + 1.121 T	{54}
	γ	-4510 + 4.060 T	-4510 + 4.060 T	(54)
Fe	Ni			
	L	-6660 + 2.200 T	-1655 + 0.650 Y	{25, 43}
	δ	+4215 -	+3585 - 2.500 T	{25}
	γ	+1914 - 2.500 T	- 850 + 0.400 T	{25, 43}
Fe	C			
	L	-39990 +11.692 T	-22000 + 2.364 T	{8}
	δ	-22900 - 6.950 T	- 8200 - 9.024 T	{8}
	γ	-38860 + 1.390 T	-23225 - 0.700 T	{8}

*Parentheses indicate reference source of the parameter and brackets indicate reference source of the original parameter which was adjusted in this study.

Table 2 (Cont'd.)

System		Parameters		References*
i	j	θ_j^ϕ	θ_i^ϕ	
Cr	Mn			
	L	-3000 + 2.500 T	-3000 + 2.500 T	(54)
	δ	-2100 + 2.500 T	-2100 + 2.500 T	(54)
	γ	-4200 + 2.500 T	-4200 + 2.500 T	(54)
Cr	Ni			
	L	-2000 -	-2000 -	(25)
	δ	-3200 - 0.500 T	+12800 - 6.500 T	(25)
	γ	+12500 - 9.000 T	-6200 + 2.300 T	{25}
Mn	Ni			
	L	-15395 + 2.600 T	-18395 + 2.600 T	(54)
	δ	-10895 + 0.870 T	-13895 + 0.870 T	(54)
	γ	-12400 + 2.600 T	-15395 + 2.600 T	(54)
Cr	C			
	L	-33000 -	-33000 -	(8)
	δ	-32000 -	-32000 -	(8)
	γ	0 -	-40000 -	-
Mn	C			
	L	-39790 +11.400 T	-23795 - 1.100 T	(55)
	δ	-64285 +11.400 T	-28295 - 1.100 T	(55)
	γ	-68885 +11.397 T	-33790 - 0.971 T	(55)
Ni	C			
	L	-23800 + 3.600 T	-2660 +10.300 T	(8)
	δ	0 -	0 -	-
	γ	-26000 +16.180 T	-19000 + 1.030 T	(8)

Table 7.3. Ternary parameters in the quasi-regular solution model determined from experimental tie-lines

Ternary system i j k	Parameters*					
	θ^L (ijk)	σ	θ^δ (ijk)	σ	θ^γ (ijk)	σ
Fe-Cr-C	-1800	± 1000	-18000	± 2000	-49000	± 1000
Fe-Mn-C	10000	± 700	-40000	± 1000	-8000	± 500
Fe-Ni-C	7000	± 3000	0	-	0	± 1000
Fe-Cr-Ni	1200	± 20	- 1000	± 20	800	± 100
Fe-Cr-Mn	0	-	0	-	0	-
Fe-Mn-Ni	0	-	0	-	0	-

* calculated from Equation (6.24)

Table 7.4. Quaternary parameters in the quasi-regular solution model determined from experimental tie-lines

Quaternary system i-j-k-l	Phase ϕ	Parameter*	
		θ (ijkl)	σ
Fe-Cr-Mn-C	L	0	± 50000
	δ	0	± 50000
	γ	0	-
Fe-Mn-Ni-C	L	0	± 100000
	δ	350000	± 100000
Fe-Cr-Ni-C	L	0	± 50000
	δ	0	± 50000
	L	-900000	± 100000
	δ	-1400000	± 100000

* determined from Direct Search subroutine.

CHAPTER 8DISCUSSION OF RESULTS8.1. Binary Systems

The majority of the experimental results of the binary systems are points locating the iron-rich liquidus, which were determined by DTA. Five points locating the solidus in the Fe-C system and one each, in the Fe-Cr and Fe-Ni systems were determined from equilibrium couples. The liquidus and solidus agree generally within the experimental error with those reported by recent investigators.

The liquidus and solidus of the iron-rich binary alloy have been calculated with the quasi-regular solution model and agree generally within the experimental error with the present measurements. The parameters chosen in the model are different than proposed by Kaufman or by Tiller. The parameters were evaluated in the present study from published thermochemical measurements and from the measurements of the liquidus and solidus, employing the optimization procedure discussed in Chapter 6. In the latter case, the parameters proposed by Kaufman provided a starting point in the optimization procedure.

Fe-C

Numerous points on the δ -liquidus and γ -liquidus were found to agree within $1/2^\circ\text{C}$ with Equations (2.2) and (2.4) and are represented as solid lines in Figure 7.1. The points on δ -solidus are also in good agreement with the phase diagram proposed by Chipman (9). The γ -solidus falls short of that determined by Benz and Elliott (51). However, if adjusted within the experimental error of both measurements, the data overlap.

The agreement between the experimental and calculated phase diagram

is well within the experimental error. Table 8.1 lists the composition and temperature of the peritectic reaction determined experimentally and calculated with the quasi-regular solution model with the parameters determined in this study and with those proposed by Kaufman (Chapter 2).

Fe-Ni

The liquidus is in good agreement with that determined by Hume-Rothery (10) (Figure 7.2) and, the average discrepancy with respect to the temperature of the calculated and experimental liquidus is within 1°C. It is noted in Table 8.1 that the composition of the δ -liquidus at the peritectic temperature is calculated to be about 0.6 and 1.0 w/o Ni less than the experimental value when the parameters of Kaufman and Tiller, respectively, are used in the model.

Fe-Mn

The average discrepancy with respect to temperature between points on the liquidus determined experimentally and calculated with the model is about 1°C.

Fe-Cr

The average discrepancy with respect to temperature of the liquidus determined experimentally and calculated with the model is about 1 1/2°C. Although the minimum in the liquidus determined experimentally is in good agreement with that calculated with the model (Table 8.2), a discrepancy of 2°C occurs in the vicinity of 10 w/o Cr. Kubachewski has shown that his power series expansion of the excess enthalpy of the liquid phase enabled the liquidus and solidus to be predicted well within 1°C of the experimental data at all compositions (41). The present calculations

Table 8.1. The peritectic reaction $L+\delta \rightarrow L+\delta+\gamma$ determined experimentally in the binary systems and calculated from the quasi-regular model*

System	Investigation	Composition (w/o)			Temp. (°C)
		L	δ	γ	
Fe-C	Exp (DK)	0.53	0.09	0.17	1496
	Cal (DK)	0.50	0.08	0.16	1498
	(LK)	0.66	0.13	0.22	1483
Fe-Ni	Exp (DK)	5.0	4.0	4.3	1517
	Cal (DK)	4.8	3.5	4.3	1518
	(LK)	4.2	-	3.5	1517
	(WT)	3.7	-	3.0	1517

* (DK), (LK), and (WT) refer to the calculations with the parameters proposed by this author, Kaufman and Tiller, respectively.

Table 8.2. Experimental and calculated minimum in the liquidus of the Fe-Cr system*

Investigation	Minimum (w/o Cr)	Temp. (°C)
Exp (DK)	20	1517
Cal (DK)	20	1516
Cal (LK)	16	1521
Cal (OK)	20	1515

* (DK), (LK), (WF) and (OK) refer to the calculations with the parameters proposed by this author, Kaufman, Tiller and Kubachewski, respectively.

expose the inadequacy of the quasi-regular solution model to represent the thermodynamic interactions in this system since the only parameters different from those proposed by Kubashewski are the parameters representing the excess enthalpies of the liquid phase which, in turn, were obtained from his power series model in the limit (see Equation (2.20)).

Ni-Cr

The liquidus determined experimentally agrees up to 25% Cr with that calculated with the model. The parameters are quite different than proposed by Kaufman and refer to a difference in the Gibbs energies between the BCC and FCC structures of chromium which was determined from the γ -loop of the Fe-Cr system and extrapolated to pure hypothetical FCC chromium (22). This quantity was chosen over that proposed by Kaufman and by Dombre (Chapter 2) on the basis of the smallest discrepancy between experimental and calculated phase relationships in the Fe-Cr-C, Fe-Ni-C as well as the Fe-Cr and Ni-Cr systems.

8.2. Ternary Systems

The phase relationships which have been determined experimentally in the ternary systems have been calculated with the quasi-regular solution model, and the discrepancy is generally within the experimental error. It was necessary to include the ternary parameters in the model in four of the six systems investigated. These parameters were determined from the experimental tie-lines as discussed in Chapter 6.

It was found that for some sets of experimental tie-lines, the minimization procedure to obtain the parameters was difficult to apply as several minima occurred in the error-parameter surface defined by Equation (6.16). Consequently, starting points (initial values of the

parameters) were calculated from models of activity data of the ternary fields. The ternary parameters $\theta^{(i,j,k)}$ in the quasi-regular solution model for the liquid phase which were calculated from this source are listed in Table (8.3).

Fe-Cr-C

The average discrepancy with respect to temperature between the experimental and calculated liquidus is about 1°C. The minimum in the liquidus in the Fe-Cr system at 20 w/o Cr continues in the ternary system at approximately the same chromium composition at increased carbon levels. Consistent with the minimum in the liquidus with respect to temperature, the isotherms of the δ -liquidus are convex relative to the iron-rich corner. On the other hand, the isotherms of the γ -liquidus are concave relative to the iron-rich corner. The intersection of these isotherms map out the line of two-fold saturation of liquid in equilibrium with the delta and gamma phases, which is observed to bend toward the Fe-C binary axis at higher carbon and chromium concentrations. Jackson has determined an experimental point (DTA) on the δ -liquidus to be: 0.56 w/o C and 8.05 w/o Cr; $T_{L \rightleftharpoons L+\delta} = 59^\circ\text{C}$, which corresponds to $T_{L \rightleftharpoons L+\delta} = 60^\circ\text{C}$ calculated from the model (21). Figure 8.1 also shows that the data of Chocholare consistent with the isotherms calculated by the model although the discrepancy is larger (about 1.5°C for the δ -liquidus and 3°C for the γ -liquidus).

The tie-lines which have been determined experimentally between the liquid and delta phases (Figure 7.6) and between the liquid and gamma phases (Figure 7.7) are predicted by the model to within the experimental error. The tie-lines of the liquid-delta equilibrium are in general

Table 8.3. The ternary parameter in the quasi-regular solution-model for the liquid phase calculated from thermochemical models reported in the literature

Ternary system i j k	Isotherm ΔT^* °C	Parameter θ_{ijk}^L		Source	Reference
		Max	Min		
Fe-Cr-C	30	-1000	-6000	Eq. (2.13)	(38)
	50	-4000	-6000		
	30	2000	-1000	Eq. (2.11)	(32)
	50	1000	-1000		
Fe-Mn-C	50	7000	7000	Eq. (2.11)	(34)
Fe-Ni-C	50	11000	1000	Eq. (2.11)	(34)
Fe-Cr-Ni	30	-10000	-2000	Eq. (2.20)	(45)
	50	-8000	-2000		
	-60	-50000	-8000	Data	(44)
	30	-25000	-9000	Eq. (2.11)	(34)
	50	-20000	-6000		
Fe-Cr-Mn	30	4000	4000	Eq. (2.11)	(33), (34)
Fe-Mn-Ni	30	-16000	-18000	Eq. (2.11)	(33), (34)

$$*\Delta T = 1538^\circ\text{C} - T$$

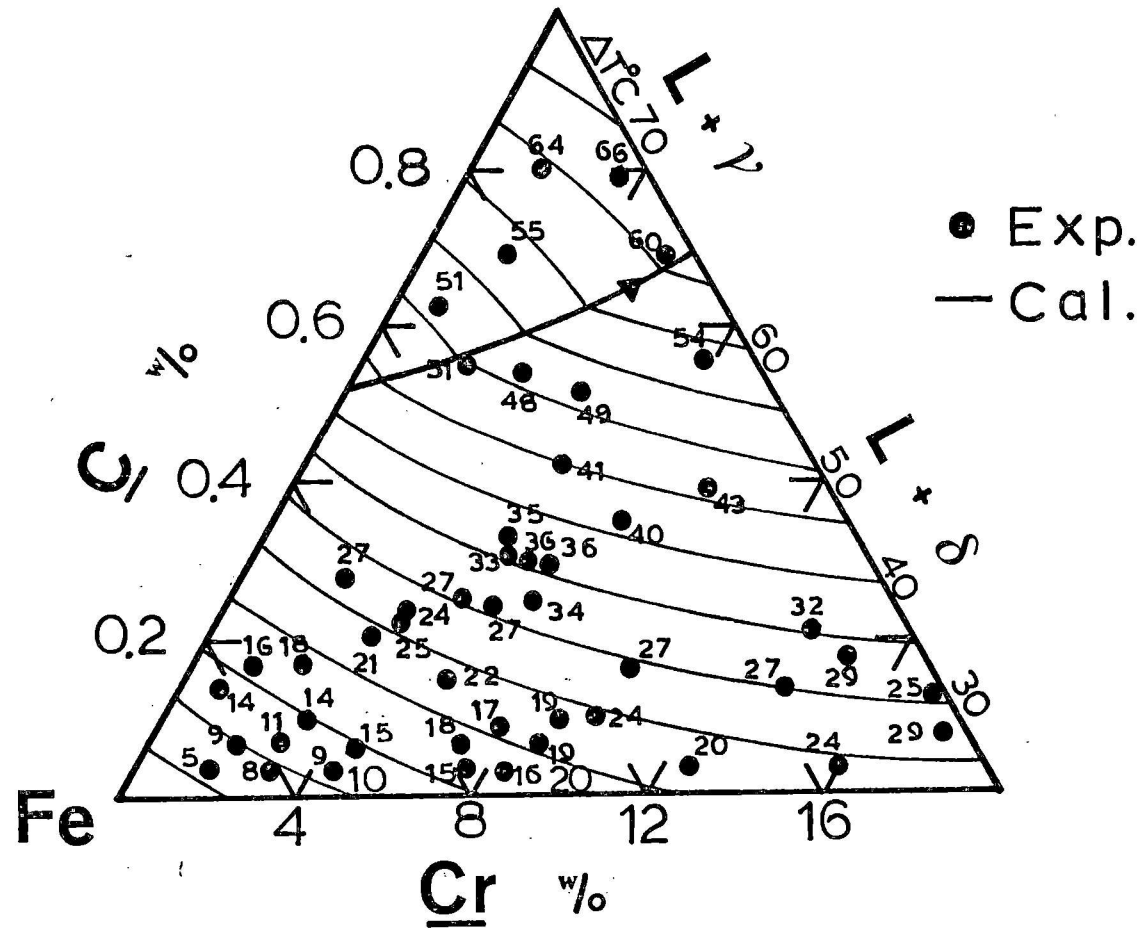


Figure 8.1 - The liquidus in the Fe-Cr-C system determined experimentally by Chochol and calculated with the quasi-regularly solution model⁽¹³⁾

parallel to the carbon axis; however, the partition coefficient of chromium, $K_{Cr} = X_{Cr}^{\delta} / X_{Cr}^L$ at a given temperature is decreased at higher chromium concentrations and then approaches unity again at the minimum in the liquidus. The tie-lines of the liquid-gamma equilibrium compared to those of the liquid-delta equilibrium are observed to change orientation, relative to the carbon axis, at lower chromium concentrations. Accordingly, the partition coefficient of chromium of the liquid-gamma equilibrium decreases continuously with chromium content at a given temperature.

Figure 8.2 compares tie-lines of the liquid-delta equilibrium determined in the present study with the tie-lines determined by Chochol. The experimental conditions that can lead to errors in the determination of the conjugate compositions of the equilibrium couple were noted to give a solidus composition in excess of the composition in equilibrium with the liquid phase (Chapter 5). The discrepancy between the two sets of tie-lines is explained on the basis that the experimental technique of the former investigator may not have accounted for these conditions at the solidification rates employed (13).

Experimented points locating the surface of the two-fold equilibrium $L + \delta \rightleftharpoons L + \delta + \gamma$ are shown in Figure (7.8). The discrepancy with respect to temperature increases to about 5°C at the higher chromium compositions. This discrepancy could be decreased by shifting the calculated isotherms of the liquidus to higher carbon concentrations in the vicinity of the line of two-fold saturation $L \rightleftharpoons L + \delta + \gamma$. This could be accomplished by evaluating the ternary parameters as a function of temperature; however, analysis of the experimental and calculated results of the two-fold equilibrium in the Fe-Ni-C, Fe-Cr-Ni and Fe-Mn-C systems suggest that

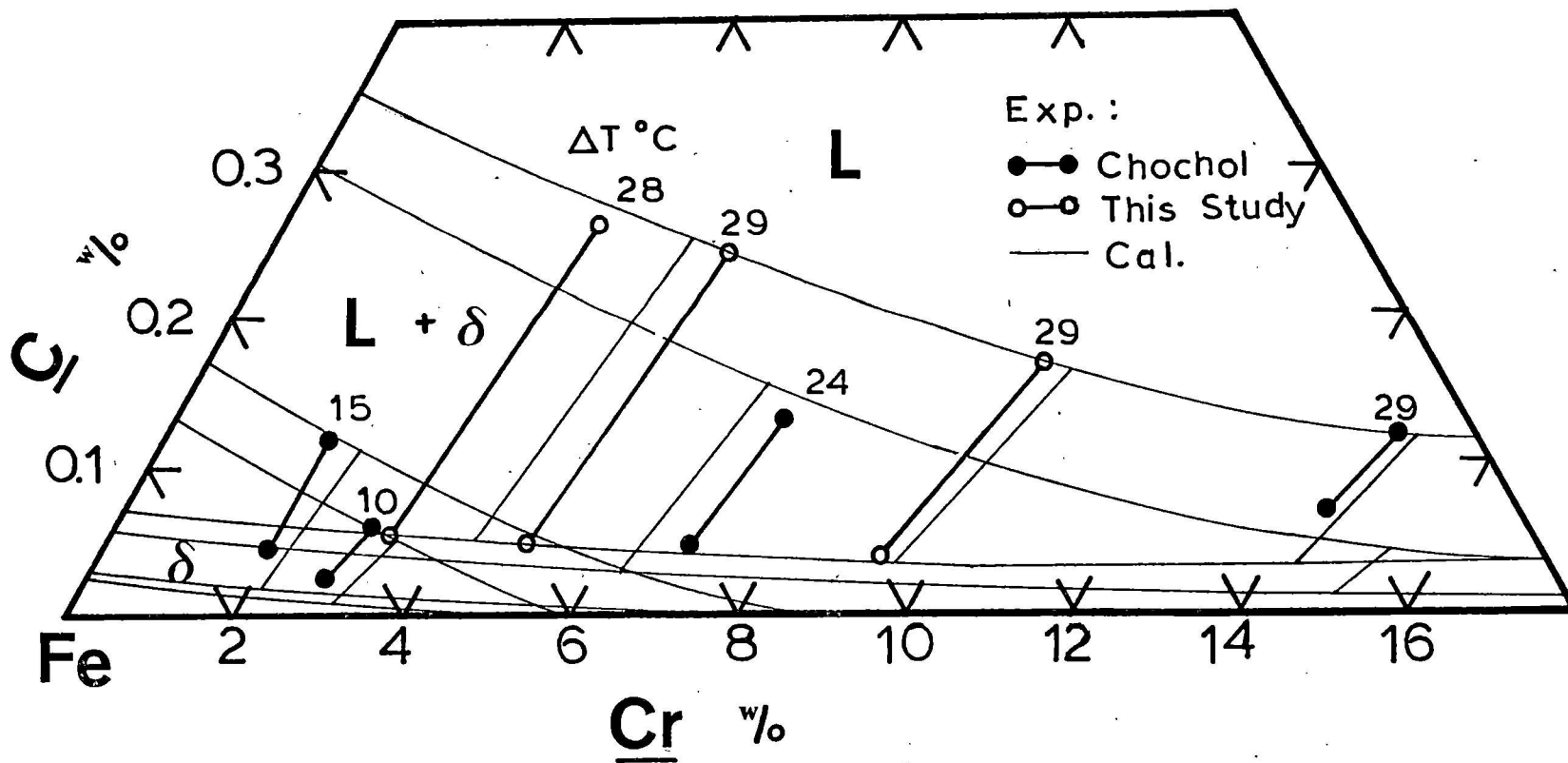


Figure 8.2 - Comparison of the equilibrium between the liquid (L) and BCC (δ) phase in the Fe-Cr-C system determined experimentally in this study and by Chochol(13)

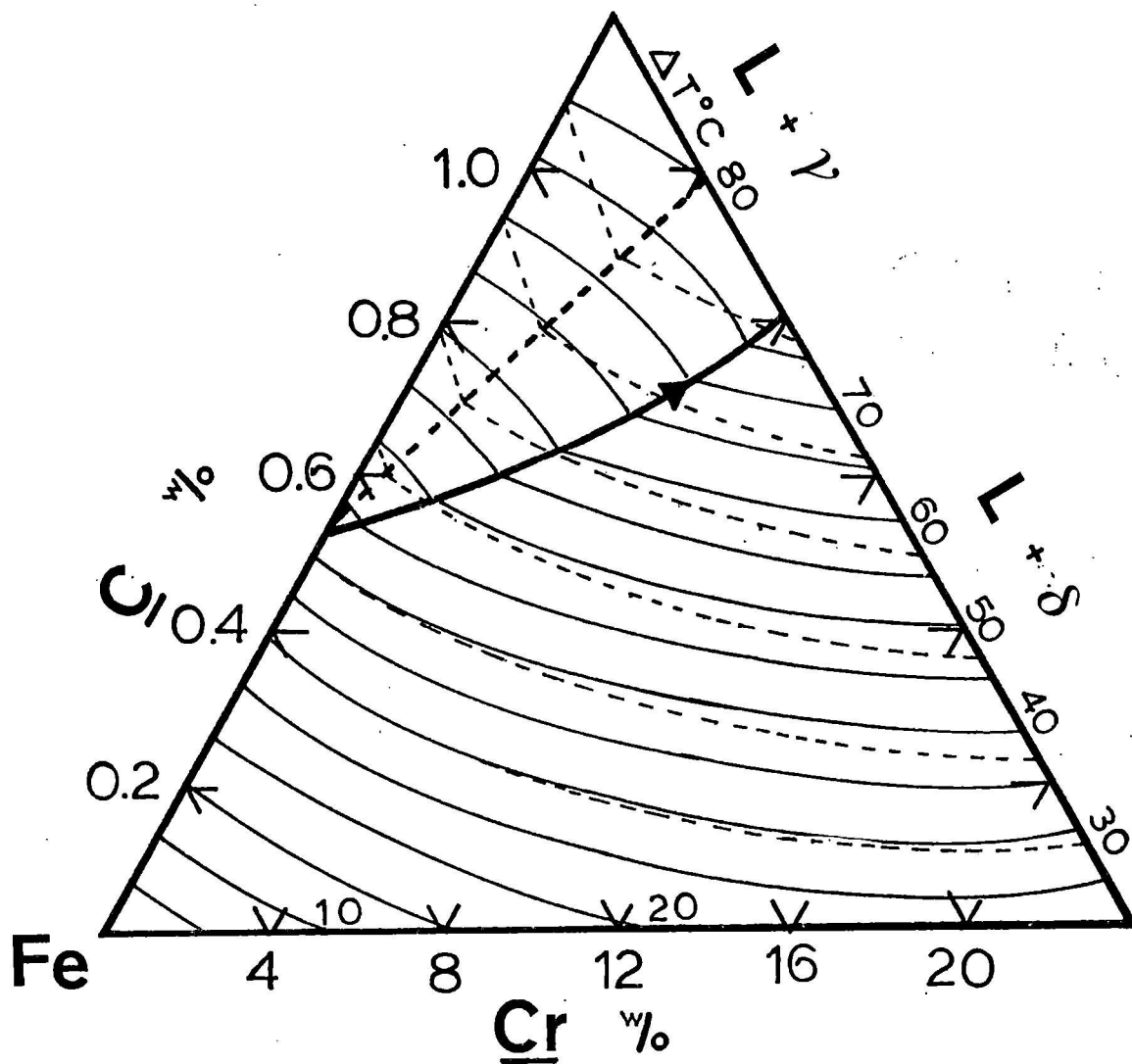


Figure 8.3 - Comparison of the isotherms of the liquidus in the Fe-Cr-C system calculated with the quasi-regular solution model with (continuous line) and without (dotted lines) the ternary parameters

the measurement of the temperature of the equilibrium is more likely to be in error than the measurements and modelling of the equilibrium.

Figure 8.3 is a comparison of the isotherms of the liquidus calculated with the quasi-regular solution model with and without the ternary parameters (set equal to zero). The difference between the two sets of calculations is most apparent at the higher chromium and carbon concentrations. The discrepancy is particularly large for the liquid-gamma equilibrium and is primarily due to the large interaction in the gamma phase which has been observed in the activity of carbon measured in the austenite field at lower temperatures (38).

Fe-Mn-C

The isotherms of the δ -liquidus and γ -liquidus tend to be concave relative to the iron-rich corner and as the isotherms of both equilibria are nearly parallel, the two-fold equilibrium is virtually an isotherm. (Figure 7.9).

The experimental and calculated tie-lines of the liquid-delta equilibrium are in good agreement with respect to the carbon concentrations but not with respect to the manganese concentrations, and the discrepancy is enhanced near the manganese axis. This is explained partially on the basis that the calculated liquidus-solidus gap of the Fe-Mn system may be too large. On the other hand, vaporization of manganese from the liquid phase of the equilibrium couples may have attributed to an error in the determination of the conjugate compositions of manganese; however, this loss was estimated to not exceed 0.3 w/o Mn. Figure 7.11 shows that the agreement between the experimental and calculated tie-lines of the liquid-gamma equilibrium is within this experimental error.

Fe-Ni-C

The average discrepancy with respect to temperature between the liquidus determined experimentally and calculated by the model is less than 1°C. And, the data of Hume-Rothery is consistent with the isotherms predicted by the model, although the discrepancy increases at the higher solute compositions (Figure 8.4).

The tie-lines of the equilibrium between the liquid and the gamma phases is predicted by the model to within 0.01 w/o C and 0.1 w/o Ni. The excellent agreement between the experimental and calculated tie-lines and liquidus suggest that the two-fold equilibrium $L+\delta \rightleftharpoons L+\delta+\gamma$ should be predicted accurately. However, the experimental points location the equilibrium are in modest disagreement with the calculated two-fold surface and, as noted in the Fe-Cr-C system, the discrepancy between calculated and experimental points of the equilibrium increases as the composition is shifted away from the carbon axis.

Fe-Cr-Ni

The discrepancy with respect to temperature between the liquidus determined experimentally and calculated by the model is about 2°C for the equilibrium between the liquid and gamma phases and less than 1°C for the equilibrium between the liquid and delta phases. The isotherms of the γ -liquidus are concave relative to the iron-rich corner (Figure 7.15). This is consistent with the contours of the liquidus determined by Jellinghams et al. (18). Although Chochol concluded that the isotherms of the γ -liquidus are convex, some of his data are in agreement with the isotherms predicted by the model (Figure 8.4) (13). It is noted that the isotherms calculated by the model employing only binary

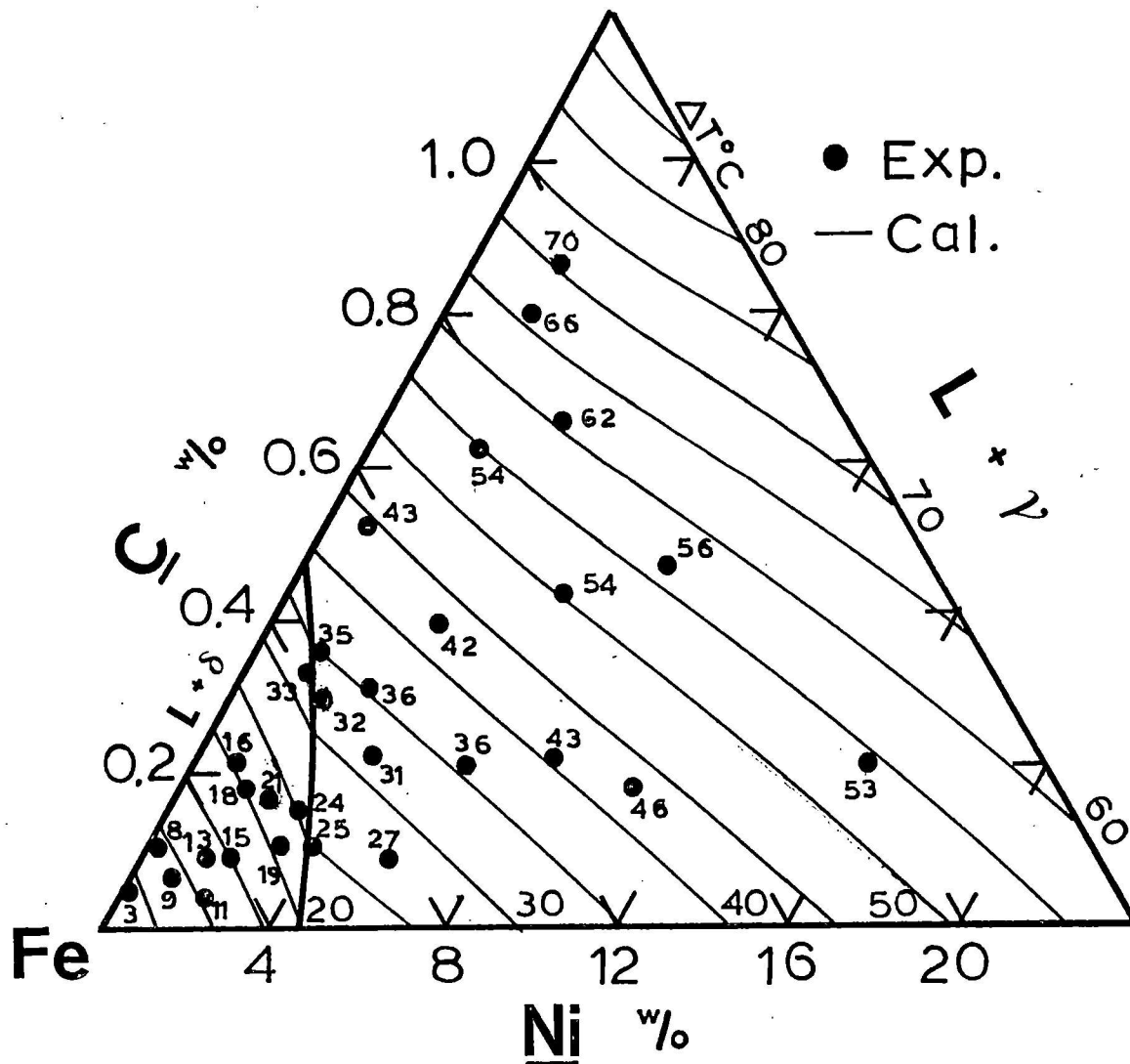


Figure 8.4 - Comparison of the liquidus in the Fe-Ni-C system determined experimentally by Hume-Rothery and calculated with the quasi regular solution model (15)

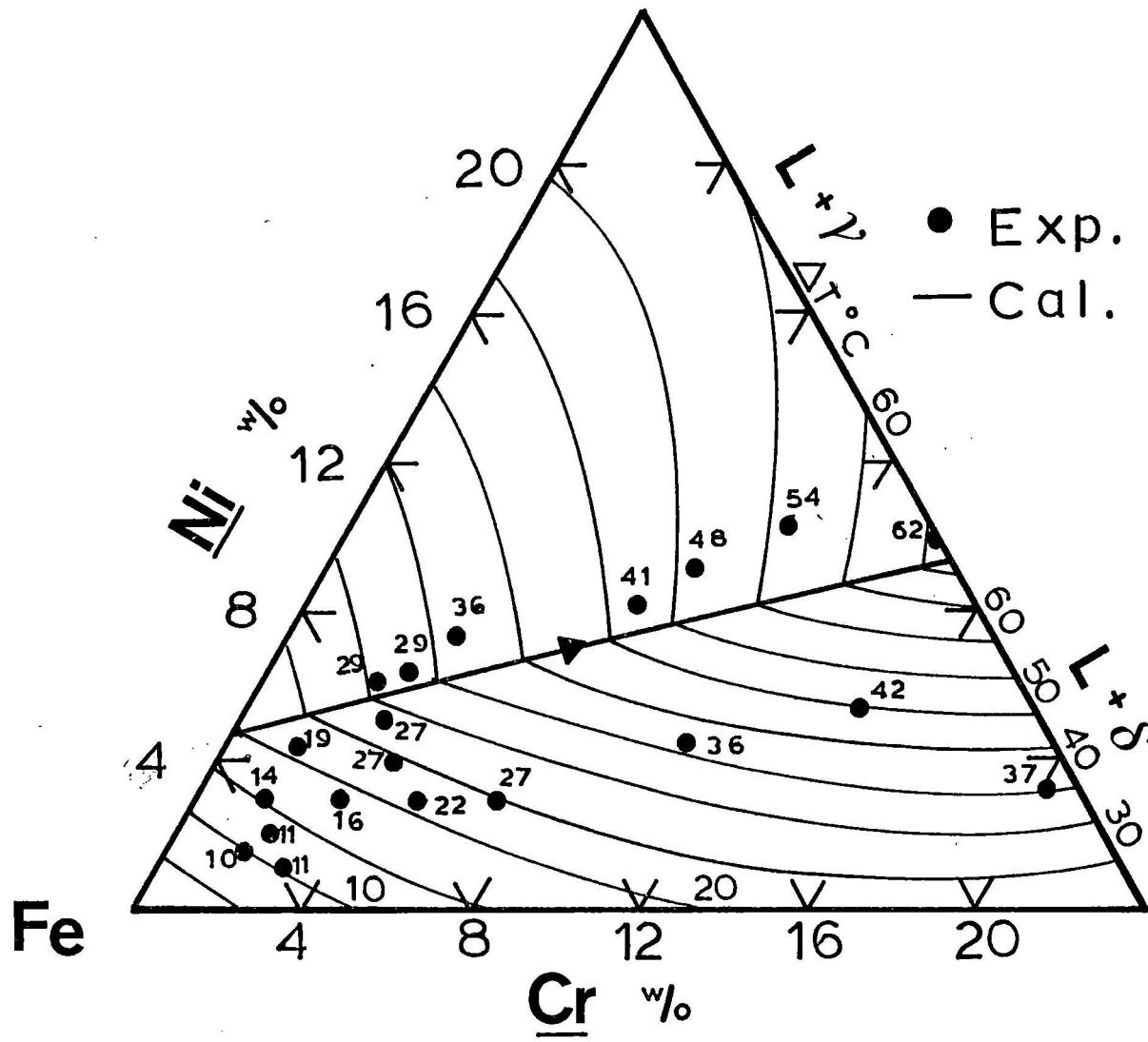


Figure 8.5 - The liquidus in the Fe-Cr-Ni system determined experimentally by Chochol and calculated with the quasi-regular solution model (13)

parameters and the difference between pure FCC chromium and pure liquid chromium proposed by Chipman are also concave, but predict the temperatures of the liquidus to be too low.

The equilibrium between the liquid and gamma phases is shown in Figure 7.16. The orientation of the tie-lines relative to the nickel axis is predicted by the model although the average composition of the solidus is of higher chromium concentration than determined experimentally by about 0.2 w/o Cr.

Figure 7.17 shows the experimental points locating the surface of the two-fold equilibrium $L+\delta \rightleftharpoons L+\delta+\gamma$. Again, as noted in the Fe-Cr-C and Fe-Ni-C systems, the predicted temperatures of the equilibrium are about 6°C too high at the higher solute composition. On the other hand, for composition less than 6% Cr, the temperatures predicted by the model are too low.

Fe-Cr-Mn

The experimental liquidus is in good agreement with the isotherms predicted by the model. The average discrepancy with respect to temperature is about 1°C (Figure 7.18). For this system, the ternary parameters in the model were not found to be statistically significant when based on the liquidus data only. The experimental tie-lines are in modest agreement with the calculated tie-lines of the equilibrium between the liquid and delta phases at all compositions except near the minimum in the liquidus with respect to temperature. Here, the experimental tie-line indicated a solidus-liquidus gap of 1% Cr.

Fe-Mn-Ni

The liquidus determined experimentally is, on the average, within 1°C of the temperature predicted by the model. The experimental tie-lines are in modest agreement with the calculated tie-lines. When based on only the liquidus data, the ternary parameters in the model were not found to be statistically significant.

Comparison of Thermodynamic Models

Models of the thermodynamic behavior of the solution phases in the ternary systems investigated in this study have been reviewed in Chapter 2. The methods of Chapters 4 and 6 provide a means to compare the models at the temperatures and compositions in which two or more of the phases are in equilibrium. The basis of comparison is the discrepancy between the phase relationships of each alloy system determined directly by experiment and calculated from the models chosen for each of the co-existing phases. However, the present study is restricted to a comparison of the parameters of the quasi-regular solution model calculated from the experimental tie-lines and from other models at the experimental compositions and temperatures. In particular, parameters for the liquid phase were calculated and are listed in Tables 7.3 and 8.3. The parameters for the liquid phase of the alloys containing carbon which were obtained from the experimental tie-lines are in modest agreement with the parameters calculated from the thermodynamic models of the activity of carbon in the ternary solution. The parameters for the liquid phase of the alloys containing only substitutional elements were obtained from temperature measurements of the liquidus only and they are not in agreement with the parameters calculated from the thermodynamic models.

However, analysis of the Fe-Cr-Ni system revealed that the location of the calculated isotherms depended considerably on the difference between the Gibbs energies of the liquid and solid phases. That is, the error-parameter surface, defined by Equation (6.17) exhibited a shallow valley that extended to the magnitudes of the parameters calculated from the thermodynamic models. This suggests that the parameters of the solid phases may be of the same sign and nearly the same magnitude as the parameters calculated from the thermodynamic models for the liquid phase.

8.3. Quaternary Systems

The phase relationships which have been determined experimentally in the quaternary systems have been calculated with the quasi-regular solution model. The discrepancy between the experimental and calculated tie-lines of the liquid-delta equilibrium is within the experimental error. However, the discrepancy between the experimental tie-lines of the liquid-gamma equilibrium justified additional modelling.

The quaternary parameters were obtained with the same procedure as for determination of the ternary parameters described in Chapter 6. The ternary parameters of the ternary systems that were not treated in the preceding section were assumed to be zero in the quaternary model; i.e.,

$$\theta_{(ijk)}^{\phi} = 0; (i,j,k) = \{C, Cr, Mn, Ni\}$$

It is recalled from Chapter 2 that the equilibrium between two phases at a constant temperature is a volume in the composition tetrahedron. And, as a consequence of the procedure to calculate the continuum, a tie-line is calculated at selected compositions of two of the independent variables. At each phase boundary; i.e., surface of saturation, the

discrepancy with respect to each component is calculated by determining the difference between the experimental and calculated compositions when two of the composition variables are set equal to their experimental compositions (See Chapter 6). In the calculations which refer to Figure 7.20 through 7.24 the composition variables set equal to the experimental compositions are: X_{Cr}^L and X_C^L in the Fe-Cr-Mn-C system and X_{Ni}^L and X_C^L in the Fe-Cr-Ni-C and Fe-Mn-Ni-C systems. Accordingly, these figures show only the discrepancy with respect to the manganese component of the liquidus in the Fe-Cr-Mn-C system and the chromium and manganese components of the liquidus in the Fe-Cr-Nr-C and Fe-Mn-Ni-C systems, respectively.

Fe-Cr-Mn-C

The experimental tie-lines of the liquid-delta equilibrium are in good agreement with the tie-lines predicted by the quasi-regular solution model. The quaternary parameters for the liquid and delta phases were not found to be statistically significant for the case in which $\theta^{\phi}(\text{CrMnC})$ is assumed to be zero. As a consequence, the tie-lines located within the composition tetrahedron shown in Figure 7.20 can be predicted within the experimental error.

The discrepancy with respect to the chromium component of the liquidus of the experimental tie-line of the liquid-gamma equilibrium (not shown) is

	w/o Cr	w/o Mn	w/o C
Liquidus	0.90	0.00	0.00
Solidus	0.95	0.40	0.02

Although the discrepancy is larger than the experimental error, quaternary parameters were not determined for this equilibrium.

Fe-Mn-Ni-C

The experimental tie-lines of the liquid-gamma equilibrium are in modest agreement with the tie-lines predicted by the model when only the ternary and binary parameters were employed. To improve the discrepancy, the quaternary parameters for both phases were determined from the experimental tie-lines. Figure 7.21 shows that, with the quaternary parameter included, the carbon compositions of the solidus calculated from the model are in excellent agreement with the experimental values. The partition coefficient of manganese calculated from the experimental tie-lines was not found to be in agreement with that predicted from the model when the quaternary parameters were set equal to zero. The discrepancy is still apparent and is larger at lower carbon and higher nickel concentrations. The partition coefficient of nickel follows a similar pattern as with manganese but only at higher nickel concentrations. This may indicate an increased thermodynamic interaction among carbon, manganese, nickel and iron at higher nickel concentrations.

Fe-Cr-Ni-C

The experimental tie-lines of the liquid-delta equilibrium are in good agreement with the tie-lines predicted by the model when only the ternary and binary parameters were employed (Fig. 7.22). However, with respect to chromium, the discrepancy between the experimental and calculated tie-lines of the liquid-gamma equilibrium is relatively large as depicted in Fig. 7.23. This suggests the need for the quaternary parameters for the liquid and gamma phases, although the investigations of Lupis and Greenbank suggest that the quaternary interactions are small (32,49). However, it is noted to be that the ternary parameters which are

assumed to be zero ($\theta_{(CCrNi)}^{\phi=\delta,\gamma}$) may, in fact, be substantial and exert considerable influence on the calculations in the iron-rich composition field. This may account partially for the discrepancy of the quaternary tie-lines since the parameters of the binary systems C-Cr and Ni-Cr were observed to affect appreciably the calculations of the tie-lines of the liquid-gamma equilibrium in the iron-rich ternary systems. Figure 7.24 in comparison with Figure 7.23 shows the improvement in the discrepancy of the liquidus when the quaternary parameters were included in the model. However, it is noted that the partition coefficient of both chromium and nickel calculated with the model is decreased below that calculated from the experimental tie-lines when the quaternary parameters were included in the model.

Figure 8.6 shows the orthogonal projection of the iso-carbon compositions of the liquidus at $T = 45^\circ\text{C}$ (1493°C) onto the Fe-Cr-Ni basal plane. The line of two-fold saturation $L \rightleftharpoons L+\delta+\gamma$ is shown to be the intersection of the iso-carbon lines of the δ -liquidus and the γ -liquidus. It is also the loci of equilibrium compositions of the liquidus traced out by the continuum of tie triangles of the L- δ - γ equilibrium. This equilibrium in the Fe-Cr-Ni-C system at a constant temperature is shown schematically in Figure 8.7.

As temperature is increased, the liquidus progresses through the composition tetrahedron and accordingly, the composition field of the three-phase equilibrium changes. The shift with temperature of the line of two-fold saturation $L \rightleftharpoons L+\delta+\gamma$ is shown in Figure 8.8. With temperature as an additional variable, the two-fold equilibrium is a surface in the composition tetrahedron, which can be depicted as a family of iso-carbon

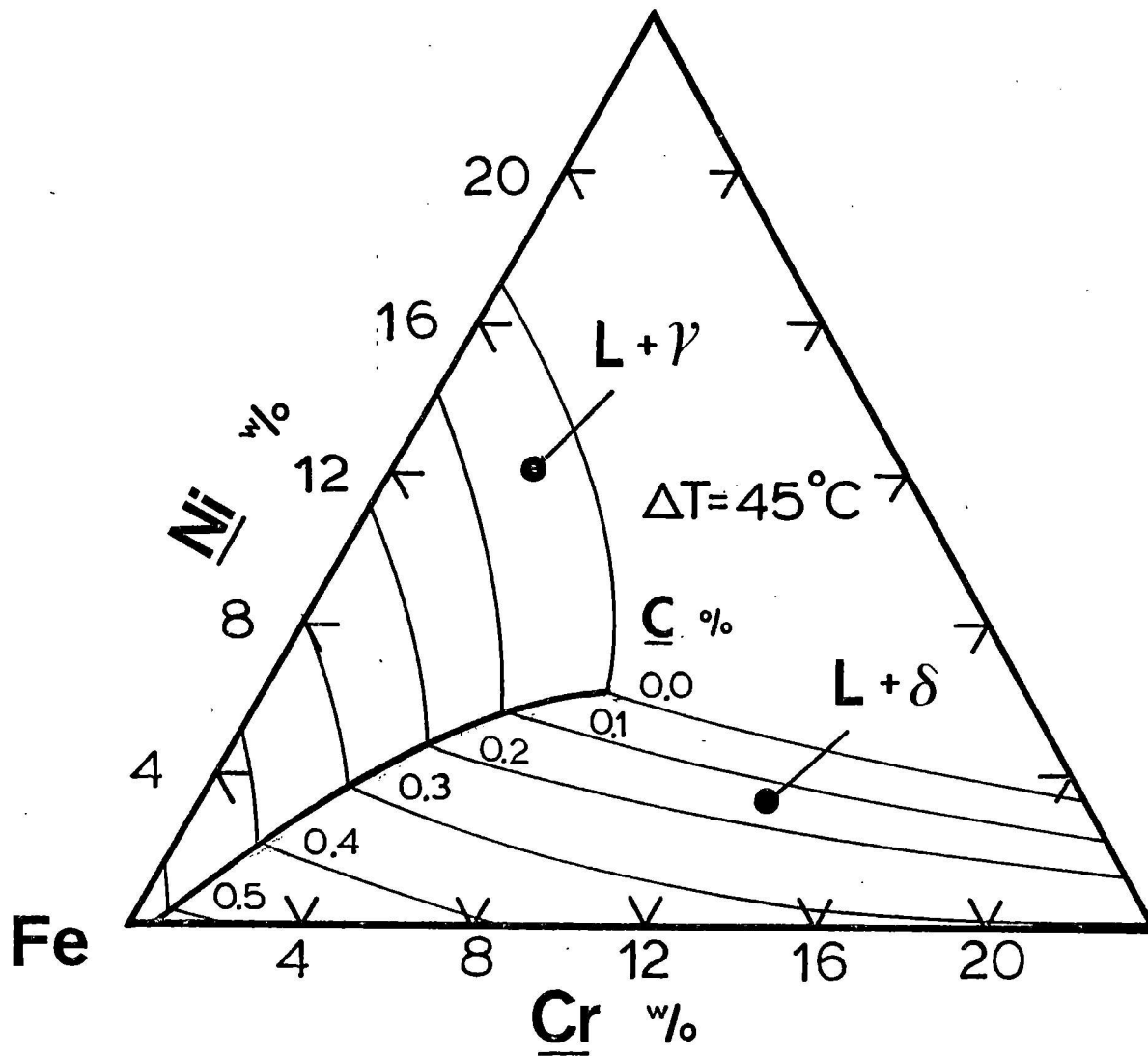


Figure 8.6 - Orthogonal projection of the liquidus in the Fe-Cr-Ni-C system at 1493°C onto the Fe-Cr-Ni basal plane. Calculated with the quasi-regular solution model ($\theta_{L(\gamma)}^{FeCrNiC} = 0$; $\theta_{L(\delta)}^{FeCrNiC} = -1000000$; $\theta_{L(\gamma)}^{FeCrNiC} = -1400000$; $\theta_{L(\delta)}^{FeCrNiC} = -1000000$;

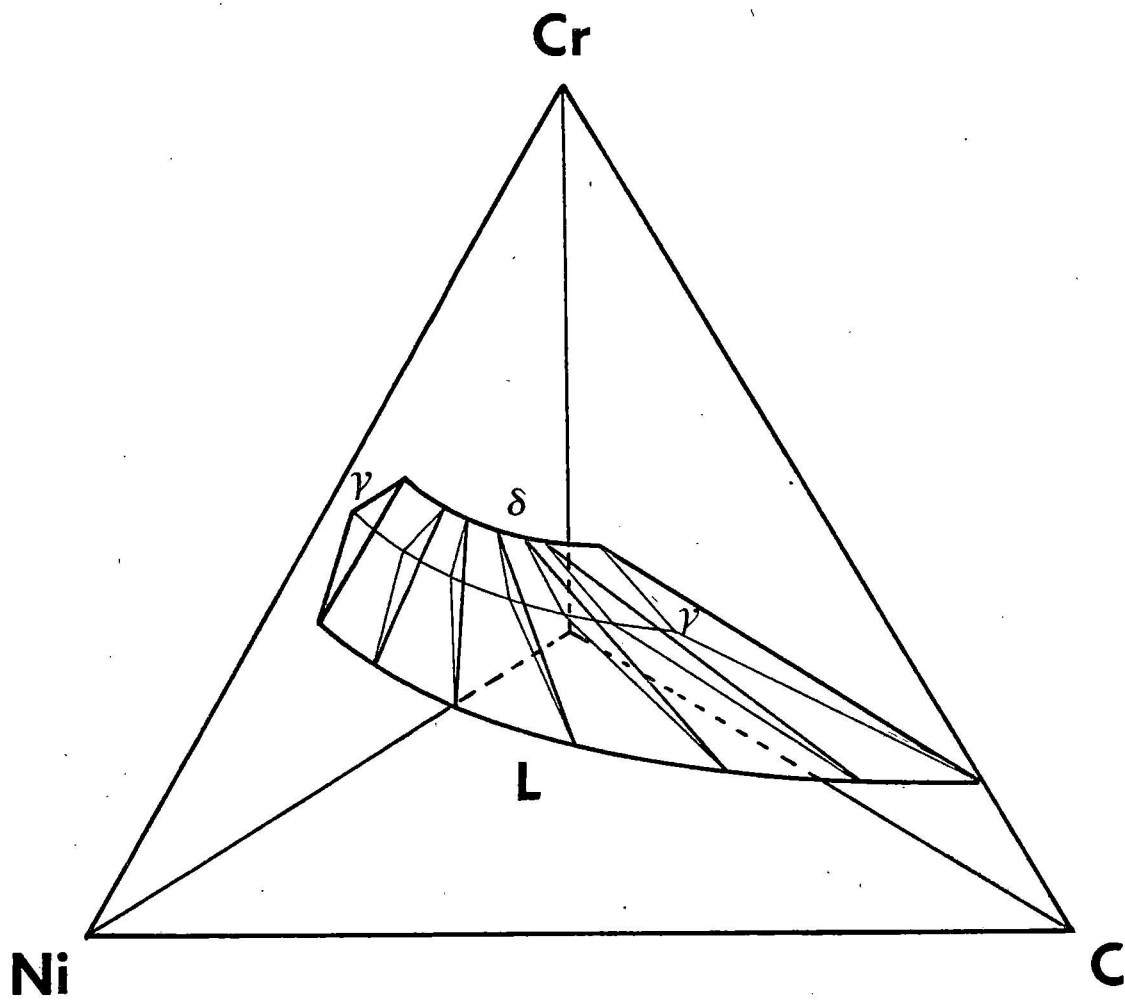


Figure 8.7 - The L- δ - γ equilibrium in the Fe-Cr-Ni-C system (Constant T,P) depicted as a continuum of tie-triangles

lines or as a family of isotherms. These lines were calculated by employing Equation (4.16) for the case of three phases and four components. From the solution matrix, the composition of saturation of each of the single-phase fields with respect to the other phases is known at each temperature and can be depicted as in Figure 8.8.

A quantity measured by DTA is the temperature of the two-fold equilibrium $L+\delta \rightleftharpoons L+\delta+\gamma$ which is depicted as a ruled surface in the quaternary system at a constant temperature. The surface is the continuum of $L-\delta$ tie-lines of the $L-\delta-\gamma$ tie-triangles. The progress with temperature of this equilibrium calculated from Equation (4.16) is shown quantitatively in Figure 8.9.

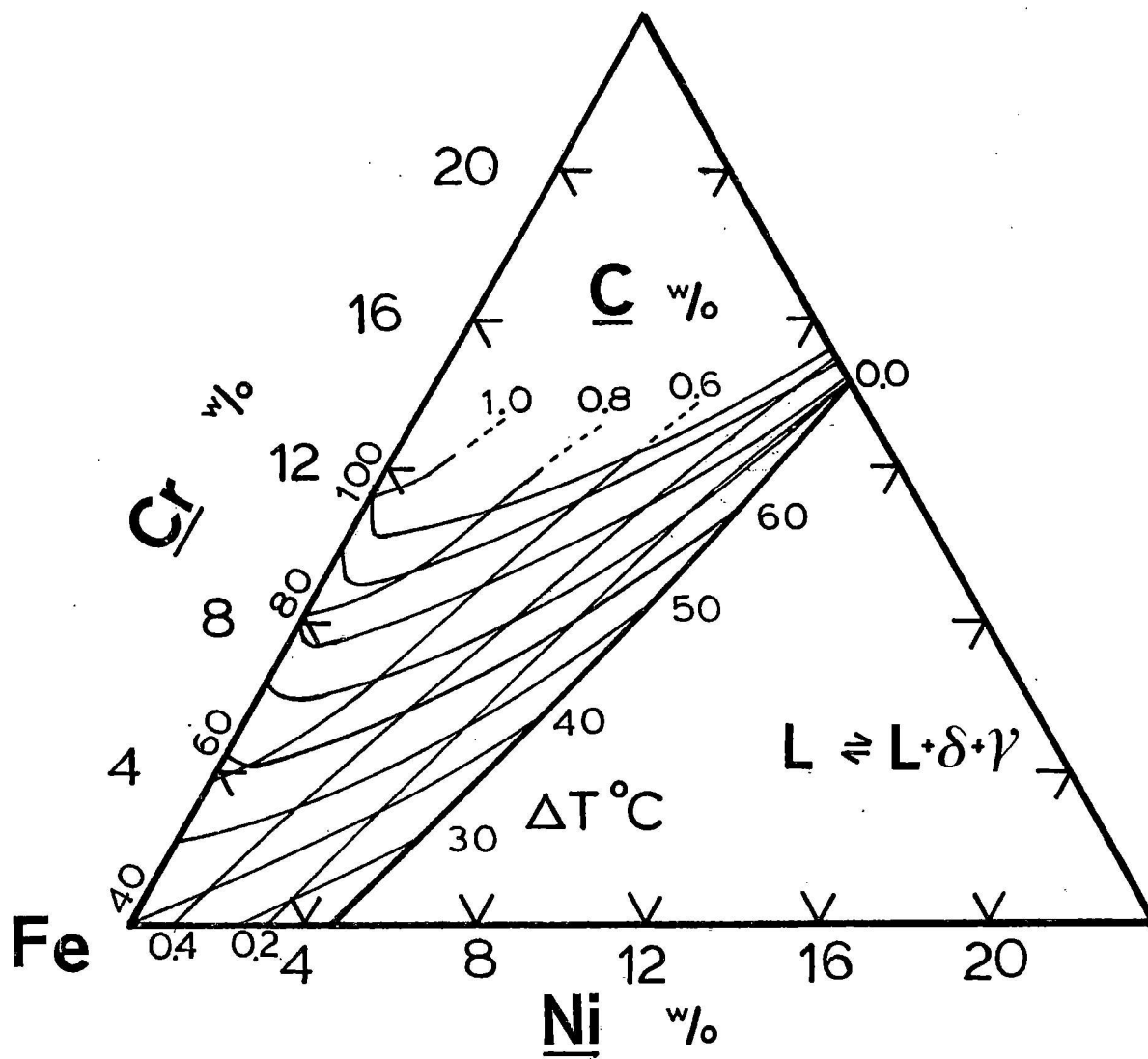


Figure 8.8 - Orthogonal projection of the surface of two-fold saturation $L \cong L+\delta+\gamma$ in the Fe-Cr-Ni-C system onto the Fe-Cr-Ni basal plane. Calculated with quasi-regular solution model ($\theta^\phi_{(\text{FeCrNiC})} = 0$; $\phi = \delta, L, \gamma$)

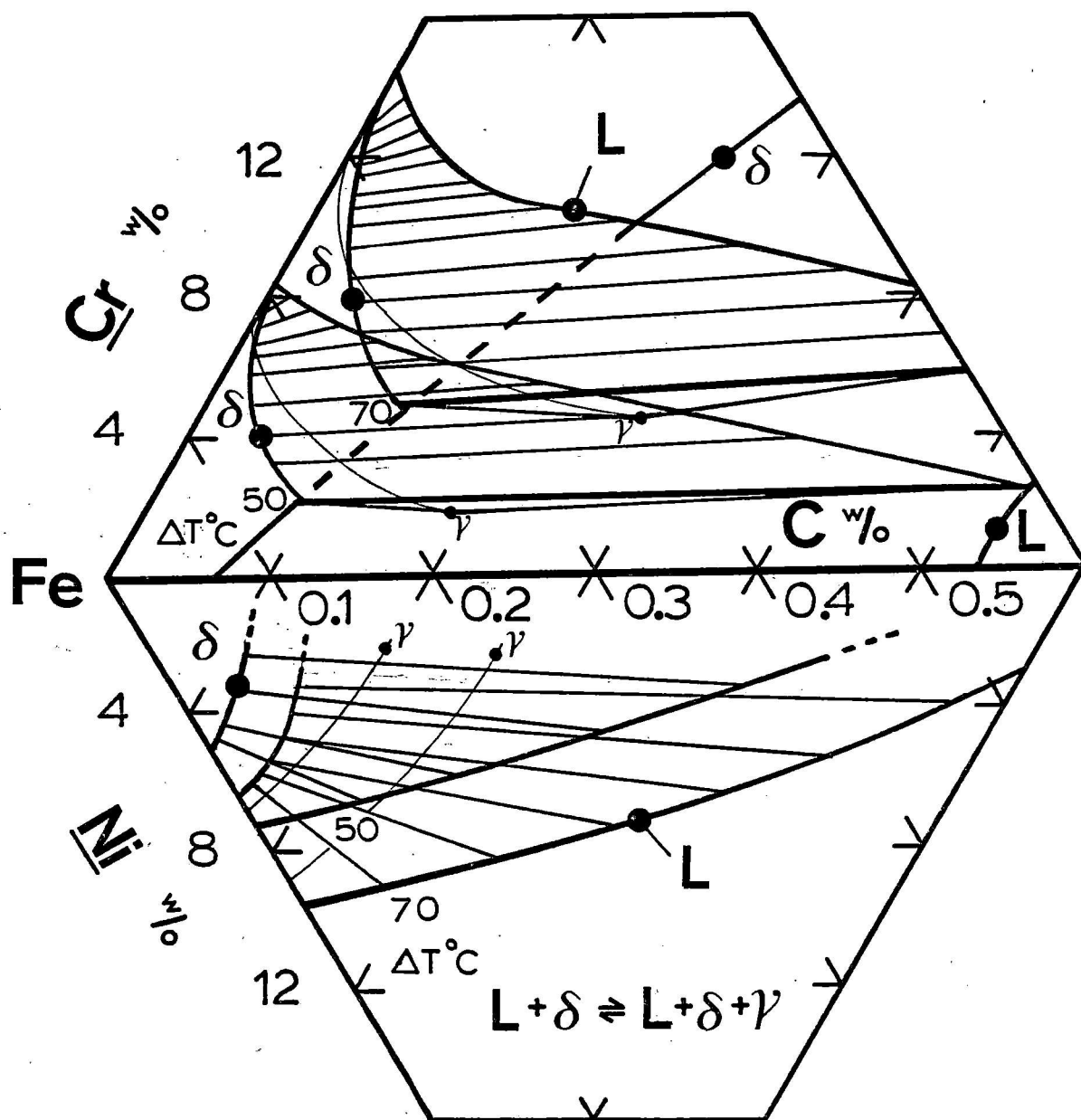


Figure 8.9 - Progress of the two-fold equilibrium $L+\delta \rightleftharpoons L+\delta+\gamma$ with temperature in the Fe-Cr-Ni-C system (orthogonal projection onto the Fe-Ni-C and the Fe-Cr-C basal planes)

CHAPTER 9CALCULATION OF CRYSTALLIZATION PATHS

Control of the processes that occur during the solidification of steels is essential to produce castings of superior quality and desired microstructure. This state-of-the-art has been largely attained in the processing of low-alloy steels. High-alloy steels are more complex. Understanding the solidification process is complicated by the number of important solute elements and may require the aid of mathematical models to accommodate the factors which determine the course of solidification.

An important aspect of this analysis would be modelling of the compositions and structures of the phases which precipitate under controlled conditions. Among these are the conditions which establish the equilibrium state of the alloy system. Knowledge of the equilibrium state is essential to predict the driving force for a process and the final state to which it should move.

The equilibrium state is expressible either as a mathematical function of the Gibbs energies of the phases partaking in the process or as maps of the equilibrium composition relationships among the stable phases at each temperature. The equilibrium phase diagram can be calculated from models of the Gibbs energies of each of the coexisting phases and is applicable directly in the analysis of the solidification process because the alloy casting is characterized by its microstructure which, in turn, is identified by the compositions and amounts of the phases present.

The process which occur during the course of equilibrium solidification of alloy steels are:

1. Precipitation of one or more solid-solution phases which may be plane-front, cellular or dendritic;
2. Precipitation of a stoichiometric and quasi-stoichiometric phase (oxide, carbide, etc.);
3. Formation of gases (H_2 , N_2 , CO, CO_2 , etc.);
4. Simultaneous occurrence of cases (1), (2), and (3).

However, the dictates of equilibrium may not be followed completely at the solidification rates encountered in the casting of ingots and in strand casting and rheo-casting. The phenomena of segregation, formation of a metastable phase, extended solubility limits of a phase and suppression of the formation of an equilibrium phase may occur from the onset, or intermittently, until solidification is completed.

These phenomena have been observed to be a function of the solidification rate. For example, segregation of the solute elements occurs when the characteristic diffusion distance^{*} is on the order of or less than the dendrite arm spacing and when the composition of the liquid phase is different from the composition of the conjugate solid phase (85). Metastable phases and non-equilibrium structures form under conditions of high cooling rates but may also form at relatively low rates when a high degree of supercooling is achieved prior to nucleation (86).

*

square-root of the diffusivity of the solute element times the local solidification rate.

An analysis of the phenomena of segregation and hindered formation of oxides (SiO_2 , Al_2O_3 , CO, etc.) in low alloy steels containing oxygen as a component has been developed by Wright and Elliott.(87). Three cases were considered:

1. Complete equilibrium solidification.
2. Complete mixing in the liquid and segregation of the solid phase during solidification, with equilibrium conditions assumed at the solid-liquid interface.
3. Segregation with the suppression for a short period of time of the formation of a third phase (i.e., oxide).

The Scheil equation for plane-front solidification was assumed. Partition coefficients of the solute elements were calculated from the limiting binary systems Fe-O, Fe-C, Fe-Al, etc.

This development is extended in the present study to high alloy steels, in particular, alloys in the Fe-Cr-Mn-Ni-C system. The partition coefficients of the solute elements in these alloys can differ appreciably from the values calculated from the limiting binary systems. In this case, the partition coefficient is calculated from the thermodynamic model of the equilibrium between two phases or among three phases, as the case may be.

9.1. Equilibrium Solidification

The equilibrium crystallization path of phase ϕ of an alloy of fixed total composition $P(x_i^o)$ is the loci of compositions of phase ϕ of the equilibria which exist in the field $P(x_i^o, T)$. The equilibrium compositions among the coexisting phases at each temperature is depicted by

the hyperconode of order S ($1 \leq S \leq (N-F+1)$) where N is the number of components and F is the degrees of freedom of the equilibrium. The solidification path is the path traced out by the compositions of the liquid phase in equilibrium with the solid phase(s) at each temperature.

9.1.1. Two-phase Equilibrium

At the temperatures in the field $P(X_i^{\circ}, T)$ where the equilibrium is between two phases, the solidification path is depicted by a continuum of tie-lines. From the tie-line at each temperature, the partition coefficient of each component can be calculated:

$$K_i = \frac{X_i^{\phi}}{X_i^L} \quad (9.1)$$

The compositions X_i^{ϕ} , X_i^L are elements of the concentration matrix

$$M = \left\| \left\| X_{ij} \right\| \right\| \quad \begin{array}{l} i = 1, N-1 \\ j = L, \phi \end{array} \quad (9.2)$$

In the temperature and composition field in which the thermodynamic behavior of the phases are known, the solidification path can be calculated by solving the set of equations expressing the equality of chemical potential of each component in the liquid phase and in the solid phase. (Chapter 4):

$$\Delta\mu_i^L = \Delta\mu_i^{\phi} + \Delta\mu_i^{\circ L \rightarrow \phi} \quad i = 1, N \quad (9.3)$$

subject to:

$$\eta_L = \frac{X_1^{\circ} - X_1^{\phi}}{X_1^L - X_1^{\phi}} = \frac{X_2^{\circ} - X_2^{\phi}}{X_2^L - X_2^{\phi}} = \dots = \frac{X_{N-1}^{\circ} - X_{N-1}^{\phi}}{X_{N-1}^L - X_{N-1}^{\phi}} \quad (9.4)$$

Equation (9.3) has (N-2) degrees of freedom. Equation (9.4) consists of (N-2) relationships which correspond to a partial mass balance of the system at $P(X_i^\circ)$. No further constraints are necessary in order that the solution matrix, Equation (9.2), can be calculated. It is noted that instead of Equation (9.4), the following equation may also be used as (N-2) constraints:

$$\eta^\phi = \frac{X_i^\circ - X_i^L}{X_i^\phi - X_i^L} = \frac{X_2^\circ - X_2^L}{X_2^\phi - X_2^L} = \dots = \frac{X_{N-1}^\circ - X_{N-1}^L}{X_{N-1}^\phi - X_{N-1}^L} \quad (9.5)$$

In practice both sets of Equations (9.4) and (9.5) could be used as constraints on Equation (9.3) since both equations must be satisfied at the solution.

9.1.2. Three-Phase Equilibrium

During the course of solidification, equilibrium among three phases may occur in the field $P(X_i^\circ, T)$. Mathematically, this is related to the fraction of liquid phase η^L which assumes a value significantly greater from zero at the temperature in the field where the equilibrium among the three phases corresponds to a lower Gibbs energy of the alloy system than that of the two-phase equilibrium. The conditions of the equilibrium among three phases is expressed as follows:

$$\Delta\mu_i^L = \Delta\mu_i^\phi + \Delta\mu_i^{\circ, L \rightarrow \phi_1} = \Delta\mu_i^{\phi_2} + \Delta\mu_i^{\circ, L \rightarrow \phi_2} \quad (9.6)$$

The set of Equations (9.6) has (N-3) degrees of freedom. For N=3, no constraints are required. The fraction of each phase at each temperature

is calculated from the following equations at the solution:

$$\eta^{\phi} = \frac{X_i^{\circ} - X_i^L}{X_i^{\circ} - X_i^L} \quad (9.7)$$

$$\eta^{\phi_1} + \eta^{\phi_2} + \eta^{\phi_3} = 1 \quad (9.8)$$

For N=4, Equation (9.6) has one degree of freedom and is subject to the following set of Equations:

$$\frac{X_i^{\circ} - X_i^{\phi_1}}{X_i^L - X_i^{\phi_1}} = \frac{X_i^{\circ} - X_i^{\phi_2}}{X_i^L - X_i^{\phi_2}} \quad i = 1,3 \quad (9.9)$$

Equations (9.7) and (9.8) can be used to calculate the fraction of each phase at the solution and partition coefficients are calculated from the elements of the solution matrix at each temperature.

9.2. Non-equilibrium solidification

The phenomena of segregation and extended (metastable) solubility limits in high-alloy steels are amenable to quantitative analysis when the equilibrium state is known quantitatively. The procedure to model each non-equilibrium process has been developed and will be presented in a future publication. Figure 9.1 shows a sample calculation of the effect of segregation of solute elements C and Cr during plane-front solidification of the γ phase in the Fe-Cr-C system. The initial composition of the melt is $P(X_i^{\circ})$. Parentheses indicate the fraction of liquid phases at selected temperatures during equilibrium solidification. Brackets indicate the fraction of liquid phase when no

diffusion of C and Cr in the solid phase but complete diffusion in the liquid phase occurs during solidification. The solidification paths were calculated from Equations (9.3) and (9.4) and are a verification of the methods to calculate the tie-lines discussed in Chapter 4.

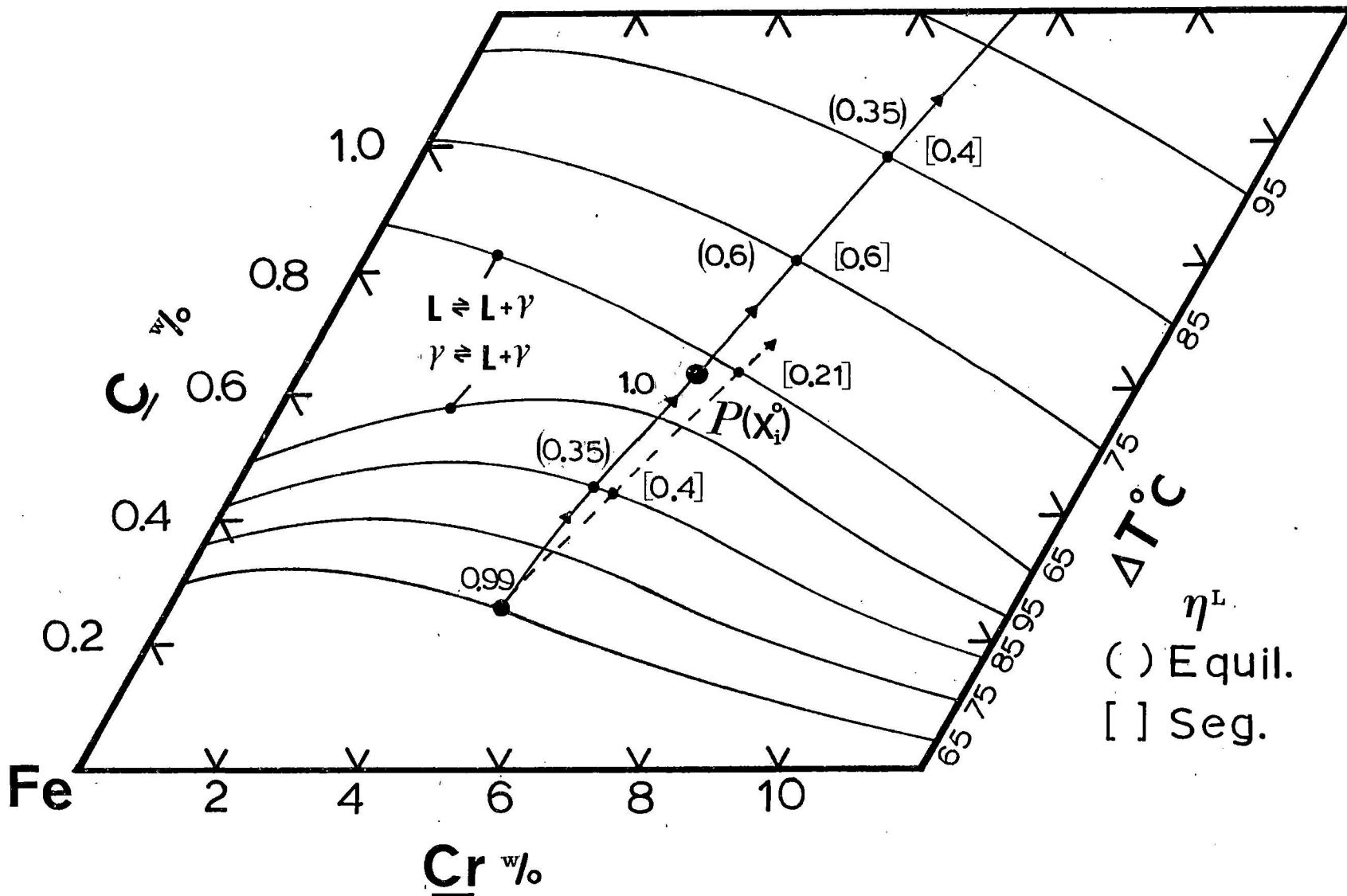


Figure 9.1 - The solidification paths of the liquid and gamma phases in the Fe-Cr-C system beginning at the composition $P(X_i^0)$. Parentheses indicate the fraction of liquid phase at selected temperatures during equilibrium solidification. Brackets indicate the fraction of liquid phase when segregation of Cr and C is assumed during solidification (see text).

CHAPTER 10SUMMARY AND CONCLUSIONS

Phase relationships have been investigated in the iron-rich Fe-Cr-Mn-Ni-C system at solidification temperatures. The composition fields investigated were the iron-rich binary systems, ternary systems and selected quaternary systems of the composition pentahedroid bounded by 0 to 1 w/o C, 0 to 10 w/o Mn, 0 to 25 w/o Cr and 0 to 25 w/o Ni (bal. Fe). The phase relationships investigated in the composition field were the tie-lines between the liquid and δ (BCC) phases and between the liquid and γ (FCC) phases, the δ -liquidus and the γ -liquidus and the two-fold equilibrium $L+\delta \rightleftharpoons L+\delta+\gamma$.

The investigation consisted of experiments and thermodynamic modelling of the results. The model consisted of parameters in the quasi-regular solution model of the thermodynamic behavior of each phase and the relative phase stabilities of the pure components. The parameters which referred to the binary systems were determined mainly from thermodynamic information reported in the literature and partly from mathematical methods applied on the experimental results. The parameters which referred to the thermodynamic behavior of the phases in the ternary and quaternary systems were determined from the experimental results.

The liquidus and the tie-lines of the equilibrium of the liquid phase and each solid phase in each binary and ternary system have been predicted within the experimental error with the model. It was necessary to include ternary parameters for the liquid and solid phases in the Fe-Cr-C, Fe-Ni-C, Fe-C and Fe-Cr-Ni systems.

The tie-lines of the equilibrium between the liquid and delta (BCC) phases in the quaternary systems Fe-Cr-Mn-C and Fe-Cr-Ni-C were predicted within the experimental error with only the binary and ternary parameters in the model. However, the tie-lines of the equilibrium between the liquid and gamma (FCC) phases in the Fe-Cr-Mn-C, Fe-Cr-Ni-C and Fe-Mn-Ni-C systems were not predicted within the experimental error with only the binary and ternary parameters. The use of the quaternary parameter in the model improved the agreement, although the discrepancy was still greater than the experimental error.

The method of equal chemical potentials was used in all the calculations of the phase equilibria. Consistent with the observations of Kubaschewski (74), the calculated results in the Fe-Cr-Mn-Ni-C system were observed to be more sensitive to the relative magnitude of the Gibbs energy of the partaking phases than on the absolute magnitude, referred to the same standard state. It is concluded that under these circumstances, the phase equilibrium determined directly by experiment may be more accurate than determined by calculation. On the other hand, under conditions when the temperature of an equilibrium is difficult to measure (e.g., minimum the surface of saturation or the three-phase equilibrium $L+\delta \rightleftharpoons L+\delta+\gamma$), the phase relationships determined by calculation from the Gibbs energies of each phase may be more accurate.

The model has been extended to calculate solidification paths for the case of complete equilibrium and for selected cases of non-equilibrium. The results of the latter calculations are intended for future publication.

APPENDIX A

THE CHEMICAL POTENTIAL EXPRESSED AS A FUNCTION OF INTENSIVE INDEPENDENT VARIABLES

The chemical potential of component i in phase ϕ in N -component system is by definition

$$\mu_i^\phi = \frac{\partial G^\phi}{\partial m_i^\phi} \left| \begin{array}{l} T, P, m_j^\phi \\ j=1, 2, \dots, N \\ j \neq i \end{array} \right. \quad (\text{A.1})$$

where G^ϕ is the Gibbs energy of phase ϕ (extensive)

m_i^ϕ is the number of moles of component i in phase ϕ .

The molar Gibbs energy of phase ϕ is related to the extensive Gibbs energy by the total number of moles of the system, n :

$$G^\phi = n^\phi G_M^\phi \quad (\text{A.2})$$

$$n^\phi = \sum_{i=1}^N m_i^\phi \quad (\text{A.3})$$

The following equation is thus obtained:

$$\mu_i = \frac{\partial m^\phi G_M^\phi}{\partial m_i^\phi} \left| \begin{array}{l} T, P, m_j^\phi \\ j=1, 2, \dots, N \\ i \neq j \end{array} \right. \quad (\text{A.4})$$

Differentiation of Equation (A.4) gives

$$\mu_i = m^\phi \frac{\partial G_M^\phi}{\partial m_i^\phi} + G_M^\phi \frac{\partial m^\phi}{\partial m_i^\phi} \quad (\text{A.5})$$

$$= m^\phi \frac{\partial G_M^\phi}{\partial m_i^\phi} + G_M^\phi \quad (\text{A.5})$$

To express Equation (A.6) as a function of the intensive rather than the extensive thermodynamic variables, the following intensive quantity is defined:

$$X_i^\phi = \frac{m_i^\phi}{m^\phi} \quad i = 1, 2, \dots, N \quad (\text{A.7})$$

And, as a consequence of Equation (A.3),

$$\sum_{i=1}^N X_i^\phi = 1 \quad (\text{A.8})$$

Application of the chain-rule to Equation (A.6) gives

$$\left. \frac{\partial G_M^\phi}{\partial m_i^\phi} \right|_{\substack{T, P, m_j^\phi \\ j=1, 2, \dots, N \\ j \neq i}} = \sum_{j=1}^N \left. \frac{\partial G_M^\phi}{\partial X_j^\phi} \right|_{\substack{T, P, X_j^\phi \\ j=1, 2, \dots, N \\ j \neq i}} \frac{\partial X_j^\phi}{\partial m_i^\phi} \quad (\text{A.9})$$

And, differentiation of Equation (A.7) gives

$$\text{for } j \neq i: \quad \frac{\partial X_j^\phi}{\partial m_i^\phi} = - \frac{m_j^\phi}{(m^\phi)^2} = - \frac{X_j^\phi}{m^\phi} \quad (\text{A.10a})$$

$$\text{for } j=i: \quad \frac{\partial X_i^\phi}{\partial m_i^\phi} = \frac{m^\phi - m_i^\phi}{(m^\phi)^2} = \frac{1}{m^\phi} (1 - X_i^\phi) \quad (\text{A.10b})$$

Combination of Equations (A.6) through (A.10) gives

$$\mu_i = G_M^\phi + \left. \frac{\partial G_M^\phi}{\partial X_i^\phi} \right|_{\substack{T, P, X_j^\phi \\ j=1, 2, \dots, N-1 \\ j \neq i}} - \sum_{j=1}^{N-1} X_j^\phi \left. \frac{\partial G_M^\phi}{\partial X_j^\phi} \right|_{\substack{T, P, X_i^\phi \\ i=1, 2, \dots, N-1 \\ i \neq j}} \quad (\text{A.11})$$

In practice, the chemical potential and the molar Gibbs energy are measured relative to a standard state.

The standard state, however, is not a function of composition. Since the following is always true:

$$G_M^\phi = \sum_{i=1}^N X_i^\phi \mu_i^\phi \quad (\text{A.12})$$

Therefore,

$$\mu_i^\phi - \mu_i^{\circ,\phi} = \Delta G_M^\phi + \left. \frac{\partial \Delta G_M^\phi}{\partial X_i^\phi} \right|_{\substack{T, P, X_j^\phi \\ j=1, 2, \dots, N \\ j \neq i}} - \sum_{j=1}^{N-1} X_j^\phi \left. \frac{\partial \Delta G_M^\phi}{\partial X_j^\phi} \right|_{\substack{T, P, X_i^\phi \\ i=1, 2, \dots, N-1 \\ i \neq j}} \quad (\text{A.13})$$

where

$$\Delta G_M^\phi = G_M^\phi - \sum_{i=1}^N X_i^\phi \mu_i^{\circ,\phi} \quad (\text{A.14})$$

and

$$\Delta \mu_i^\phi = \mu_i^\phi - \mu_i^{\circ,\phi} \quad (\text{A.15})$$

Finally, Equation (A.13) can be re-arranged as

$$\Delta \mu_i^\phi = \Delta G_M^\phi + \sum_{j=1}^{N-1} (\delta_{ij} - X_j) \frac{\partial \Delta G_M^\phi}{\partial X_j} \quad (\text{A.16})$$

where δ_{ij} is the Kronecker delta which equals one, when $i=j$ and equals zero when $i \neq j$. The superscript ϕ on the variable X_j^ϕ has been dropped for convenience.

APPENDIX B

THE EFFECT OF CONTAMINATION ON THE MEASUREMENT OF TEMPERATURE AND THE COMPOSITION OF THE TWO-PHASE EQUILIBRIUM

Any alloy system under experimental analysis contains impurities of measurable concentrations. The alloy system of N components is in fact an N+M component system where M is the number of impurity components. To assess the effect of the concentrations of the impurities on the tie-lines determined by experiment, one could calculate the equilibrium in the (N+M)-component system and calculate the discrepancy between the experimental and calculated tie-lines as a function of the concentrations of the impurities. The system of equations for the equilibrium between the α and β phases are

$$\Delta\mu_i^\alpha = \Delta\mu_i^\beta (X_i^\beta) + \Delta\mu_i^{\alpha \rightarrow \beta} \quad (\text{B.1})$$

$$i = 1, 2, \dots, N+M$$

However, a model of the thermodynamic interactions of each of the (N+M) components and its relative phase stability must be known for the concentrations and temperatures at which the equilibrium has been measured. Nonetheless, in the present study, a simplified analysis can be made.

A simple analysis is to calculate the effect of the impurity concentrations on the melting points of the pure components. This analysis is particularly useful in the present study because the measurement of temperature is confined to the iron-rich composition field and is determined in the same manner at each point in the composition field. Furthermore, if the temperature depression of the

melting point due to a given concentration of impurities can be assumed to be equal for pure iron and the concentrated alloy, measurements of the liquidus of the N-component system can be calibrated by the discrepancy between the accepted melting point of hypothetically pure iron and the measured melting point of the iron used in the experiment. This calculation is determined by assuming Raoult's law for each impurity in Equation (B.1) for $i=Fe$.

$$\ln (1 - \sum X_i^l) \approx \frac{\Delta H_{Fe}^{\circ, \delta \rightarrow L} \theta_{Fe}^{L \rightarrow \delta}}{R(T_{mp}^{hyp.})^2} \quad (B.2)$$

from page , $(\sum X_i)_{max} \approx 0.001$

and

$$\theta_{Fe}^{L \rightarrow \delta} = T_{mp}^{hyp.} - T_{mp}^{Exp.} \approx 2.5^\circ C$$

where $\Delta H_{Fe}^{\circ, \delta \rightarrow L}$ is the enthalpy of fusion of pure iron (Table 2.5).

It is noted, however, that at the higher concentrations of the major components in the alloy, the effect of the impurities on the temperature of the liquidus may change significantly (on the order of a degree or more) from the value calculated at low alloy concentrations, due to the thermodynamic interactions that may exist at the higher alloy concentrations. This effect can only be verified by an analysis of the entire N+M component system. In addition, the foregoing analysis does not take into account the effect of the impurities on the partitioning of the solute elements in the equilibrium between the liquid and solid solution phases.

A more complete analysis is to calculate the equilibrium by employing Equation (B.1) for the components in which the thermodynamic

interactions in iron are known. For iron, the interaction coefficients at infinite dilution can be employed (Equation 2.10). The first and second-order interaction coefficients can be used for the major components but only the first-order interaction coefficients for the impurity components. The Gibbs-Duhem relationship can then be applied to determine the interaction coefficients of the other $(N+M-1)$ to determine the interaction coefficients of the other $(N+M-1)$ components. Alternatively, when only one or two impurities such as O and Si are to be considered, the quasi-regular solution model of the $N+M$ components could be employed, with only the binary parameters included for the interactions with the impurity component.

The interaction coefficients of the impurities have been determined in dilute liquid iron. However, there has been little or no thermodynamic investigation of the behavior of the impurities in delta or in gamma iron. An approach to overcome this limitation would be to calculate the phase equilibria in the Fe-C-X-Y system where X is the major component (Cr, Mn, Ni, etc.) and y is the impurity component (O, Si, Al, etc.). Parameters in the model for the solid solution phases could be determined by application of the methods of Chapter 6 to the iron-rich systems Fe-O, Fe-Si, Fe-Al, etc.

APPENDIX C

TABULATED RESULTS

Table 1. Transformation temperatures in the Fe-Ni system:
 δ -liquidus ($L \rightarrow L + \delta$) and peritectic reaction ($L + \delta \rightarrow L + \delta + \gamma$)

Composition w/o Ni	Temperature *	
	ΔT^L	ΔT^P
1.01	4	-
2.04	8	-
2.99	13	-
3.96	17	-
4.95	21	22

$$* T = 1538^\circ\text{C} - \Delta T$$

Table 2. Transformation temperatures in the Fe-Ni system:
 γ -liquidus ($L \rightarrow L + \gamma$)

Composition w/o Ni	Temperature	
	ΔT^L	T^L
5.99	25	1513
8.02	27	1511
10.00	31	1507
12.00	35	1503
14.00	39	1498
15.97	43	1495
17.98	46	1492
19.99	50	1488
22.00	54	1484
24.98	60	1478

Table 3. Transformation temperatures in the Fe-Cr system:
 δ -liquidus ($L \rightarrow L + \delta$)

Composition w/o Cr	Temperature	
	ΔT^L	T^L
2.10	4	1534
4.01	7	1531
5.97	10	1528
8.09	13	1525
10.18	15	1523
12.16	18	1520
14.01	19	1519
15.91	20	1518
17.78	21	1517
20.12	21	1517
22.64	21	1517

Table 4. Transformation temperatures in the Fe-Mn system:
 δ -liquidus ($L \rightarrow L + \delta$)

Composition w/o Mn	Temperature	
	ΔT^L	T^L
5.20	24	1514
6.00	27	1511
6.50	29	1509
10.10	46	1492

Table 5. Transformation temperatures in the Cr-Ni system:
 γ -liquidus ($L \rightarrow L + \gamma$)

Composition w/o Cr	Temperature	
	ΔT^L	T^L
5.0	8	1447
10.0	16	1439
15.0	25	1430
20.0	34	1421
25.0	45	1410
32.0	59	1396

Table 6. Transformation temperatures in the Fe-Cr-C system:
 δ -liquidus ($L \rightarrow L+\delta$) and peritectic reaction ($L+\delta \rightarrow L+\delta+\gamma$)

Composition		Temperature*		Composition		Temperature*	
w/o	w/o Cr	ΔT^L	ΔT^P	w/o	w/o Cr	ΔT^L	ΔT^P
0.092	2.18	11	--	0.131	15.87	30	-
0.091	4.06	14	-	0.187	10.53	31	-
0.154	1.62	15	-	0.259	6.00	32	-
0.089	5.90	17	-	0.285	6.00	33	67
0.151	3.18	17	-	0.182	13.12	33	-
0.149	4.57	19	-	0.177	15.57	34	-
0.100	6.22	19	-	0.284	7.98	34	-
0.087	7.97	20	-	0.172	17.78	35	-
0.147	5.99	21	-	0.167	20.07	35	-
0.085	10.00	22	-	0.280	8.00	35	78
0.145	7.44	23	-	0.373	3.85	37	-
0.202	3.76	23	-	0.410	2.00	37	48
0.083	12.02	24	-	0.269	11.10	38	-
0.141	9.20	25	-	0.260	14.00	39	-
0.081	13.99	26	-	0.400	4.02	39	55
0.270	1.99	26	-	0.365	5.92	39	-
0.197	6.00	26	-	0.254	16.00	40	-
0.079	16.00	27	-	0.250	18.20	41	-
0.077	18.09	27	-	0.390	6.02	41	63
0.075	20.11	27	-	0.357	8.16	42	-
0.074	22.06	27	-	0.495	2.02	43	-
0.138	11.07	27	-	0.350	10.06	43	-
0.300	2.05	28	50	0.380	9.00	44	78
0.264	4.01	29	-	0.341	12.06	45	-
0.135	13.13	29	-	0.485	3.97	46	-
0.193	8.09	29	-	0.474	6.12	48	-
0.290	4.00	30	57	0.465	7.97	50	-

Table 6 (Cont'd.)

Composition		Temperature*	
w/o C	w/o Cr	ΔT^L	ΔT^P
0.455	9.84	51	-
0.446	11.78	53	-
0.520	5.24	53	57
0.514	6.60	54	-
0.490	9.08	55	-
0.555	6.51	57	66
0.54	8.10	59	74
0.537	9.57	60	81
0.530	10.16	61	84
0.527	11.21	61	-
0.516	13.17	62	-
0.563	9.80	62	-
0.620	7.84	65	72
0.620	10.00	66	-
0.630	8.95	66	76
0.644	8.80	67	-

Table 7. Transformation temperatures in the Fe-Cr-C system:
 δ -liquidus ($L \rightarrow L + \delta$)

Composition		Temperature*	Composition		Temperature*
w/o C	w/o Cr	ΔT^L	w/o C	w/o Cr	ΔT^L
0.540	2.05	47	0.770	3.86	66
0.660	1.52	54	0.787	4.03	67
0.680	1.46	55	0.730	6.81	69
0.650	3.05	57	0.771	5.94	69
0.673	2.50	57	0.712	8.46	71
0.662	4.06	59	0.920	1.99	73
0.640	4.48	59	0.754	8.01	73
0.760	2.00	61	0.910	3.46	75
0.649	6.01	62	0.738	10.00	76
0.770	2.00	62	0.892	5.09	77
0.750	3.54	63	1.020	2.04	78
0.803	2.02	63	0.913	6.11	79
0.755	3.58	63	0.880	6.33	79
0.795	3.03	65	1.000	3.75	81
0.740	5.16	66	0.890	8.30	82
0.742	5.21	66	1.000	6.70	86

$$*T = 1538^\circ\text{C} - \Delta T$$

Table 8. Transformation temperatures in the Fe-Mn-C system:
 δ -liquidus ($L \rightarrow L + \delta$) and peritectic reaction ($L + \delta \rightarrow L + \delta + \gamma$)

Composition		Temperature*	
w/o C	w/o Mn	ΔT^L	ΔT^P
0.051	1.20	9	-
0.117	1.01	14	-
0.116	2.01	18	-
0.131	1.95	20	-
0.165	1.55	20	45
0.130	2.65	22	-
0.100	3.12	22	-
0.221	1.10	22	43
0.115	2.98	22	-
0.113	4.02	26	-
0.096	4.42	27	-
0.120	4.20	28	-
0.241	2.00	29	45
0.112	5.00	31	-
0.111	6.01	35	-
0.130	5.60	36	-
0.237	3.90	37	49
0.33	2.50	38	46
0.36	2.50	40	47
0.128	7.07	42	-
0.125	9.04	50	-

* $T = 1538 - \Delta T$

Table 9. Transformation temperatures in the Fe-Mn-C system:
 γ -liquidus ($L \rightarrow L+\gamma$)

Composition		Temperature [*]
w/o C	w/o Mn	ΔT^L
0.460	1.62	43
0.344	4.01	45
0.450	3.00	48
0.280	6.12	49
0.450	4.00	50
0.336	6.23	52
0.600	2.80	55
0.270	8.00	55
0.510	4.70	57
0.590	3.97	58
0.750	1.01	60
0.600	4.40	60
0.740	2.05	61

$$*T = 1538^{\circ}\text{C} - \Delta T$$

Table 10. Transformation temperatures in the Fe-Ni-C system
 δ -liquidus ($L \rightarrow L + \delta$) and peritectic reaction ($L + \delta \rightarrow L + \delta + \gamma$)

Composition		Temperature*	
w/o C	w/o Ni	ΔT^L	ΔT^P
0.112	0.98	12	38
0.111	2.04	16	33
0.143	1.00	16	38
0.142	2.00	20	34
0.110	2.97	21	31
0.130	2.65	22	-
0.222	0.97	22	38
0.109	4.01	24	27
0.141	2.99	24	30
0.219	1.97	26	34
0.284	0.98	27	37
0.139	4.00	27	27
0.360	1.00	33	42

$$*T = 1538^\circ\text{C} - \Delta T$$

Table 11. Transformation temperatures in the Fe-Ni-C system:
 γ -liquidus ($L \rightarrow L + \gamma$)

Composition		Temperature*	Composition		Temperature*
w/o C	w/o Ni	ΔT^L	w/o C	w/o Ni	ΔT^L
0.106	6.03	29	0.197	12.00	46
0.136	5.98	31	0.095	16.01	48
0.104	7.98	33	0.371	8.03	49
0.133	8.00	35	0.122	15.99	50
0.270	3.95	35	0.192	14.03	50
0.275	4.04	35	0.252	12.05	50
0.210	5.99	36	0.494	3.98	50
0.150	8.50	36	0.327	10.00	51
0.102	10.04	37	0.093	17.99	52
0.356	3.03	37	0.610	1.98	52
0.130	9.99	39	0.363	10.03	53
0.206	8.03	39	0.483	5.97	53
0.270	6.03	39	0.119	18.00	54
0.396	1.99	39	0.188	16.00	54
0.349	3.99	40	0.246	14.06	54
0.100	11.98	41	0.320	11.99	54
0.387	4.02	42	0.600	3.93	55
0.201	10.00	43	0.413	8.00	56
0.264	7.99	43	0.355	12.04	56
0.127	12.01	43	0.241	16.01	57
0.400	4.20	43	0.183	17.99	57
0.342	6.04	43	0.116	20.03	58
0.097	14.03	45	0.313	14.02	58
0.125	13.98	46	0.235	17.99	60
0.258	9.93	46	0.347	14.00	60
0.335	8.02	46	0.462	10.03	60
0.379	6.00	46	0.590	6.00	60
0.503	2.04	46	0.640	4.69	60

Table 11 (Cont'd.)

Composition		Temperature*
w/o C	w/o Ni	ΔT^L
0.179	19.97	61
0.306	15.99	61
0.770	2.00	63
0.570	7.98	63
0.452	12.03	63
0.334	16.01	63
0.620	7.94	65
0.299	17.88	65
0.760	4.01	66
0.560	10.02	66
0.780	3.55	67
0.440	14.00	67
0.840	1.96	68
0.610	9.71	68
0.740	5.96	69
0.550	12.03	69
0.830	3.97	71
0.760	5.99	71
0.730	8.03	73
0.740	7.97	74
0.810	5.92	74
0.710	9.99	75
0.960	2.04	76
0.940	4.04	78

$$*T = 1538^{\circ}\text{C} - \Delta T$$

Table 11 (Cont'd.)

Composition		Temperature*	Composition		Temperature*
w/o C	w/o Ni	ΔT^L	w/o C	w/o Ni	ΔT^L
0.241	16.01	57	0.840	1.96	68
0.183	17.99	57	0.610	9.71	68
0.116	20.03	58	0.740	5.96	69
0.313	14.02	58	0.550	12.03	69
0.235	17.99	60	0.830	3.97	71
0.347	14.00	60	0.760	5.99	71
0.462	10.03	60	0.730	8.03	73
0.590	6.00	60	0.740	7.97	74
0.640	4.69	60	0.810	5.92	74
0.179	19.97	61	0.710	9.99	75
0.306	15.99	61	0.96	2.04	76
0.770	2.00	63	0.94	4.04	78

$$*T = 1538 - \Delta T$$

Table 12. Transformation temperatures in the Fe-Cr-Mn system:
 δ -liquidus ($L \rightarrow L + \delta$)

Composition		Temperature [*]
w/o Mn	w/o Cr	ΔT^L
2.00	5.15	17
2.25	8.10	23
3.30	5.05	24
1.00	13.80	24
2.05	13.70	29
3.15	8.80	29
2.00	17.30	30
4.75	4.15	30
2.15	13.60	30
3.00	12.20	31
2.90	16.25	33
4.60	6.75	33
3.20	17.05	35
5.95	5.00	36
3.80	13.30	36
4.30	12.00	37
5.60	9.05	40

$$*T = 1538^{\circ}\text{C} - \Delta T$$

Table 13. Transformation temperatures in the Fe-Mn-Ni system:
 δ -liquidus ($L \rightarrow L + \delta$) and peritectic reaction ($L + \delta \rightarrow L + \delta + \gamma$)

Composition		Temperature *	
w/o Mn	w/o Ni	ΔT^L	ΔT^P
1.50	3.00	19	46
2.80	2.60	24	-
4.20	2.00	29	-
4.50	2.10	30	-
3.80	3.85	34	37

$$*T = 1538^\circ\text{C} - \Delta T$$

Table 14. Transformation temperatures in the Fe-Mn-Ni system:
 γ -liquidus ($L \rightarrow L + \gamma$)

Composition		Temperature [*]
w/o Mn	w/o Ni	ΔT^L
1.40	6.25	29
1.90	6.85	33
1.40	10.00	37
2.55	7.65	38
4.20	5.70	40
1.75	12.05	43
5.50	5.50	44
3.60	9.85	46
4.70	7.50	47
3.90	9.20	47
2.80	11.55	47
1.80	14.70	49
3.80	11.45	51
5.60	9.00	53
1.25	18.05	53
3.45	13.50	54
4.80	11.30	55
5.80	11.20	59

$$*T = 1538^\circ\text{C} - \Delta T$$

Table 15. Transformation temperatures in the Fe-Cr-Ni system:
 δ -liquidus ($L \rightarrow L + \delta$) and peritectic reaction ($L + \delta \rightarrow L + \delta + \gamma$)

Composition		Temperature *	
w/o Cr	w/o Ni	ΔT^L	ΔT^P
2.06	2.02	12	-
3.19	2.01	14	-
4.00	1.98	16	-
5.03	2.02	17	-
5.91	1.94	19	-
7.00	2.05	20	-
8.02	1.89	21	-
8.00	3.97	21	36
8.92	2.00	23	-
3.06	4.04	23	43
3.99	3.89	24	-
10.02	1.85	24	-
4.93	4.00	25	45
12.03	1.79	26	-
11.11	2.02	26	-
6.03	3.81	27	-
14.01	1.77	27	-
15.98	1.73	29	-
8.03	3.72	29	-
6.86	4.02	29	-
18.07	1.66	30	-
20.16	1.64	30	-
8.74	3.97	30	-
3.00	6.01	31	-
3.97	5.85	31	33
10.02	3.65	31	-
12.00	3.57	35	-
14.03	3.48	35	-
6.00	5.73	35	-

Table 15 (Cont'd.)

Composition		Temperature*	
w/o Cr	w/o Ni	ΔT^L	ΔT^P
10.88	4.01	35	-
7.98	5.02	35	-
15.98	3.40	36	-
4.83	6.20	36	-
10.03	4.91	37	-
18.03	3.32	38	-
20.00	3.24	38	-
8.00	5.61	38	-
12.04	4.80	39	-
8.55	6.03	39	60
5.99	6.91	40	42
10.03	5.48	40	-
14.04	4.69	41	-
12.05	5.36	42	-
7.99	6.76	42	50
16.03	4.58	42	-
18.02	4.48	42	-
19.30	4.41	42	-
10.65	6.04	43	-
14.03	5.24	44	-
15.98	5.12	45	-
18.00	5.00	45	-
10.00	6.61	45	-
12.00	6.45	46	-
14.02	6.32	48	-
16.00	6.17	49	-
17.87	6.04	49	-
10.40	7.99	51	52
14.13	8.77	59	-
14.04	9.37	61	65

* $T = 1538 \text{ }^\circ\text{C} - \Delta T$

Table 16. Transformation temperatures in the Fe-Cr-Ni system:
-liquidus (L L+)

Composition		Temperature*	Composition		Temperature*
w/o Cr	w/o Ni	ΔT^L	w/o Cr	w/o Ni	ΔT^L
2.01	7.20	30	2.68	16.00	48
2.00	8.02	31	8.00	10.02	48
2.01	10.01	35	6.04	13.15	50
2.01	10.68	36	8.01	12.00	51
3.98	9.81	38	2.61	17.98	51
4.02	10.46	40	10.00	9.81	52
6.01	9.60	41	10.20	10.03	53
2.81	12.00	42	5.91	15.01	53
2.05	13.70	43	7.98	14.07	54
6.03	10.24	43	12.03	8.99	55
8.37	8.02	45	2.55	20.00	55
8.01	9.40	46	11.98	9.59	56
2.74	14.01	46	9.97	12.03	56
4.04	13.42	46	5.78	16.95	57
8.19	9.98	48	7.64	15.99	58
			14.13	8.77	59
			9.75	14.02	59

$$^*T = 1538^\circ\text{C} - \Delta T$$

Table 17. Transformation temperatures of the quaternary peritectic reaction ($L+\delta \rightarrow L+\delta+\gamma$)

<u>Fe-Cr-Ni-C system</u>			
w/o C	Composition		Temperature*
	w/o Cr	w/o Ni	ΔT^P
0.250	10.15	4.50	63
0.090	9.80	5.40	56
<u>Fe-Cr-Mn-C system</u>			
0.260	3.90	2.00	58
0.350	5.20	2.85	64
0.320	5.20	2.00	64
0.280	5.10	4.00	66
0.290	9.40	2.50	87

* $T = 1538^\circ\text{C} - \Delta T$

Table 18. Experimental tie-lines between the liquid and solid phases in the iron-rich binary systems

Solute	Phases	Composition**		Temperature*
		Liquidus	Solidus	ΔT
C	L- δ	0.08	0.02	7
C	L- δ	0.37	0.07	30
C	L- γ	0.62	0.25	39
C	L- γ	0.74	0.31	58
C	L- γ	0.93	0.40	71
Cr	L- δ	6.10	5.75	10
Ni	L- δ	2.10	1.60	9

* $T = 1538^{\circ}\text{C} - \Delta T$

** w/o solute in Fe

Table 19. Experimental tie-lines between the liquid and solid phases in the Fe-Cr-C system

Liquidus Composition		Solidus Composition		Temperature	Solid phase
w/o C	w/o Cr	w/o C	w/o Cr	ΔT	
0.10	6.30	0.02	5.75	19	δ
0.14	8.00	0.03	7.40	24	δ
0.26	3.80	0.05	3.40	28	δ
0.24	5.30	0.05	5.05	29	δ
0.17	9.95	0.04	9.40	29	δ
0.21	11.90	0.07	11.15	35	δ
0.27	11.10	0.08	10.50	38	δ
0.39	9.10	0.09	8.15	45	δ
0.31	14.75	0.09	13.55	43	δ
0.50	3.95	0.11	3.50	48	δ
0.63	8.95	0.17	7.90	66	δ
0.77	3.85	0.30	3.40	66	γ
0.89	3.70	0.39	3.05	74	γ
0.91	6.10	0.40	5.00	79	γ
1.00	3.75	0.45	3.10	81	γ
1.00	6.70	0.44	5.55	86	γ

$$*T = 1538^{\circ}\text{C} - \Delta T$$

Table 20. Experimental tie-lines between the liquid and solid phases in the Fe-Mn-C system

Liquidus Composition		Solidus Composition		Temperature *	Solid phase
w/o C	w/o Mn	w/o C	w/o Mn	ΔT	
0.05	1.20	0.01	0.90	9	δ
0.16	1.55	0.03	1.30	19	δ
0.13	2.05	0.03	1.60	20	δ
0.10	3.10	0.03	2.75	22	δ
0.13	2.65	0.03	2.40	22	δ
0.22	1.10	0.04	0.90	22	δ
0.12	4.25	0.04	3.80	28	δ
0.13	5.60	0.04	5.00	35	δ
0.24	3.90	0.07	3.50	36	δ
0.33	2.50	0.06	2.00	37	δ
0.35	2.60	0.09	2.10	40	δ
0.45	1.55	0.17	1.25	43	γ
0.28	6.10	0.13	5.30	49	γ
0.60	2.75	0.23	2.20	55	γ
0.51	5.00	0.23	4.05	57	γ
0.73	2.00	0.28	1.50	61	γ

$$* T = 1538^{\circ}\text{C} - \Delta T$$

Table 21. Experimental tie-lines between the liquid and solid phases in the Fe-Ni-C system

Liquidus Composition		Solidus Composition		Temperature [*]	Solid phase
w/o C	w/o Ni	w/o C	w/o Ni	ΔT	
0.10	2.10	0.03	1.80	16	δ
0.13	2.65	0.02	2.15	22	δ
0.27	3.95	0.10	3.65	35	γ
0.15	8.50	0.07	7.95	37	γ
0.15	10.80	0.05	9.85	41	γ
0.40	4.20	0.15	3.85	43	γ
0.34	6.20	0.11	5.70	44	γ
0.29	8.20	0.12	7.60	45	γ
0.15	14.20	0.06	13.40	48	γ
0.26	15.00	0.10	13.90	56	γ
0.48	9.40	0.22	8.90	60	γ

$$*T = 1538^{\circ}\text{C} - \Delta T$$

Table 22. Experimental tie-lines between the liquid and solid phases in the Fe-Cr-Mn system

Liquidus Composition		Solidus Composition		Temperature [*]	Solid phase
w/o Mn	w/o Cr	w/o Mn	w/o Cr	ΔT	
3.50	5.05	3.05	4.85	24	δ
2.10	17.30	1.85	16.30	30	δ
4.80	6.75	4.15	6.35	33	δ

$$*T = 1538^{\circ}\text{C} - \Delta T$$

Table 23. Experimental tie-lines between the liquid and solid phases in the Fe-Cr-Ni system

Liquidus Composition		Solidus Composition		Temperature *	Solid phase
w/o Cr	w/o Ni	w/o Cr	w/o Ni	ΔT	
5.80	5.90	5.30	5.00	36	δ
2.95	10.70	2.70	9.90	39	γ
2.95	14.80	2.80	13.50	46	γ
6.00	11.90	5.30	10.80	48	γ
7.20	13.90	6.50	13.10	53	γ
3.75	17.00	3.45	15.90	51	γ

* $T = 1538^{\circ}\text{C} - \Delta T$

Table 24. Experimental tie-lines between the liquid and solid phases in the Fe-Mn-Ni system

Liquidus Composition		Solidus Composition		Temperature*	Solid phase
w/o Mn	w/o Ni	w/o Mn	w/o Ni	ΔT	
1.50	3.00	1.20	2.45	19	δ
2.00	6.90	1.60	6.20	33	γ
1.90	14.70	1.35	13.20	49	γ

$$*T = 1538^{\circ}\text{C} - \Delta T$$

Table 25. Experimental tie-lines between the liquid and solid phases in the Fe-Cr-Ni-C system

Liquidus Composition			Solidus Composition			Temperature *	Solid phase
w/o C	w/o Cr	w/o Ni	w/o C	w/o Cr	w/o Ni	$\Delta T(^{\circ}\text{C})$	
0.09	9.80	5.40	0.02	9.10	4.40	46	δ
0.22	9.85	5.25	0.05	8.80	4.30	55	δ
0.25	10.10	4.50	0.06	9.40	3.80	55	δ
0.16	5.00	4.10	0.07	4.70	3.85	41	γ
0.12	6.10	5.20	0.05	5.80	5.00	44	γ
0.12	5.20	9.85	0.05	4.70	9.10	51	γ
0.24	5.20	9.75	0.09	4.70	9.40	56	γ
0.28	5.30	8.80	0.10	4.45	8.20	57	γ
0.37	5.40	8.00	0.14	4.60	7.40	61	γ
0.47	5.30	5.10	0.10	4.45	4.60	62	γ

* $\Delta T = 1538^{\circ}\text{C} - T$

Table 26. Experimental tie-lines between the liquid and gamma phases of the Fe-Mn-Ni-C system

Liquidus Composition			Solidus Composition			Temperature [*]
w/o C	w/o Mn	w/o Ni	w/o C	w/o Mn	w/o Ni	$\Delta T(^{\circ}\text{C})$
0.18	3.85	5.20	0.07	3.45	4.60	47
0.14	3.95	10.10	0.06	3.20	8.95	56
0.32	3.85	6.40	0.12	3.10	5.80	57
0.23	3.85	8.20	0.11	3.30	7.50	58
0.46	4.00	4.15	0.19	3.40	3.80	60

* $\Delta T = 1538^{\circ}\text{C} - T$

Table 27. Experimental tie-lines between the liquid and solid phases of the Fe-Cr-Mn-C system

Liquidus Composition			Solidus Composition			Temperature [*]	Solid Phase
w/o C	w/o Cr	w/o Mn	w/o C	w/o Cr	w/o Mn	$\Delta T(^{\circ}\text{C})$	
0.10	5.05	1.90	0.02	4.60	1.50	26	δ
0.26	3.90	2.00	0.05	3.50	1.60	38	δ
0.13	12.40	3.80	0.03	12.00	3.10	45	δ
0.16	8.00	4.10	0.05	7.30	3.55	46	δ
0.32	5.20	2.00	0.06	4.65	1.60	45	δ
0.28	5.10	4.00	0.05	4.65	3.40	49	δ
0.23	8.10	3.90	0.07	7.60	3.40	50	δ
0.35	5.25	2.90	0.09	4.65	2.40	50	δ
0.29	9.40	2.55	0.09	8.80	2.30	50	δ
0.41	14.65	2.90	0.13	13.75	2.50	64	δ
0.57	5.35	2.10	0.24	4.45	1.70	64	γ

* $\Delta T = 1538^{\circ}\text{C} - T$

RECOMMENDATIONS FOR FURTHER RESEARCH

The present investigation has been restricted to carbon concentrations in iron below 1.0 w/o C, and has been confined to temperature range (1538°C to 1450°C) in the iron-rich Fe-Cr-Mn-Ni-C system. The influence of alloying elements on the activity of carbon in liquid and in FCC iron and on the phase relationships of iron-carbon alloys at temperatures near 1000°C has been reported in the literature. Some of the latter work included an investigation of the carbide phases which are stable in the iron-rich ternary system.

It is recommended that the present investigation be extended to the measurement and modelling of the equilibrium phase relationships in the iron-rich Fe-Cr-Mn-Ni-C system at the higher carbon concentrations up to and including saturation of the liquid phase with respect to graphite (1100°C < T < 1538°C). This research should also include an investigation of the influence of alloying elements in the metastable equilibrium of the liquid phase and the carbide M_3C where M is the atom fraction of the solute elements Cr, Mn and Ni.

REFERENCES

1. Hanson, M., Constitution of Binary Alloys, Sec. Ed., McGraw-Hill, New York, 1958.
2. Elliott, R. P., Constitution of Binary Alloys, First Supplement, McGraw-Hill, New York, 1965.
3. Shunk, F.A., Constitution of Binary Alloys, Second Supplement, McGraw-Hill, New York, 1969.
4. Hultgren, R., Desai, P.D., Hawkins, O.T., Gleiser, M. and Kelley, K.K., Selected Values of the Thermodynamic Properties of Binary Alloys, American Society for Metals, Ohio, 1973.
5. Metallography, Structures and Phase Diagrams, vol. 8, American Society for Metals, Ohio, 1973.
6. Prince, A., Multicomponent Alloy Constitution Bibliography 1955-1973, The Metals Society, London, 1974.
7. Orr, R.L. and Chipman, J., Trans. TMS-AIME, 1967, vol. 239, p. 630.
8. Kaufman, L. and Nessor, H., Treatise on Solid State Chemistry, Hanney, ed., vol. 5, Plenum Press, New York, 197 , p. 179.
9. Chipman, J., Met. Trans., 1972, vol. 3, p. 55.
10. Hellewell, A. and Hume-Rothery, W., Phil. Trans. Royal Society of London, vol. A-249, 1957, p. 417.
11. Austin, C., J I S I, vol. 108, 1923, p. 235.
12. Griffing, N.R., Foreng, W.D. and Healy, G.W., Trans. TMS-AIME, vol. 224, 1962, p. 148.
13. Chochol, M., Sc.D. Thesis, Massachusetts Institute of Technology, June, 1976.
14. Benz, R., Elliott, J. and Chipman, J., Met. Trans., vol. 5, 1974, p.2235.

15. Buckley, R.A. and Hume-Rothery, W., J I S I, 1964, p. 895.
16. Isobe, M., Sci. Rep., R I T U, vol. A-3, 1951, p. 540.
17. Benz, R., Elliott, J. and Chipman, J., Met. Trans. vol. 4, 1973, pp. 1975.
18. Wever, F. and Jellinghaus, W., Mitteilungen aus dem Kaiser-Wilhelm-Institute fur Eisenforschung, vol. 13, 1931, p. 93.
19. Jenkins, C.H., Bucknall, E., Austin, C. and Mellor, G., J I S I, vol. 138, 1937, p. 187.
20. Burgess, C. and Forgem, W., Trans. AIME, 1938, p. 277.
21. Jackson, R.S., J I S I, 1970, p. 163.
22. Chipman, J., Met. Trans., vol. 5, 1974, p. 521.
23. Jaufman, L., Phase Stability in Metals and Alloys, Rudman, P., Stringer, J. and Jaffee, R., eds., McGraw-Hill, New York, 1967, p. 125.
24. Kirchner, G., Nishizawa, T. and Uhrenius, B., Met. Trans., vol. 4, 1973, p. 167.
25. Kaufman, L. and Nessor, H., Zeitschrift fur Metalkurde, band 64, heft 4, 1973, p. 249.
26. Domre, M., Thesis de Docteur-Ingenieur, L'institut National Polytechnique de Grenoble, 1978.
27. Lupis, C.P. and Elliott, J.F., Acta, Met., vol. 14, 1966, p. 529.
28. Lupis, C.P. and Elliott, J.F., J I S I, 1966, p. 739.
29. Kaufman, L. and Bernstein, H., Computer Calculation of Phase Diagrams, Academic Press, New York and London, 1970.
30. Foo, E. and Lupis, C.P., Acta Met., vol. 21, 1973, p. 1409.

31. Chipman, J., Met. Trans., vol. 3, 1972, p. 879.
32. Foo, E. and Lupis, C.P., Acta Met., vol. 3, 1972, p. 2125.
33. Mukai, K., Uchida, A., Tagami, T. and Wasai, Y., Third Int. Iron and Steel Congress, Chicago, 1978, p. 236.
34. Sigworth, G. and Elliott, J., Metal Science, vol. 8, 1974, p. 298.
35. Fuwa, T. and Chipman, J., Trans. TMS-AIME, vol. 215, 1959, p. 708.
36. Chipman, J. and Brush, E., Trans. TMS-AIME, vol. 242, 1968, p. 35.
37. Wada, T., Wada, H., Elliott, J. and Chipman, J., Met. Trans., vol. 2, 1971, p. 2199.
38. Ibid., vol. 3, 1972, p. 2865.
39. Foo, E. and Lupis, C.P. Proceedings, ICSTIS, Suppl. Trans. I S I U, vol. 11, 1971, p. 404.
40. Chipman, J., Ibid, p. 239.
41. Kubaschewski, O. and Müller, F., High Temperatures-High Pressures, 1969, vol. 1, p. 543.
42. Rao, M. and Tiller, W., Mats. Sci. and Eng., vol. 15, 1974, p. 87.
43. Ibid., vol. 14, p. 47.
44. Gilby, S. and St. Pierre, G., Trans. AIME, vol. 245, 1969, p. 1749.
45. Belton, G. and Fruehan, R., Met. Trans, vol. 1, 1970, p. 781.
46. Rao, M. and Tiller, W., Mat. Sci. and Eng., vol. 11, 1973, p. 61.
47. Smith, J., Paxton, H. and McCabe, C., Journal of Physical Chem., vol. 68, No.6, 1964, p. 1345.
48. Zupp, R. and Stevenson, D., Trans. AIME, vol. 242, 1968, p. 862.
49. Greenbank, J., JISI, 1972, p. 111.
50. Hultgren, R., Desai, P.D., Hawkins, D.T., Wagman, D., Gleiser, M. and Kelley, K.K., Selected Values of the Thermodynamic Properties of the Elements, American Society for Metals, Ohio, 1973.

51. Benz, R. and Elliott, J., Trans. AIME, vol. 221, 1961, p. 323.
52. Maz and Arany, F. and Pehlke, R., Met. Trans., vol. 4, 1973, p. 2067.
53. Bodsworth, T., Davidson, I. and Atkinson, D., Trans. AIME, vol. 242, 1968, p. 1135.
54. Kaufman, L., Calphad, vol. 2, 1978, p. 117.
55. Ibid., p. 295.
56. Lux, A. L. and Flemings, M.C., Met. Trans. B, vol. 10B, 1979, p. 71.
57. Kelly, T., Private Communication.
58. Null, H.R., Phase Equilibrium in Process Design, Wiley-Interscience, New York, 1970.
59. Henri, H. and Lupis, C.P., Met. Trans. A, vol. 6A, 1975, p. 1057.
60. Ansara, I., Int. Metall. Rev., No.1, 1979, p. 20.
61. Chart, T.G., Counsell, J.F., Jones, G.P., Slough, W. and Spencer, P.J., Int. Metall. Rev., No.20, 1975, p. 57.
62. Hurle, D.J. and Pike, E.R., J. Mat. Sci. vol. 1, 1966, p. 399.
63. Course 10.38, Dept. Chemical Engineering, M.I.T.
64. Nelder, J.A. and Mead, R., Comp. J., 1965, vol. 7, p. 308.
65. Project MACK, Dept. of Elect. Eng. and Computer Sci., M.I.T.
66. Prince, A., Met. Rev. vol. 8, No.30, 1968, p. 213.
67. Palatnik, L.S. and Landau, A.I., Phase Equilibria in Multicomponent Systems, Holt, Rinehart and Winston Inc., New York, 1964.
68. Prince, A., Applications of Phase Diagrams in Metallurgy and Ceramics, vol. 1, NBS pub. 496, 1978, p. 660.
69. Rhines, F., Phase Diagrams in Metallurgy, McGraw-Hill, New York, 1956.
70. Meijering, J.L., Philips Technical Review, vol. 26, No.1, 1965, p. 12.
71. Flemings, M.C., Solidification Processing, McGraw-Hill, New York, 1974.

72. Duwez, P. Wille, R.H. and Klement, W., J. Appl. Phys., vol. 41, 1960, p.1136.
73. Holiday, P.R., Cox, A.R. and Patterson II, R.J., Rapid Solidification Processing Principles and Technology, Mehrabian, R., Kear, B.H. and Cohen, M., Claitor's Publishing Div., Baton Rouge, 1978.
74. Kubaschewski, O. and Alcock, C.B., Metallurgical Thermo-Chemistry, Pergamon Press, Oxford, 1979.
75. Bale, C.W. and Pelton, A.D., Met. Trans., vol. 5, 1974, p. 2323.
76. Luraschi, A., Private Communication.
77. Hiskes, R. and Tiller, W.A., Mats. Sci. and Eng., vol. 2, 1967/68, p.320.
78. Ibid.
79. Ibid.
80. Rao, M.V., Hiskes, R. and Tiller, W.A., Acta Met., vol. 21, 1973, p. 733.
81. Hasebe, M. and Nishizawa, T., Applications of Phase Diagrams in Metallurgy and Ceramics, vol. 2, NBS Publ. No.496, p. 911.
82. Sillen, L.G., Acta Chemica Scand., vol. 16, 1962, p. 169.
83. Kirchner, G. and Uhrenius, B., Acta Met., vol. 22, 1974, p. 523.
84. Beers, Y., Theory of Error, Addison-Wesley, Massachusetts, 1957.
85. Brody, H.D. and Flemings, M.C., Trans. AIME, vol. 236, 1966, p. 615.
86. Rasmussen, D.H. and Loper, Jr., C.R., Acta. Met., vol. 24, 1976, p.117.
87. Wright, J.F. and Wright, J.K., Can. Met. Quart., vol.11, 0.4, 1972, p. 573.
88. Denbigh, K., Principles of Chemical Equilibrium, Cambridge University Press, London, 1973.

BIOGRAPHICAL NOTE

The author was born July 14, 1952 in Steubenville, a small steel town in the hills of Eastern Ohio. He attended several elementary schools in the Ohio Valley and graduated from Wintersville High School in 1970. He enrolled in the College of Engineering at the University of Cincinnati and became the first co-operate student with National Steel Research and Development. He graduated summa cum laude in June 1975 and joined subsequently the chemical metallurgy group at M.I.T. At the completion of the thesis he will join Armco Steel Research in Middletown, Ohio.

His hobbies are oils, photography and some athletics. He enjoys particularly a good game of tennis and bike touring in New England.

The author is a member of Alpha Sigma Mu, American Society of Metals, the Metallurgical Society of AIME and the Electrochemical Society.